Institut für Physikalische und Theoretische Chemie der Technischen Universität München

EXCITED STATE DYNAMICS IN FLUORESCENT PROTEINS (GFP, RFP) AND FLAVOPROTEINS

Tanja Angela Schüttrigkeit

Vollständiger Abdruck der von der Fakultät für Chemie der Technischen Universität München zur Erlangung des akademischen Grades eines

Doktors der Naturwissenschaften

genehmigten Dissertation.

Vorsitzender: Univ.-Prof. Dr. Klaus Köhler

Prüfer der Dissertation: 1. Univ.-Prof. Dr. Maria E. Michel-Beyerle i.R.

2. Univ.-Prof. Dr. Sevil Weinkauf

Die Dissertation wurde am 22.03.2004 bei der Technischen Universität München eingereicht und durch die Fakultät für Chemie am 27.07.2004 angenommen.

Table of Contents

Table of Figures

Table of Amino Acids

A	Ala	Alanine
B	Asx	Asparagine or asparaginic acid
C	Cys	Cysteine
D	Asp	Asparaginic acid
E	Glu	Gluthaminic acid
F	Phe	Phenylalanine
G	Gly	Glycine
H	His	Histidine
I	Ile	Isoleucine
K	Lys	Lysine
L	Leu	Leucine
M	Met	Methionine
N	Asn	Asparagine
P	Pro	Proline
Q	Gln	Gluthamine
R	Arg	Arginine
S	Ser	Serine
T	Thr	Threonine
V	Val	Valine
W	Trp	Tryptophane
Y	Tyr	Tyrosine
Z	Glx	Glutamine or gluthaminic acid

1 Introduction

One of most interesting topics in photobiology is the detailed nature of interactions between chromophores and their protein environment. Specific problems will be addressed in studies of excited state decay mechanisms in fluorescent proteins, where the chromophore is formed auto-catalytically from amino acid residues and proteins, which contain oxidized flavin as cofactor.

Green and Red Fluorescent Proteins

The Green Fluorescent Protein (GFP) from the jellyfish *Aequorea victoria* has become one of the most widely studied and exploited proteins in biochemistry and cell biology. [Tsi98, Pal99] Due to its high fluorescence quantum yield [Mor74], GFP is utilized as a non-invasive marker of gene expression and protein targeting in intact cells and organisms. The wildtype exhibits two absorption maxima at 397 nm and 477 nm originating from the chromophore in its protonated state RH and its deprotonated state R^-. Both species lead to green fluorescence with slightly shifted maxima. The underlying mechanism of this phenomenon is an Excited State Proton Transfer (ESPT) occurring after excitation of the chromophore in its protonated state RH. In the spirit of this ESPT mechanism the slowing of the kinetics in deuterated samples has been studied at low temperatures in transient absorption experiments and has been utilized as a central argument for supporting ESPT. In order to perform low-temperature absorption measurements, good optical quality of the sample is absolutely necessary. For this purpose glycerol has been used as cryoprotector. Yet it has been shown, that glycerol affects strongly the sensitive ground-state equilibrium (equilibrium constant K≈1) between protonated and deprotonated state in GFP at room temperature as well as at 150 K. [Los96] Therefore the role

of changes in the hydrogen bonding network of the chromophore's binding site is not clear and the large deuterium effect may also reflect a change in the structure of the binding site induced by the glycerol component. Theoretical models, which are based on the assumption of only minor structural changes cannot explain the large isotope effect of a factor 3-5. [Cha96, Bub98]

A process competing with ESPT in GFP is thermally activated internal conversion (IC). In order to study in absorption measurements the influence of temperature on this process, leading to excited-state lifetimes in the picosecond range in some GFP-mutants, [Kum98,Kum00a], the consequences of a polymer matrix on the spectroscopic behavior of GFP will be tested **(Chapter 4.3)**.

If ESPT from the chromophore's hydroxy group is prevented, e.g. upon replacement of the tyrosine by a phenylalanine or a histidine, there is no green fluorescence. Instead blue fluorescence at ~450 nm is observed. However, the usefulness of such blue mutants is limited by their low fluorescence intensity and photobleaching, especially in the case of the single-site mutants. [Cub95, Hei94, Hei95] The origin of the of their low quantum yield will be studied in picosecond time-resolved fluorescence experiments the origin of the loss of fluorescence quantum yield in the single-site mutants Y66F and Y66H **(Chapter 4.4)**.

Another series of experiments relates to the photophysical properties of some Red Fluorescent Proteins (RFPs). Although blue and yellow GFP mutants already allowed for the simultaneous localization of two and more fusion proteins as well as Fluorescence Resonance Energy Transfer (FRET) experiments, [Tsi98] red fluorescent mutants could not be constructed. A novel class of RFPs has been isolated from corals. [Mat99, Luk00] These distant GFP homologues offer a dramatic extension of the spectral range.

The first RFP investigated closer in this context is a protein from the coral *Discosoma sp. 'Red'* drFP583 (DsRed), which fluoresces at 583 nm. The origin of this large red-shift of fluorescence compared with GFP is an additional oxidation step during chromophore formation. The resulting double bond extends the chromophoric π-system (Figure 1-1).

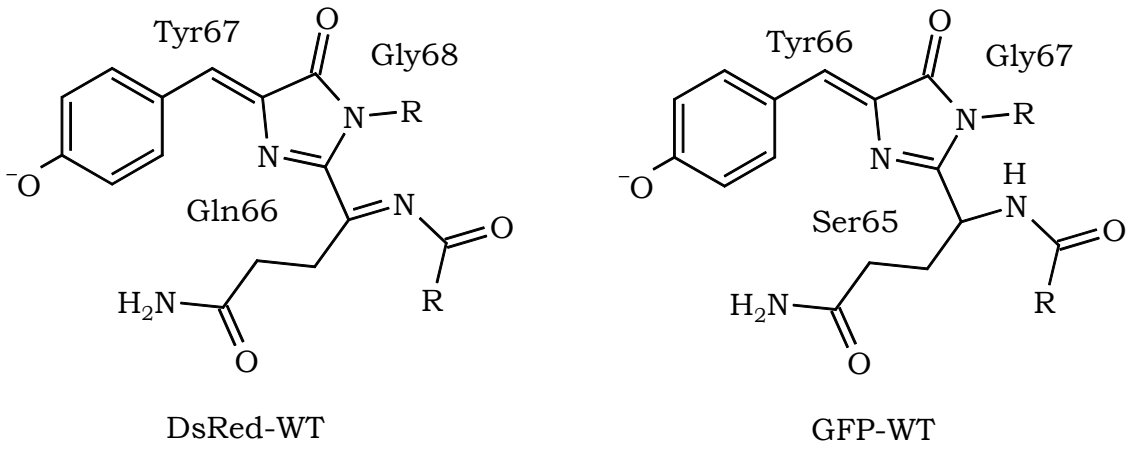

Figure 1-1: Chromophore of DsRed-WT and GFP-WT

However, for most applications in biotechnology DsRed-WT suffers from two major drawbacks: slow maturation from the green emitting precursor to the final red emitting chromophore and a strong tendency to form aggregates. [Bai00, Hei00, Gro00, Wie01] Most relevant in the context of the work presented here is the structure based conjecture of FRET from the π-electronic system of immature green emitting to mature red emitting chromophores. This conjecture is supported by a detailed characterization of FRET kinetics in picosecond time-resolved measurements **(Chapter 5)**.

The slow and incomplete maturation of the DsRed chromophore and its tendency for tetramerization triggered the search for better suited RFPs. A chromoprotein isolated from the sea anemone *Anemonia sulcata* (asFP595) shows a most interesting spectroscopic behavior. Its fluorescence is red-shifted 12 nm with respect to DsRed, but its quantum yield is extremely small (< 0.001). [Luk00] Surprisingly the

asFP595 wildtype protein becomes fluorescent upon irradiation. This Light Induced Fluorescence Enhancement (LIFE effect is reversible in the time range of seconds. [Luk00, Chu03] **Chapter 6** is dedicated its mechanism. Also here immobilization in a solid polymer matrix is necessary to minimize diffusion effects. Finally, the role of mutations in this chromoprotein on the fluorescence quantum yield has been studied.

Pathways of Excited-State Deactivation Competing With Fluorescence in Proteins Containing Flavin in its Oxidized Redox State

A wide range of phenomena in the life of plants including seed germination, pigment biosynthesis, stomatal opening, floral induction, circadian rhythms, and phototropism is initiated by sensoric photoreceptors [Bri99]. Depending on the spectral region, the photoactive cofactors may be bilins in phytochromes responding to red light [Fan99] and flavins in the blue light photoreceptors, i.e. the cryptochromes [Cas99,San00a] and phototropins [Hua97].

Intersystem Crossing. Phototropins bind Flavin MonoNucleotide (FMN) in two Light-, Oxygen-, and Voltage-sensitive domains, LOV1 and LOV2. Their absorption and fluorescence excitation spectra were found to be similar and to resemble closely the action spectrum of phototropin. [Sal00] The fingerprint for the sensoric function in this class of blue photoreceptors is the dramatic bleaching under high excitation intensity. Comparison of the absorption spectra of the LOV domains under bleaching conditions and of mercuric ion reductase [Mil90] led to the conclusion that the transient product state is a flavin carbon C(4a)-thiol adduct, which is reached from the triplet state of LOV2. Triplet formation may in principle proceed via two different mechanisms: singlet-triplet Inter System Crossing (ISC) and singlet-triplet spin-

conversion in a primary radical pair induced by hyperfine interaction [Mic79, Vol99]. In the past the transient triplet state of the LOV2 domain has been studied on time scales longer than 30 ns, [Swa02] and more recently, while this work was in progress, with femtosecond time resolution. [Ken03] The conclusions of these most recent investigations of LOV2-WT from *Adiantum capillus-veneris* phy3 and *Avena sativa* Phot1 are based on a comparison of the primary photodynamics of the LOV2-WT protein and FMN free in aqueous solution. The goal of this work is the investigation of the photophysical primary processes in LOV2-WT from *Avena sativa* Phot1 and the single-site mutant C39A, where cysteine has been replaced by alanine, in fs- to ps- time-resolved absorption and fluorescence spectroscopy. In contrast to the approach of Kennis et al. we performed a comparative study in similar chromophore surroundings **(Chapter 7)**.

Excitation energy transfer in (6-4) photolyase and cryptochrome 2. Cyclobutane Pyrimidine Dimer (CPD) and pyrimidine-pyrimidone (6-4) photoproduct are light-induced (by UV light) lesions in the DNA duplex. Each of these lesions is repaired specifically by a special photolyase enzyme. While CPD-photolyase was subject to a great number of published reports, only little is known about the structure and the reaction mechanism of (6-4) photolyase. Here, we report for the first time the evidence for excitation energy transfer in *Xenopus laevis* (6-4) photolyase from a second chromophore functioning as a photoantenna, to the flavin cofactor by Förster dipole-dipole interaction **(Chapter 8)**, derived from steady-state and time-resolved fluorescence measurements.

Cryptochromes are sensoric protein systems, widespread in nature, [San03], which exhibit high sequence homology to photolyases. [Ahm93, Lin95, Cas99] Despite this similarity to photolyase, they do not show any signs of DNA repair activity. [Hsu96] Instead they function as photoreceptors in circadian rhythms and regulate some of

the blue-light responses in plants. They also contain both an antenna pigment and a flavin in its oxidized state as cofactors. [Mal95] In **Chapter 9** we investigate a human cryptochrome 2 still containing its antenna pigment and establish energy transfer from the antenna to the flavin cofactor as main deactivation channel. As a reference system we examined cryptochrome1 from *Arabidopsis thaliana*. As this protein should have lost its antenna during the purification procedure, the fluorescence lifetime of the flavin cofactor is indicative of the primary photophysics of this sensoric protein.

2 Experimental

In this section the methods are described, which were used to achieve the results presented in this work. Common in all methods is the continuous-flow cryostat (Leybold VSK 3-300) cooled with liquid nitrogen, in which cuvette was placed to perform low-temperature experiments.

2.1 Steady-State Spectroscopy

Steady-state absorption and fluorescence spectra are measured in order to characterize new samples, test their optical quality and to trace damage of the proteins caused by the high-intensity excitation light of the time-resolved fluorescence and transient absorption measurement setups.

2.1.1 Absorption measurements

Absorption spectra were recorded alternatively with a Perkin-Elmer Lamda 2S or a Varian Cary BIO100 UV-VIS spectrometer. Both have 2.0 nm resolution or better.

2.1.2 Fluorescence measurements

Fluorescence spectra were measured using a spectrofluorometer (Spex Fluorolog-2 Model F212I) with a typical resolution of 1.7 nm or better. Fluorescence was collected in Front Face geometry. The entrance/exit slits of the monochromators were adjusted to the fluorescence intensity of each sample.

2.2 Picosecond Time-Resolved Fluorescence Measurements

Time-resolved fluorescence measurements were carried out with an apparatus as shown in Figure 2-1, based on [Pöl93, Los98, Kum00]. In this setup two different excitation light sources were used, i.e. either a Ti:Sapphire laser (Coherent MIRA) providing a 100 fs pulse in combination with a pulse picker or a dye laser (Satori 702-CD1) for picosecond excitation pulses. The fluorescence decay kinetics can be observed by two detection methods. The Time-Correlated Single Photon Counting setup (TCSPC) provides a time resolution of ~10 ps. For faster decay dynamics a streak camera was used, with a resolution of ~3 ps.

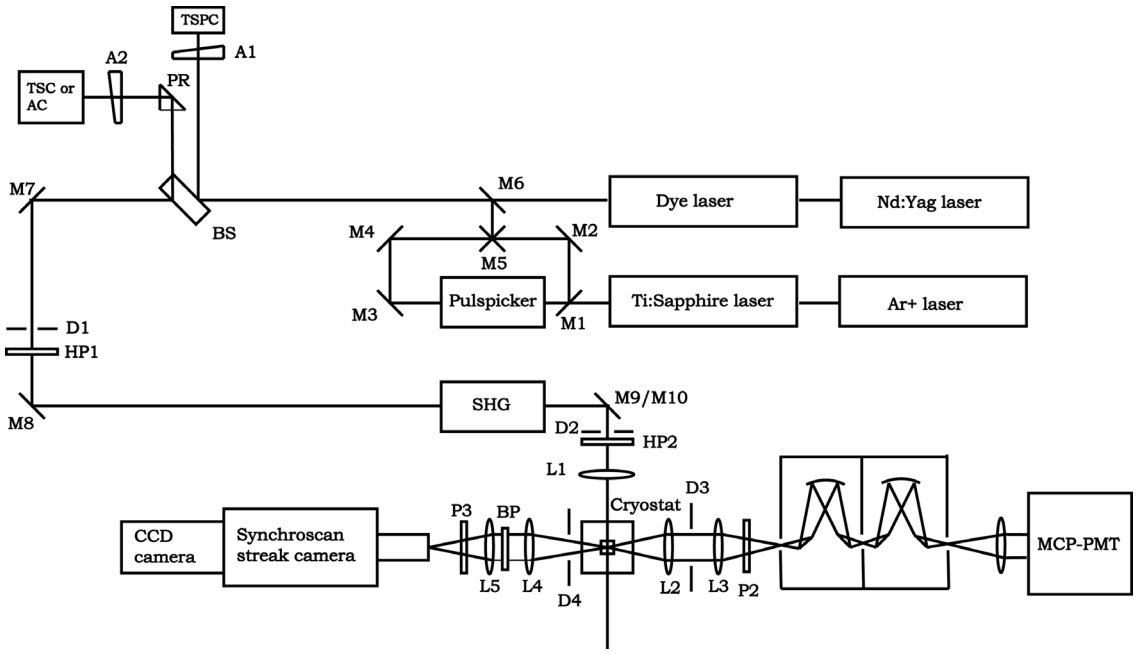

Figure 2-1: Apparatus for time-resolved fluorescence measurements

M = Mirror, BS = Beam Splitter, At = Attenuator, P = Polarizer, HP = λ/2 plate, T-SPC = Trigger diode for TCSPC, T-SC = Trigger diode for Streak Camera, AC = AutoCorrelator, L = Lens, D = Diaphragm, SHG = Second Harmonic Generation, MCP-PMT = MicroChannel Plate PhotoMultiplier Tube, BP = BandPass filter

All data are measured under magic angle conditions (54°) not to fudge the results by rotational depolarization. Using standard deconvolution procedures, average lifetimes shorter than the Full Width Half

Maximum (FWHM) of the instrument response function (6 ps in case of the streak camera, 25 ps in case of TCSPC) are considered to have an ambiguity of a factor of 2, all other lifetimes carry an approximate error of ~20%.

2.2.1 Fs-pulse excitation

Excitation at high repetition rate. The excitation light used in most measurements of this work is provided by the frequency-doubled output of a Ti:Sapphire laser (Coherent MIRA), pumped by an Ar^+ laser [Coherent Innova 310].

By actively stabilizing the Ar^+ laser (Power Track, Light Track) the noise caused by instability of amplitudes is below 0.5 % over 30 min. The emerging beam is vertically polarized with a ratio of 100:1 and has a diameter of 1.9 mm with a divergence of 0.4 mrad.

After entering the linear, multi-folded cavity of the MIRA the pump beam is focused into the crystal, which is thermally stabilized at 14°C. The emission of the gain medium is collimated by two concave mirrors before it traverses a Lyot-filter (birefringent filter) for tuning the wavelength (600 nm-1100 nm). In our setup only two mirror sets are employed, the so called short-wave (700 nm-820 nm) and midwave (785 nm–925 nm) mirror sets. Hence the tuning range of the laser system is limited by the reflection range of these mirrors. In the Continuous Waves modus (CW modus) the power output of the MIRA reaches 1.2 W. Short pulses are produced in this laser by passive mode-locking, which is achieved by the optical Kerr effect in the Ti:Sapphire crystal. Kerr lensing causes the material to alter its refractive index at very high light intensities, making it transparent. Mode-locking is started when some wave modes are in resonance and the light intensity of the wave peak is high enough to cause formation of the Kerr lens. Furthermore, Kerr lensing not only produces short pulses, but also causes collimation of the pulsed beam. As the light beam is narrowed it

can pass a slit placed directly in front of the output coupler uninterrupted, whereas the large diameter laser beam associated with continuous operation will be chipped at its edges and therefore be suppressed very effectively. Finally, the resulting pulses are restricted to ~100 fs duration with a maximal peak power of 12 nJ by an integrated chirp compensation consisting of two quartz prisms. Due to the resonator length the repetition rate is 75.9 MHz.

Elongation of the Time Window by a Pulse Picker. The time window between two pulses of 13.2 ns (repetition rate 75.9 MHz) is too short to determine lifetimes longer than 2 ns reliably. Thus the system is extended by a pulse picker (Coherent Model 9200) which can be optionally included into the light path.

The 10 cm input focus mirror directs the incoming collimated MIRA beam onto a high speed acousto-optic modulator. This Bragg cell consists of a TeO_2 plate, cut at Brewster's angle and matched to an acousto-optic transducer. The controller electronics supplies a sufficiently short RF pulse for creation of an acoustic wave in the crystal, producing density variations within the material. These density variations act like parallel planes having different indices of refraction. In this way it is possible to diffract a single pulse out of a 76 MHz pulse train with an efficiency of more than 60 % and a contrast ratio better than 500:1. The controller works at an internal repetition rate of 380 MHz. It uses the output from the MIRA's fast photodiode as input signal for synchronization to the laser. By integer division of the fundamental 38 MHz repetition rate of the pulse picker by a factor between 8 and 520 pulses at variable repetition rates can be produced, generating repetition rates from 9.5 MHz to 146 KHz.

2.2.2 Ps-pulse excitation

Alternatively to the Ti:Sapphire laser a dye laser (Satori 702-1CD), equipped with a cavity dumper (Coherent, Model 7220) can be used for

exciting the samples. This laser is pumped by an actively mode-locked Nd:YAG laser (Coherent Antares 76S).

The 9 cm long Nd:YAG rod is symmetrically pumped by dual krypton arc lamps and emission extrudes through its cut ends into the single folded cavity. A Brewster window forces vertical polarization of the circulating pulse. Mode-locking is achieved by an acousto-optic modulator placed in the cavity. The modulator forces phase coupling of longitudinal modes establishing in this way a pulse train with a pulse duration of ~100 ps and a repetition rate of 75.9 MHz. The power output of the IR beam is ~20 W as specified. After passing the output coupler, the IR beam (1064 nm) is frequency doubled in a KTP crystal integrated in the laser housing. The resulting green (532 nm) light beam has ~2 W power. Before leaving the laser housing, the green light passes a Polarization Rotation and Discrimination Device (PROD). This combination of three dichroitic mirrors not only separates the green beam from the residual IR light, but also turns its polarization back to vertical. The polarization of the beam leaving the Second Harmonic Generation (SHG) is 45° with respect to the vertical polarization of the YAG cavity. The signal to noise ratio of the frequency doubled YAG beam is with 8 % twice as high as that of the IR beam (4 %) caused by the non-linearity of the frequency doubling process. The noise is determined by the AC:DC ratio, measured with an IR photodiode, placed behind the high reflecting output coupler. It consists mainly of two components: i) a high frequent part (>1 KHz) which has its origin in the power supplies etc. but with a very low amplitude of <1 %, and ii) the low frequent part (<10 Hz) with an amplitude of ~4 %. The latter is caused by beam pointing (spatial walking of the beam in the cavity) as well as vibrations of the resonator mechanics. Additionally thermal lensing can be produced by inhomogeneous pumping of the YAG rod, which fluctuates with low frequency. Optically beam movement of more than 10 % of the beam diameter can be observed leading to amplitude noise caused by the change of the beam path.

The frequency doubled output of the Nd:YAG laser is used for pumping a dye laser (Satori 701-1CD). Its linear cavity is folded into a vertical Z-direction and is equipped with a cavity dumper instead of the original output coupler. The liquid dye is inserted into the cavity as a free-standing jet stream oriented in Brewster's angle for low loss. The dye, Rhodamine 6G (570 nm-600 nm) in the case of the measurements done in this work is solved in 50 ml methanol and added to ~1 l ethylene glycol. The concentration is adjusted to be 80 % absorption by monitoring the pumping light transmitted through the jet. Pulse amplification occurs by the synchronous pumping of the dye laser. By the pump pulse the lasing medium is converted into the excited state while the dye pulse arriving shortly afterwards causes depopulation of the dye molecules by stimulated emission and is in this way amplified. The leading edge of the dye pulse is amplified more than the trailing edge. This causes a shortening of the pulse after some circulations. For achieving synchronous pumping it is important, that the cavity length of the dye laser matches exactly the cavity length of the pump laser. The laser provides the possibility of inducing a second dye jet as saturable absorber for reducing the pulse width to ~1 ps, but as long excitation pulses were needed, the saturable absorber is not employed. The pulse width (10 ps in our case) is constantly monitored with an autocorrelator (Femtochrom FR 103). The noise of the dye laser is mainly due to instabilities of the pump laser and is typically <15 %.

The cavity dumper works in principle like the external pulse picker. As it is included into the cavity it not only provides selectable repetition rates but increases at the same time the power output level of the system. The cavity dumper driver provides a RF pulse to a Bragg cell at a basic repetition rate of 38 MHz. The light pulse circulating in the resonator has to arrive in time with the RF pulse. Then it is deflected in the sonic field of the Bragg cell and afterwards separated from the resonator beam by a quartz prism. By dividing the basic rate of 38 MHz

by an integer factor of 4 to 259, the repetition rate can be easily changed. In this work it was adjusted to be either 3.8 MHz or 0.38 MHz.

2.2.3 The time-correlated single photon counting method

For measuring picosecond to nanosecond fluorescence kinetics a Time-Correlated Single-Photon Counting setup (TCSPC) was used as described in [Los96]. In principle TCSPC means measuring the time between the excitation of the sample and the consecutive emission of a single photon. The fluorescence signal is attenuated, that typically only one photon per 100 excitation pulses is detected. Accumulation of a manifold of such measurements yields a histogram depicting the time dependence of the fluorescence of the sample.

The wavelength of the photons to be detected is selected with a subtractive double monochromator (2 x Jobin Yvon H10). The signal of the detector, a high speed MicroChannel Plate PhotoMultiplier Tube (MCP-PMT, Hamamatsu R2809U-07) cooled to –30°C to reduce noise, is fed to a pre-amplifier (Nucleotudes S.C.D. 60.20.1) and then converted to a NIM pulse utilizing a Constant Fraction Timing Discriminator (CFTD, Tennelec TC455). The resulting almost jitter-free signal starts a Time-to-Amplitude Converter (TAC, Ortec 567)- the picosecond stop watch. In parallel, a small fraction of the excitation light is used to generate a constant sequence of stop pulses (BS, TSPC, CFTD, Delay). This inverted mode (the subsequent excitation pulse serves as a timing reference) drastically reduces the TAC's dead time while it is possible to maintain the high repetition rates of the laser system. The TAC's amplitude output is stored digitally in a multichannel buffer (Ortec 918). Finally, a multichannel analyzer software (EG&G Ortec MAESTRO) displays and saves the results on a PC. The Instrument Response Function (IRF) of the TCSPC setup is typically in the range of 23 ps to 29 ps and does not depend on the excitation source.

2.2.4 The streak camera method

For detection of fluorescence kinetics affording a time resolution better than 25 ps the emission light was launched into a synchroscan streak camera (Hamamatsu C1578). [Kum98] The principle of operation is a conversion of temporal information to a spatial coordinate.

The fluorescence light of the sample is collected and focused into the horizontal entrance slit of the streak camera. A 10 nm bandpass filter is used to select the detection wavelength. By the input optics the slit image is formed on the photo cathode plane of the streak tube, where it is converted into an electronic image. After being accelerated in a static electric field (Voltage U_b) the electrons enter the deflecting field. A high-speed ramp voltage (U_s) is applied to the deflecting plates to sweep the electron image in the vertical direction.

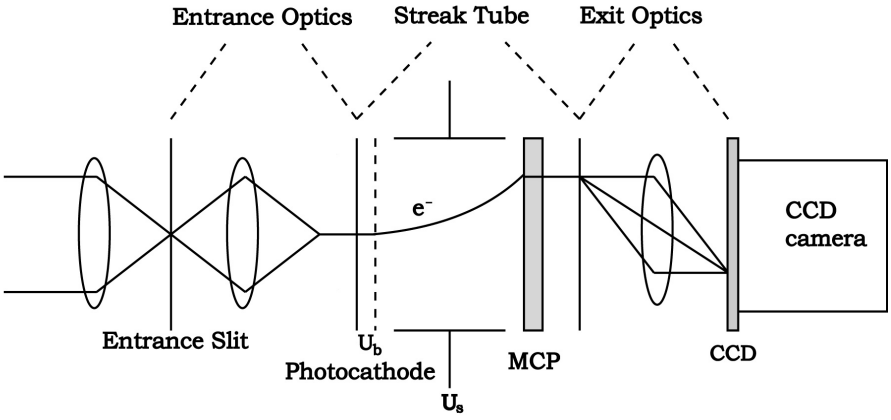

Figure 2-2: Scheme of the streak camera

In the so-called synchroscan mode used in this work the sweep is synchronized with the excitation light pulses by an external trigger signal (TSC). The swept electron image is projected onto a Microchannel Plate, amplified electronically and then applied to the phosphor screen where it is converted to light again. Formed by the output optics on the light-sensitive surface of the CCD camera (Hamamatsu C3140) the image of the phosphor screen is saved on a chip (integration time is

typically 100 s). Transmitted to a PC consecutive images (510 x 492 pixels) are be summed up to yield an overall measuring period of up to 800 s. This integration period is limited by slow drift of the sweep/trigger synchronization. Are long measuring periods necessary, the single images can be stored on the PC hard disk and summarized half-automatically afterwards. In this procedure the images can be shifted, so that rising edge of the measurement signal is overlaid and in this way the walk of the excitation/trigger synchronization can be suppressed.

Since long-lived components of the fluorescence signal are still contributing to the image when the sweep voltage has declined, another synchronized voltage (phase-shifted by 90°) is applied to deflection plates perpendicular to the ramp voltage plates. This so-called synchronous blanking causes the return path to be horizontally translated in the image. The acquired image has to be corrected for the background signal (requiring a measurement with otherwise unchanged conditions but blocked excitation light) and the non-uniform sensitivity of the MCP channels (shading correction). In Figure 2-3 such a streak image is shown. The signal intensity is encoded by different colors, to the right the long fluorescence components are visible as the dark blue back trace.

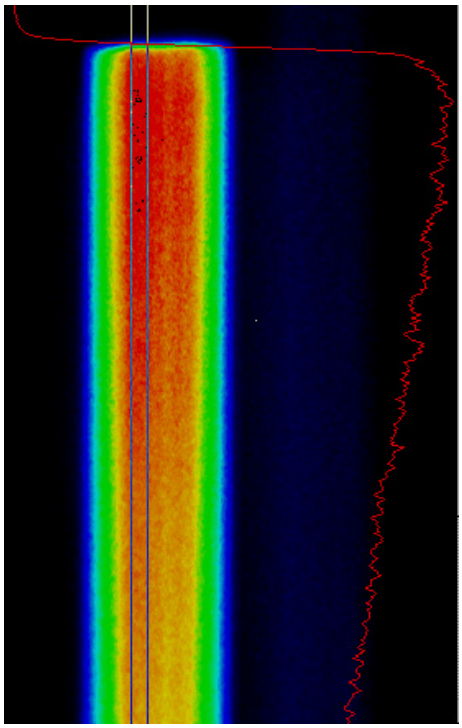

Figure 2-3: Picture of a streak measurement

A vertical strip of the corrected image with a width between 10 and 30 pixels, depending on the signal intensity is used to extract a profile (red line, Figure 2-3) for further analysis.

With this system it is possible to achieve FWHM of the IRF of 6 ps in the fastest time regime (0.88 ps per channel), the corresponding time window being 450 ps. The signal to noise ratio is better than 500:1.

2.2.5 Numerical analysis of the measurements

The goal of the numerical analysis is to describe the fluorescence kinetics measured in TCSPC or with the streak camera by an analytical function, which depends on statistical and systematical perturbations. In the cases relevant here, the profiles derived from the measurements Y(t) are in principle a convolution of the intrinsic fluorescence kinetics f(t) of the sample and the instrument response function IRF(t).

$$Y(t) = \int_{-\infty}^{+\infty} IRF(t') \cdot f(t - t')dt' \qquad (2\text{-}1)$$

The profiles Y(t) include further statistical noise, remains of the background signal and long-lived components of the fluorescence excited by the previous laser pulse. The IRF itself is a convolution of the actual excitation light pulse and the response of the apparatus to excitation. In practice it is determined by replacing the sample by a scattering solution (Ludox, Fa. Aldrich) simulating a fluorophore with a lifetime of 0 ps and measuring the response of the whole system to the excitation pulse.

In this work deconvolution of the measured profiles was carried out with the programs FAPGNU and GNUAP [Hae95] based on the algorithm for non-linear least squares fits developed by Marquardt [Mar63, Pre92]. In this method the parameters of a defined theoretical test function are changed iteratively until the sum of the square deviation, weighted with the error of measurement between measured decay and the theoretical test function is minimized. The convolution integral is estimated numerically. The criterion to be minimized is given by

$$X^2 = \sum_{i=1}^{N} \left\{ \frac{Y_i - F(t_i)}{\sigma_i} \right\}^2 \qquad (2\text{-}2)$$

where N is the number of data points in the profile, Y_i the i^{th} data point, σ_i its statistical error and $F(t_i)$ the theoretical test function. [Bev92] F(t) can be written as the sum of three terms:

i) a constant background signal O, which is due to environmental stray light and the dark count rate of the detection electronics;

ii) an exponential term for the long-lived fluorescence components left over from the excitation by the previous laser pulse $A_i e^{-t/\tau_j}$;

iii) the convolution of the IRF I(t) and the model function f(t) used to describe the fluorescence kinetics of the sample:

$$F(t) = O + A_i e^{-t/\tau_j} + \int_{-\infty}^{\infty} I(t')f(t-t')dt' \qquad (2\text{-}3)$$

In general, f(t) has to be derived from the applied physical model, in case of fluorescent species it is commonly written as a sum of exponential terms: $f(t) = \sum_i A_i e^{-t/\tau_i}$ with the amplitudes A_i and the time constants τ_i. In case of a decay component is $A_i > 0$. For $A_i < 0$ it represents a rise component. However, one should keep in mind that other sets of functions could exist that might fit the profiles equally well.

Three criteria are employed to evaluate the quality of the fit results:

i) the reduced $X_r^2 = \frac{X^2}{(N - n_p)}$, which represents X^2 (Equation 2-2), normalized by the difference between the number of data points N and the number of free parameters n_p. X_r^2 should be close to unity, i. e. the

mean squared deviation of the data points from the test function is close to the statistical error.

ii) the weighted residuals $R_i = \frac{(Y_i - (F(T_i))}{\sigma_i}$ should be distributed statistically about zero with an amplitude of less than 4.

iii) the autocorrelation function $C_j = \frac{\sum_{j=1}^{N/2} R_j \cdot R_{j-i}}{1/N \sum_{j=1}^{N} R_j^2}$ of the weighted residuals enhances correlated deviations in the residuals and should also be distributed statistically about zero.

2.3 Femtosecond Transient Absorption Measurements

Transient absorption measurements were performed using a Ti:Sapphire oscillator/regenerative amplifier system which has been described in detail in [Pöl96]. Briefly, the output at 780 nm of an Ar^+ laser pumped commercial Ti:Sapphire oscillator (MIRA/Coherent, repetition rate 76 MHz, pulse width 100 fs) was temporarily broadened to 150 ps before seeding a regenerative amplifier system (BMI Alpha 1000 S) pumped at 10 W by a Nd:YLF laser (BMI 621D) at 526 nm. The amplified pulses (1.4 mJ) were split into pump and probe beam (9:1). After separate recompression optical pulses at 780 nm with a pulse duration of 120 fs were obtained. The more intense pulses were frequency-doubled and directed through an OPG/OPA setup to produce a signal wave tunable from 450 nm to >1000 nm for excitation. The weaker probing pulses were sent to a variable delay line two times allowing a total delay between pump and probe pulses of 10 ns with increments of 66 fs before they were focused in a 2 mm sapphire crystal to produce a white light continuum. By means of a chirp-compensated, stepper motor controlled spectrometer, a spectral regions with a bandwidth of 12 nm was selected from this continuum. The relative

polarizations between pump and probe beam were set to the magic angle to avoid rotational depolarization effects. Pump and probe beams were focused under an angle of 8° at a 2 mm fused silica cuvette containing the sample.

3 Theory

After excitation of a molecule into a higher electronic state it has different possibilities to loose its energy and relax back to the electronic ground state. Besides the radiationless internal conversion between states of the same multiplicity and fluorescence it can convert via intersystem crossing into the triplet state and afterwards emit phosphorescence. These latter processes are considerably slower than IC and fluorescence, as spin conversion is forbidden. If a partner is present, the excited molecule can transfer its excitation energy, an electron or a proton, either intra-molecular or intermolecular to a molecule nearby. In this chapter the different processes are shortly introduced.

3.1 Energy Transfer

For Excitation Energy Transfer (EET) two mechanisms can be discussed. [Gro85, Spe96] The Förster [För59, För65] and the Dexter [Dex53, Raz80] mechanism differ in the strength of pigment coupling and distance dependence.

3.1.1 The Förster energy transfer

EET in weakly coupled pigments can be described by the Förster mechanism. Here the Donor (D) and Acceptor (A) are seen as vibrating dipoles. The field produced by the vibration of the donor pigment forces the acceptor into a resonant motion. The transfer rate k_{EET} is proportional to the oscillator strength of D and A as well as to the spectral overlap of the fluorescence emission $F_D(\nu)$ of D and the absorption of A. The dipole-dipole distance R contributes with $1/R^6$.

$$k_{EET} = \frac{C}{\tau_{F,D} R^6} \int_{\nu} \frac{\varepsilon_A(\nu) \cdot F_D(\nu)}{\nu^4} \, d\nu \tag{3-1}$$

$\tau_{F,D}$ represents the fluorescence lifetime of the initial state and contains therefore the oscillator strength of the dipole-dipole transition. The oscillator strength of the acceptor is given by the extinction coefficient $\varepsilon_A(\nu)$. F_D represents the normalized fluorescence spectrum.

$$C = \left(\frac{9000 \cdot \kappa^2 \cdot c^4 \cdot \ln 10}{128 \cdot \pi^5 \cdot n^4 \cdot N_A} \right) \tag{3-2}$$

In the factor C is c the speed of light, n the refraction index and N_A is Avogadro's constant. The orientational factor of both dipoles κ has a value between 0 and 4. For isotropic distributions of D and A is $\kappa^2 = 2/3$. Although EET between the antenna complexes in photosynthesis can be described very well by Förster theory, [Gro85, Gro94] problems arise in the description of ultrafast processes. The fastest rates applicable by the Förster theory are 1/(2 ps). [Jea88]

3.1.2 The Dexter energy transfer

If the wave functions of donor and acceptor pigments overlap, description of EET via electron exchange is possible. In this model the oscillator strength of the involved transitions can be disregarded, because only the normalized absorption and fluorescence spectra participate in the transfer rate:

$$k_{EET}^{ex} = \frac{2\pi}{\hbar} \cdot U^2 \int_{\nu} F_D(\nu) \cdot E_A(\nu) \cdot d\nu \cdot \tag{3-3}$$

The rate is highly distance dependent because the exchange interaction U decreases exponentially with distance. The absolute value of the oscillator strength of D and A does not contribute to the transfer rate due to normalization.

While in the Förster mechanism strong fluorescence and absorption bands are essential for fast EET, in the Dexter mechanism small oscillator strengths are sufficient, but the distance between donor and acceptor must be very short. In both mechanisms the fluorescence band of the donor and the absorption band of the acceptor must overlap to obey the law of energy conservation.

3.2 Electron Transfer

One of the most important elementary reactions in chemistry and biological systems is the Electron Transfer (ET). More detailed description can be found in the literature. [Mar56, Lev66, Duy74, Jor76, Mar85, Jor99] Most ET systems in non-viscous solvents can be described by the non-adiabatic theory.

3.2.1 The non-adiabatic electron transfer

In case of weak electronic coupling ET is described as a non-adiabatic transfer in a super molecule consisting of the electron Donor (D), the Acceptor (A) and the surrounding medium. The system can be described by a non-charge separated state (D*A) and a charge separated state (D^+A^-). For the description of charge separation in this super molecule the Born-Oppenheimer-approximation is applied. It is assumed that the nuclei move very slow due to their much larger mass than the electrons do. In this case the nucleic wave function can be separated from the electronic wave function. Additionally it is assumed that the electrons can adapt instantaneously to changes in the configuration of the nuclei and the electronic transition takes place at nearly unchanged nucleic coordinates (Condon approximation). For the transition an electron of the donor interacts with the nucleic potential of the acceptor (*one electron two-center exchange interaction*).

Important for ET are only the electronic coupling V and the overlap of the nucleic wave functions. Depending on the magnitude of V, which links each vibronic niveau of the initial state to a diversity of charge-separated product states, two cases can be distinguished:

i) If the interaction is large the potential surfaces of the transitional area are disturbed so strongly, that an adiabatic transition between initial and product state occurs without explicit change of the potential surface.

ii) If the interaction is small, the states (D*A) und ($D+A^-$) are not mixed. The transition occurs only after passing the crossing sector of their potential surfaces several times. In this case of non-adiabatic ET the transition probability is proportional to V^2.

Due to vibronic excitation ET does not occur from a single state. During excitation more nucleic vibronic states are populated, so the product state has to be treated as a diversity of states. In this diversity relaxation takes place on a typical time scale of 100 fs to few ps. If it is assumed that this relaxation is fast compared to ET, the macroscopic ET rate k is given by the averaging of microscopic rates, derived from Fermi's golden rule, weighted with the thermal population of the excited states ρ_ν. It can be written as:

$$k = \frac{2\pi}{\hbar}|V|^2 \, FC \tag{3-4}$$

with the thermal averaged Franck-Condon-Factor (FC):

$$FC = \sum_{\nu}\sum_{\omega} \rho_\nu \left|\langle \chi_{a\nu} \,|\, \chi_{b\omega} \rangle\right|^2 \delta(E_{b\omega} - E_{a\nu}) \tag{3-5}$$

The delta function guarantees energy conservation of initial and product states with the energies $E_{a\nu}$ and $E_{b\omega}$. $X_{a\nu}$ and $X_{b\omega}$ are the nucleic wave functions of the initial and product state, ν and ω are two sets if vibronic quantum numbers.

3.2.2 The Franck-Condon factor

The Franck-Condon factor describes the reaction of the nucleic configuration to ET in the non-adiabatic borderline case. It contains the position of equilibrium changed by the reaction and the altered vibronic modes of the whole system (including the reaction of the surrounding medium).

Single-mode approximation. In the single-mode approximation all vibronic modes of the initial state (D*A) and the charge separated state (D^+A^-) are combined to a single mode with average frequency ω. The multi dimensional potential surfaces of both states are reduced to one dimension and can be approximated by harmonic oscillators. The difference of the free enthalpy at the potential minimum for both states has the value of ΔG. In exothermal reactions is ΔG negative. The energy necessary to reach equilibrium position is called reorganization energy.

Due to the Franck-Condon principle ET occurs at fixed nucleic coordinates (vertical transition). During the radiationless transition energy is preserved (horizontal transition). The only point where both conditions for an electronic transition hold, is the crossing point of the parables. The activation barrier can be written as:

$$E_A = \frac{(\Delta G + \lambda)^2}{4\lambda} \tag{3-6}$$

For low temperatures ($k_BT << \hbar\omega$) the Franck-Condon factor describes a temperature independent tunneling process from the lowest vibronic niveau of the initial state (D*A) into the isoenergetic vibronic niveau of the charge separated state (D^+A^-). For high temperatures ($k_BT >> \hbar\omega$) the Franck-Condon Factor corresponds to classical Arrhenius behavior with the activation energy $E_A = (\Delta G-\lambda)^2/4\lambda$. The transition energy between these two borderline cases is in the range of $k_BT \approx \hbar\omega/4$. [Jor80] Typical vibronic frequencies $\hbar\omega$ in proteins have values in the range of 100 cm^{-1}

to 300 cm^{-1} and are equivalent to transition temperatures of 35 K to 100 K.

In case of the high temperature approximation different areas with different temperature and energy dependence of the rates can be distinguished, depending on the position of the potential curves of donor and acceptor (Figure 3-1).

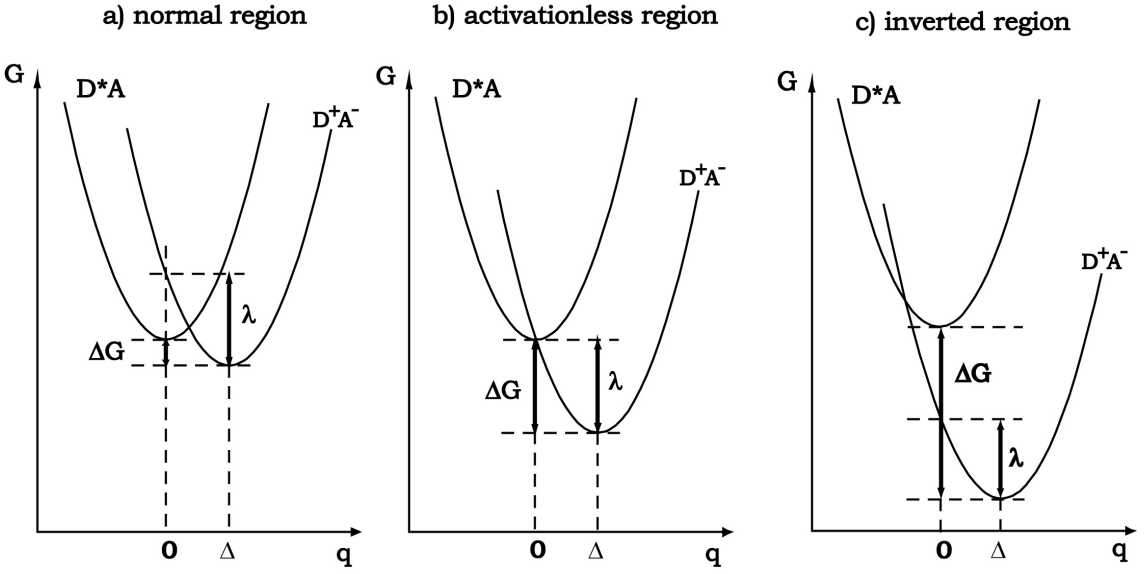

Figure 3-1: Scheme of relative positions of the nucleic potential surfaces for different values of the driving force ΔG and reorganization energy λ.

a) Normal region, $-\Delta G < \lambda$:

The ET rate shows activated behavior. It increases with increasing temperature and growing absolute value of ΔG.

b) Activationless region, $-\Delta G \approx \lambda$:

The activation energy is nearly zero and rates become maximal. The transition rate is in the high temperature case proportional to $1/\sqrt{T}$ so it increases with falling temperature.

c) Inverted region, $-\Delta G > \lambda$:

The ET rate decreases with growing absolute value of ΔG. For the single-mode approximation the temperature dependence is the same as in the

normal region. For the multi-mode approximation where further high energetic modes are added, discussed in the following section, the temperature dependence is much weaker.

Multi-mode approximation. The vibronic spectrum of complex molecules can not be represented properly by the single-mode approximation. The multi-mode approximation allows for an additional averaged high energetic vibronic mode besides an averaged low frequency mode. Now n^{th} vibronic states of the high energy mode are possible ET product states. The corresponding free enthalpy ΔG increases by $n\hbar\omega$ compared to ET into the lowest vibronic state.

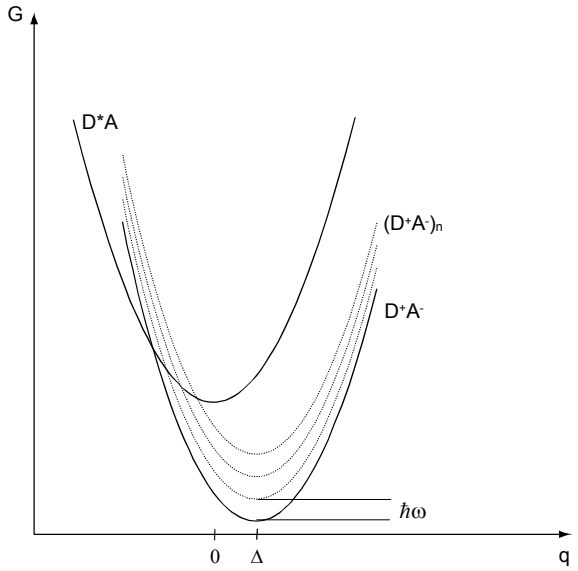

Figure 3-2: Coupling of a high energetic mode to ET in the inverted region.

The Franck-Condon factor for the high energy case in this model [Jor76] contains the reorganization energy of the surrounding environment, intra-molecular vibrations with higher energies and the electron-phonon coupling of the high frequency mode.

In the normal and the activationless region the activation energy for transitions into excited vibronic levels is higher than for transitions into the vibronic ground state. Thus the ET rates do hardly depend on

coupling of modes with high frequency. Therefore times are comparable in multi-mode and single-mode approximation. In the inverted region (Figure 3-2) transitions into excited vibronic states can have a lowered activation barrier. Transition rates are therefore accelerated in comparison to the single-mode approximation and are less dependent on ΔG. As a consequence the temperature dependence is much smaller.

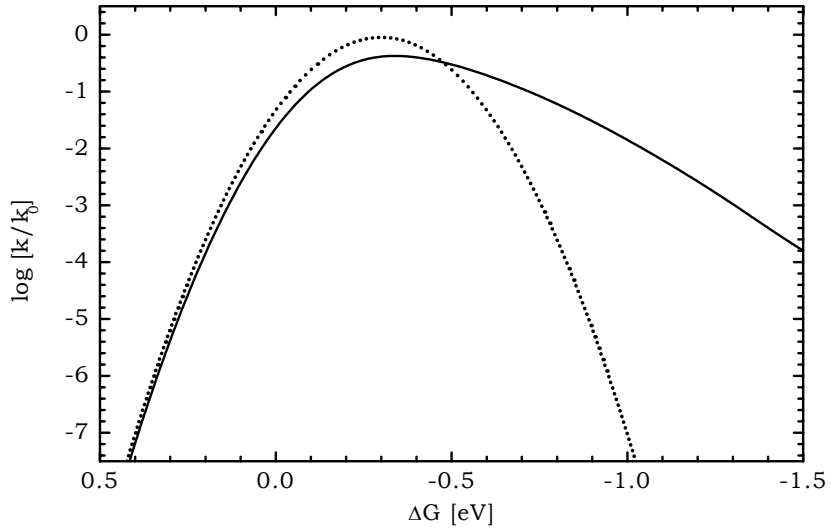

Figure 3-3: Dependency of the ET rate *k* on the driving force ΔG

In the single-mode approximation (···) and multi-mode approximation (–)

3.2.3 Electronic coupling

The electronic coupling is defined by the overlap of the nucleic wave functions of initial and product state

Direct coupling. If the distance between donor and acceptor is large, only foothills of the wave functions contribute to the overlap integral, which depends on the orientation of the pigments. The value of this overlap integral can be reduced by thermal expansion of the wave function. [Jor80] On the other hand possible reorientation of the molecules at higher temperatures can enlarge the electronic coupling. Its matrix element can be described by exponential dependence on the distance. [Mar85] It contains an attenuation parameter, which is constant

and has to be determined by experiments. Its value for proteins is between 0.9 $Å^{-1}$ and1.5 $Å^{-1}$. [Mut76, Win92, Pag99]

Coupling via Superexchange. If another molecule (S) is located between donor and acceptor the electronic coupling between the states D*A and D^+A^- can be considerably enlarged via superexchange. [Hei85, Bix89] In this mechanism virtual states of S are mixed with states of initial and product state. The intermediate state can either be characterized by (D^+S^-A) or (DS^+A^-). Thus even high energy levels can contribute to the exchange interaction. δE_S represents the vertical energy gap between the potential surface of S and the crossing point of the potential surfaces of A and D (transition point). it contributes to the electronic coupling by $1/\delta E_S$. The contribution of superexchange can surpass direct coupling by far, if S was spatially located between A and D.

3.2.4 The driving force of electron transfer reactions

The driving force of ET reactions can by calculated by the Rehm-Weller equation (Equation 3-7). This equation contains the overall electronic excitation energy E_{00} and the electrochemical potentials of the ET partners. [Wel82] In case of charge separation the electrostatic attraction of the radical pair has to be taken into account. The driving force of the charge separation step (Forward Electron Transfer) is given by:

$$\Delta G_{FET} = E^0[D/D^{+*}] - E^0[A/A^{-*}] - E_{00} - E_{Coulomb} \qquad (3\text{-}7)$$

The coulomb term $E_{Coulomb}$ contains the distance R between donor and acceptor and the dielectric constant ε of the surrounding medium and reduces the remaining driving force:

$$E_{Coulomb} = \frac{q^2}{4\pi\varepsilon_0 \varepsilon R\, 1{,}602 \cdot 10^{-19}} \qquad (3\text{-}8)$$

The driving force of the charge recombination (Back Electron Transfer) can be written as:

$$\Delta G_{BET} = E_{00} - \Delta G_{FET} \tag{3-9}$$

The overall electronic excitation energy E_{00} for the transition from the electronic ground state S_0 to the first excited state S_1 without vibronic contributions $S_{0,0} \rightarrow S_{1,0}$ is generally determined from the cross point of steady-state absorption and fluorescence spectra.

3.3 Internal Conversion

The isoenergetic radiationless transition from an excited state into a excited vibronic level of a lower state of the same multiplicity is called Internal Conversion (IC). The corresponding transition into a state with different multiplicity is named Intersystem Crossing (ICS).

IC as well as electron transfer represent borderline cases of a general theory [Jor99] In contrast to ET the electronic coupling V dominates the reorganization energy λ. For weak electron-phonon coupling the transition rate is given by the „energy gap law“. [Eng70]

$$k_{IC} = \frac{2\pi}{\hbar} C^2 \frac{1}{\sqrt{2\pi \Delta E \hbar \omega}} e^{-\frac{\gamma \Delta E}{\hbar \omega}} \tag{3-10}$$

The highest excited vibration mode ω and the coupling parameter C, which corresponds to the matrix element of the electronic coupling V in the electron transfer theory, contribute to this equation. The rate depends exponentially on the energy gap ΔE between initial and product state. Its factor γ depends just weakly on temperature. Due to the strong dependency on ΔE a molecule favors the conformation with minimal distance of the potential surfaces of S_1 and S_0 before the transition to the ground state takes place. The motion necessary for the conformational change can strongly depend on temperature. If this is the case it can be possible to inhibit IC by freezing the sample.

3.4 Fluorescence

3.4.1 Radiative lifetime

Spontaneous fluorescence is connected to induced absorption and fluorescence by Einstein coefficients. From this context Strickler and Berg deduced the following equation for the rate of spontaneous fluorescence: [Str62]

$$k_{FL} = \frac{2.88 \cdot 10^{-9} n^2}{< \nu^{-3} >_{FL}} \int \frac{\varepsilon(\nu)}{\nu} d\nu \tag{3-11}$$

$$\text{with } < \nu^{-3} >_{FL} = \frac{\int F(\nu)\nu^{-3} d\nu}{\int F(\nu) d\nu} \tag{3-12}$$

where n represents the refractive index, ν the wave number, ε(ν) the molar extinction coefficient in [$mol^{-1}cm^{-1}$] and F(ν) the amplitude of fluorescence. If the fluorescence spectrum is unknown, a simplified Strickler-Berg equation can be used. Here the Stokes-shift is neglected and the absorption spectrum is used for determining $<\nu^{-3}>$. The radiative lifetime is defined as $1/k_{FL}$.

3.4.2 Quantum yield and transition probability

The fluorescence quantum yield is defined by $\Phi_{FL} = \frac{k_{FL}}{k} = k_{FL}\tau$. Not only the fluorescence rate k_{FL} contributes to the fluorescence quantum yield, but the sum of all decay rates or lifetimes of the fluorescing state has to be included, respectively. The fluorescence intensity FI is proportional to the number of absorbed photons per second I, divided by the speed of light c and Planck's constant h:

$$FI\ (\lambda_{EXC.}, \lambda_{DET.}) = \frac{[I_0(\lambda_{EXC.}) - I(\lambda_{EXC.})] \cdot \lambda_{EXC.}}{hc} \tag{3-13}$$

If the fluorescing state is not excited directly, the transition probability from the excited to the fluorescing state Φ_{ABFL} ($\lambda_{EXC.}$, $\lambda_{DET.}$) has to be

taken into account. Thus follows for the fluorescence excitation spectrum (normalized to the number of excitation photons) [Har95b]:

$$F\ (\lambda_{EXC.}, \lambda_{DET.}) \equiv \frac{FI(\lambda_{EXC.}, \lambda_{DET.})}{I_0 \cdot \frac{hc}{\lambda_{EXC.}}} \tag{3-14}$$

$$F\ (\lambda_{EXC.}, \lambda_{DET.}) \sim \Phi_{ABFL}\ (\lambda_{EXC.}, \lambda_{DET.}) \cdot \Phi_{Fl}\ (\lambda_{EXC.}, \lambda_{DET.})\ (1 - 10^{-OD(\lambda_{EXC.})}) \tag{3-15}$$

This imports that the fluorescence is not proportional to the absorbance

$$OD = -\log\ (\ I \diagup I_0\ ), \tag{3-16}$$

but that it correlates to the absorption

$$abs = (1 - I \diagup I_0\ ) = (1 - 10^{-OD \cdot (\lambda_{EXC.})}) \tag{3-17}$$

For small absorbance (OD<<1) the relation abs ≈ OD is valid. In the absorption band of the fluorescing state Φ_{ABFL} is 1 by definition. If the fluorescence excitation spectrum is normalized to the absorption spectrum in this area, the deviation between the two spectra gives a clue of the transition probability Φ_{ABFL} from excited to the fluorescent state against the excitation wavelength. This procedure can be used as well for EET ($\Phi_{ABFL} \equiv \Phi_{EET}$) as for ESPT ($\Phi_{ABFL} \equiv \Phi_{ESPT}$).

If a sample contains several fluorescing species with relative concentrations ρ_i and different lifetimes τ_i equation 3-15 has to be written more generally. The steady-state fluorescence signal is a sum of the fluorescence signals of each species:

$$\begin{aligned} F(\lambda_{EXC.}, \lambda_{DET.}) &= F_0 \cdot \sum_i \rho_i \Phi_{ABFL,i}(\lambda_{EXC.}, \lambda_{DET.}) \cdot 1 - 10^{-OD(\lambda_{EXC.})} \\ &\cdot k_{FL,i}(\lambda_{EXC.}, \lambda_{DET.}) \cdot \tau_i(\lambda_{EXC.}, \lambda_{DET.}) \\ F(\lambda_{EXC.}, \lambda_{DET.}) &= F_0 \cdot \sum_i a_i(\lambda_{EXC.}, \lambda_{DET.}) \cdot \tau_i(\lambda_{EXC.}, \lambda_{DET.}) \end{aligned} \tag{3-18}$$

F_0 is a proportional constant. The amplitudes a_i are derived from time-resolved measurements as well as the transition rates $k_{FL,i}$.

4 Influence of the Chromophore Environment on Fluorescence and fast Internal Conversion in Wildtype GFP and Mutants

4.1 Structure and Properties of GFP

GFP is composed of 238 amino acids and weighs ~28 kDa. [Pra92] The X-ray structure analysis reveals an 11-stranded β-barrel with a diameter of ~30 Å and a length of ~40 Å. [Orm96, Yan96] Its chromophore is formed in an autocatalytic reaction from the tripeptide motif -Ser65-Tyr66-Gly67- in the presence of molecular oxygen and is located on a helix through the center of the barrel. [Cub95,Hei94] Thus it is tightly packed and protected from bulk solvent. [Cha96] The currently accepted mechanism for formation of the 4(*p*-hydroxybenzylidene)-imidazolinone chromophore is depicted in Figure 4-1. [Hei94]

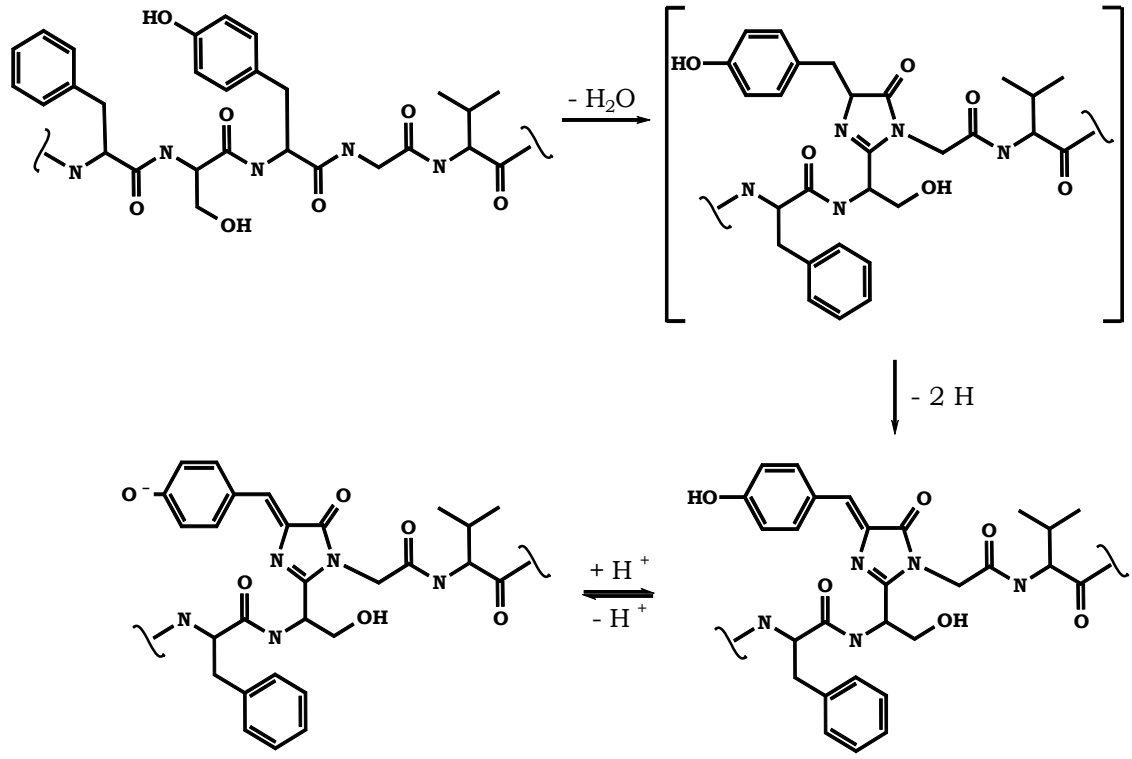

Figure 4-1: Chromophore formation in the *Aequorea* GFP

This 3-dimensional structure not only provides the environment for chromophore formation [Dop96], but is also responsible for the high fluorescence quantum yield (0.8 [Tsi98, Mor74]); denatured GFP and model compounds of the fluorophore in aqueous solution are dark at room temperature but become fluorescent upon cooling below the glass point. [Niw96] This behavior is explained by fast internal conversion (IC) competing with fluorescence. IC can be efficiently suppressed by restricting of motional freedom, e.g. by freezing the sample or increasing the viscosity of the medium. [Kum02a] The chromophore is fixed by a complex hydrogen bonding network provided by a large number of polar groups and structural water in the protein pocket (Figure 4-2). [Bre97]

From this complex protein environment results the photophysical behavior of native GFP and its genetically engineered mutants. A high energy absorption band at 277 nm is commonly founded in the presence of aromatic residues in the protein barrel [Tho98]. It might also include minor contributions from higher electronic transitions of the chromophore as comparative spectra of model compounds show. [Koj97, Voi01] Wildtype GFP (GFP-WT) exhibits two main absorption bands at 397 nm and 477 nm (Figure 4-4 A). These bands have been attributed to a ground state equilibrium between two chromophoric species differing in the protonation state of the phenolic group (Figure 4-2). [Cub95, Hei94] Excitation in any of these absorption bands leads to dominant green emission.

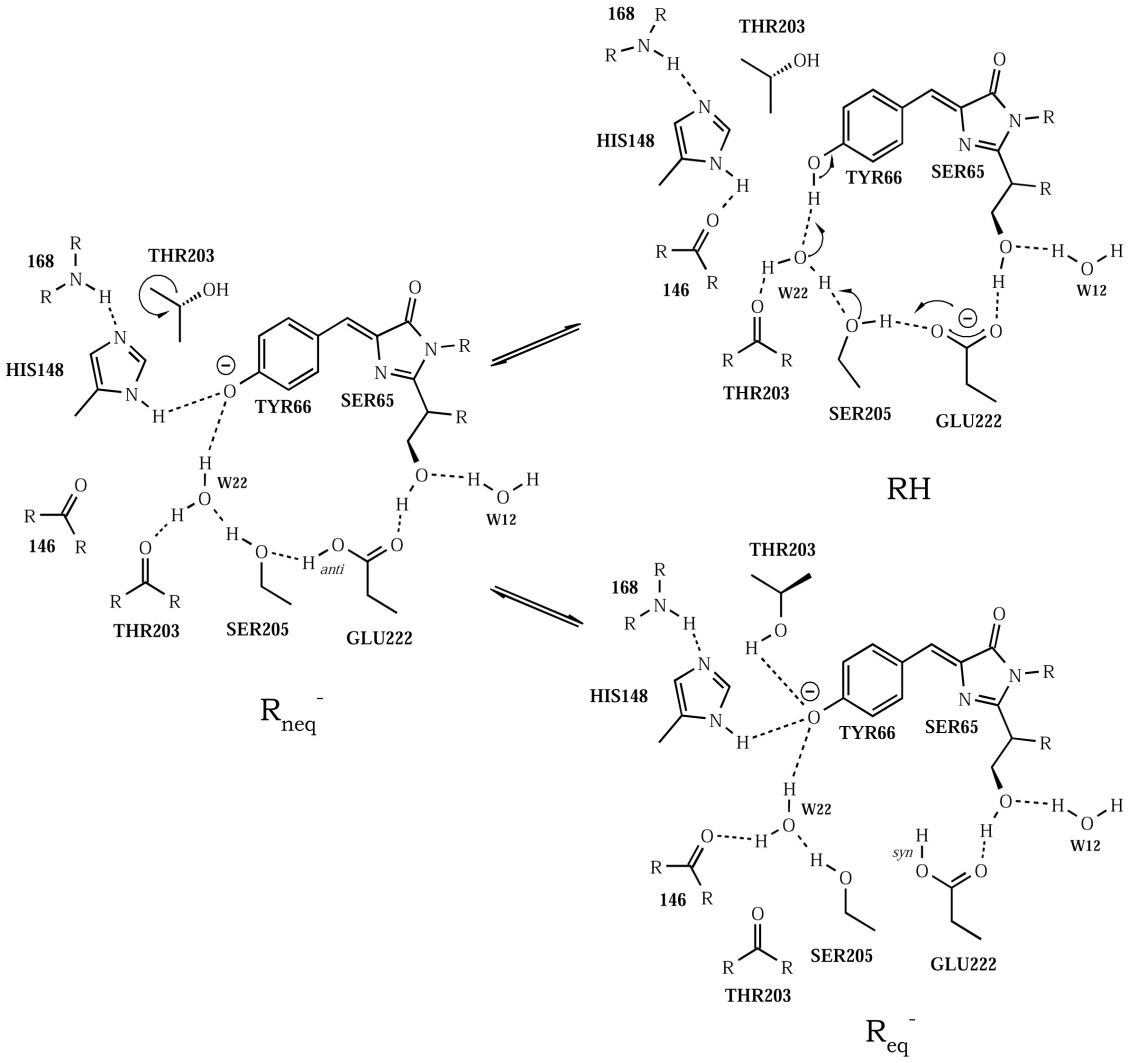

Figure 4-2: Main features of the mechanism for the photo-isomerization of GFP-WT [Bre97]

The underlying process of this spectroscopic behavior is known as Förster cycle. [För49, För50a, För50b] The acidity of proton donors coupled to a delocalized π-system like tyrosyl increases upon excitation into the first excited singlet state. In the presence of suitable proton acceptors Excited State Proton Transfer (ESPT) occurs, resulting in the excited deprotonated state. After deactivation via fluorescence or alternative radiationless processes, the proton is transferred back and the initial protonated ground state is restored. The resulting fluorescence spectrum is generally dominated by the low energy emission of the deprotonated state.

The characteristics of ESPT in GFP-WT are summarized in Figure 4-3. Excitation of the protonated form (RH) at ~400 nm triggers ESPT on a picosecond time scale with a quantum yield of 0.8 [Cha96], leading to an intermediate state R^{-*}_{neq}, which fluoresces at 510 nm. The following adjustment of the environment to the changed electronic conditions results in the equilibrated excited state R^{-*}_{eq} (Figure 4-2). This state exhibits its fluorescence maximum at 506 nm. [Cha96, Los96, Bre97]

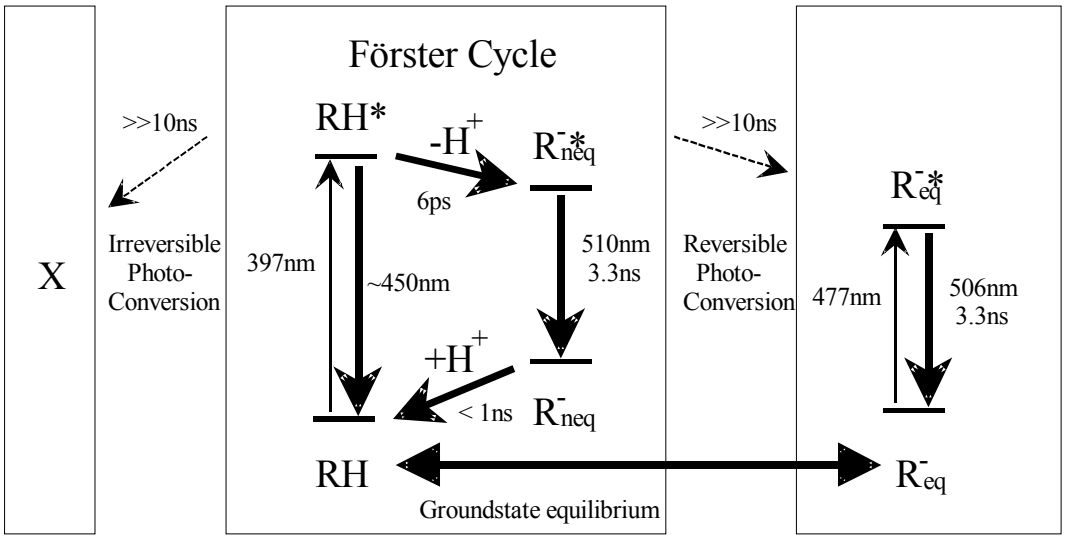

Figure 4-3: Application of the Förster cycle to absorption and emission phenomena in GFP-WT in 50 % glycerol at 295 K

The ground state species RH and R^{-}_{eq} are assumed to be in thermal equilibrium, whereas the deprotonated states R^{-}_{neq} and R^{-*}_{neq} are formed by excited state deprotonation. Low-probability photoconversion processes (reversible and irreversible) are indicated by dashed arrows.

The major evidence for ESPT is the absence of the green fluorescence after replacement of tyrosine Y66 against phenylalanine or histidine, both without the hydroxyl group for deprotonation (Chapter 4.4). [Kum02b] The attempt to proof ESPT in GFP by deuteration experiments failed. The isotope effect measured in low-temperature time-resolved fluorescence measurements is larger by a factor of 2 than by theoretical models predicted. [Cha96, Bub98] As these models are based on the

assumption of only minor structural changes, the discrepancy can only be explained by secondary isotope effects, induced by a different chromophore environment after H-D exchange. [Los98]

4.2 Experimental

4.2.1 Protein expression and purification of GFP

GFP-WT and the mutant RS8/Org18 were provided by KAIROS Scientific Inc., 3350 Scott Blvd., Bldg. 62, Santa Clara, CA 95054, USA.

The GFP-WT gene [Pra92] was subcloned between the unique BamHI and XhiI sites in the pET28a(+) plasmid (Novagen) under control of the T7 promoter.

The RS8/Org18 mutant was identified during construction of a mutant library in which the Tyr145, His148, Val150, Phe165 and Ile167 amino acid positions were simultaneously randomized. The RsGFP8 gene cloned into the pET28a(+) vector was used as the DNA template as described in [Kum00b]. A part of these clones showed orange pigmented colonies. The sequence of one of those clones, RS8/Org18, contained the substitutions F64L, S65T, Y145W, H148V, V150A and I167V. Protein expression and purification was performed essentially as described in [Mit96]. Experiments were performed in 10 mM phosphate buffer, pH 6.5. For low temperature measurements ~50 % glycerol was added.

The single-site mutants GFP-Y66H and GFP-Y66F were provided by J. Wiehler, Genzentrum der Ludwig-Maximilians-Universität, Feodor-Lynen-Str. 25, 81377 München, Germany.

GFP-Y66F. The construction of the Y66F vector as well as protein expression (at 25°C) and purification was performed as described previously. (Kum00a)

GFP-Y66H. This GFP variant was found in a random library constructed by mutagenic PCR of the complete GFP-WT gene. [Kun85, Kum02a] The DNA of the Y66H single site mutant was expressed in *E. coli* XL1 Blue and confirmed by DNA sequencing.

Both proteins were solubilized in PBS buffer pH 7.4 (4 mM KH_2PO_4, 16 mM Na_2HPO_4, 115 mM NaCl). For low temperature measurements ~50 % glycerol was added.

4.2.2 Preparation of PVA-films

500 µl of a 10 % solution of polyvinylalcohol (PVA, Polyviol W25/150, Fa. Wacker) in distilled water was mixed with 500 µl to 700 µl sample in its storage buffer solution (depending on the concentration of the sample). The mixture is centrifuged for 10 min at 5000 rpm. The clear solution is transferred in 1 cm^2 tupperware® forms. After drying at 4°C under nitrogen for three days, the PVA film was wrapped in aluminum foil and stored at –20°C.

4.3 Effects of the Protein Environment on the Spectroscopic Behavior of GFP-WT and its Mutant RS8/Org18

4.3.1 GFP-WT in buffer, glycerol and PVA

Figure 4-4 A shows the well known steady-state absorption and fluorescence spectra of GFP-WT in aqueous solution at room temperature. The fluorescence spectra from excitation in both absorption maxima result, from differing environmental relaxation of the deprotonated state R^-. The fluorescence excitation spectrum deviates from the absorption spectrum in the ratio of its peak heights. When the spectra are normalized to the R^- band, the RH band in the fluorescence excitation spectrum is smaller than in the absorption

spectrum in the present preparation. This shows, that excited state deprotonation of RH is competing with another deactivation process and contributes only approximately 60 % to the green fluorescence.

Addition of 50 % glycerol leads to a pronounced increase of the R^- absorption peak along with a roughly proportional decrease of the high-energy absorption band (Figure 4-4 B). Normalized to RH, the fluorescence excitation spectrum shows a loss in the R^- band with respect to the absorption spectrum. The relative peak ratios of absorbance and fluorescence excitation are given in Table 4-1.

	in buffer 298 K	with 50 % glycerol 298 K	in PVA 298 K	in PVA 150 K
Absorbance	3.3	1.4	2.0	2.5
Fluorescence excitation	2.0	1.7	1.4	2.0

Table 4-1: Relative peak ratios RH/R^- of GFP-WT

This spectral change exhibits a well-defined isosbestic point at 430 nm and is fully reversed after elimination of glycerol. Besides its effect on the ground-state equilibrium between R^- and RH, addition of glycerol causes a blue-shift of 2 nm in the fluorescence of R^-. The green fluorescence excited in RH is not affected.

The most interesting observation is, that the fluorescence spectra excited in RH and R^- are completely invariant against the excitation wavelength when GFP-WT is immobilized in a solid PVA matrix (Figure 4-4 C). This implies a similarity of R^{-*}_{neq} and R^{-*}_{eq}.

Comparison of the absorption spectra of GFP-WT in buffer with and without glycerol or in PVA leads to the conclusion, that PVA affects the protein structure less than glycerol.

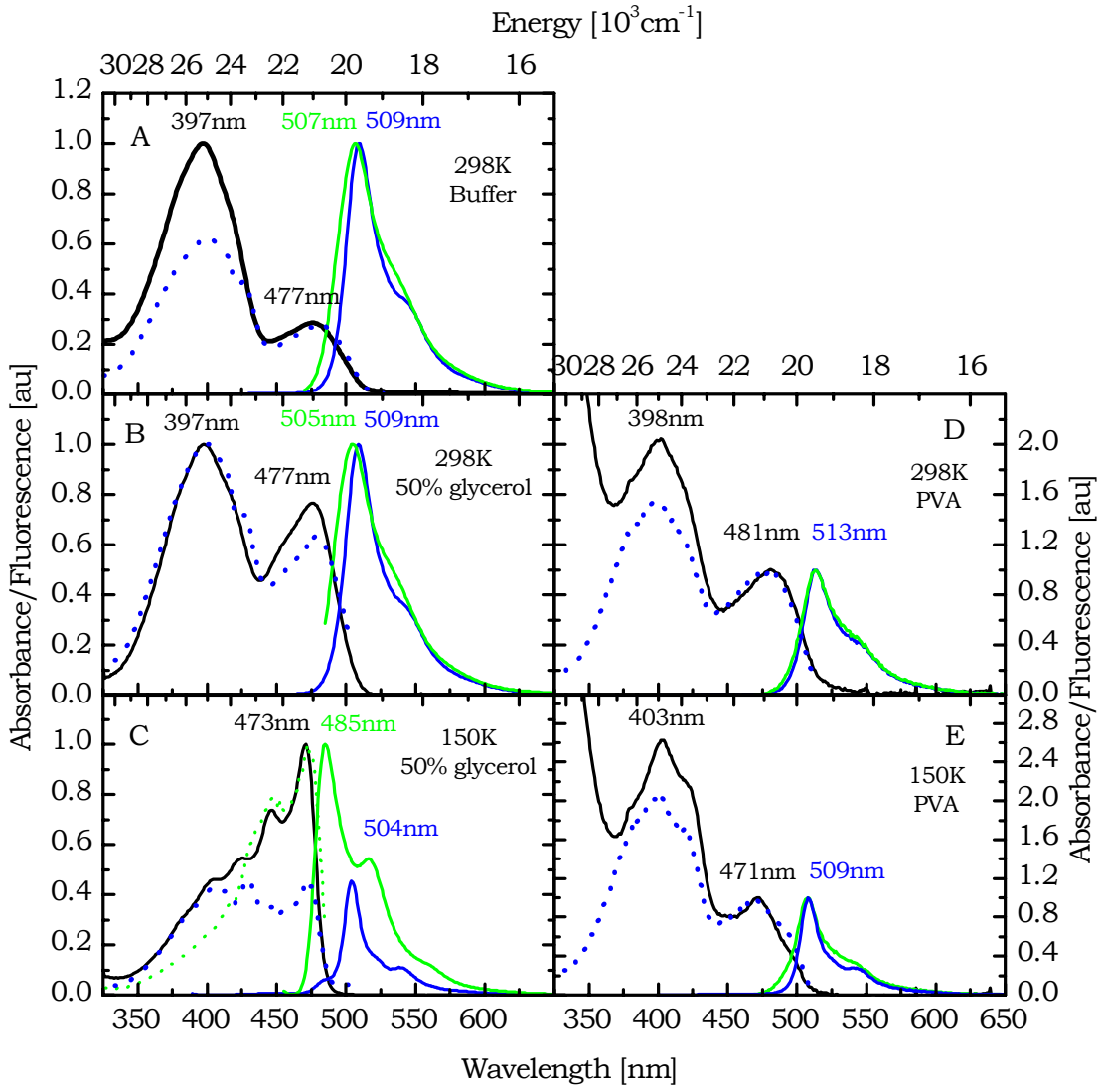

Figure 4-4: Steady-state spectra of GFP-WT

Absorption (black); **Panel A)** in buffer solution, pH 6.5, 298 K, fluorescence blue ($\lambda_{EXC.}$=393 nm) and green, ($\lambda_{EXC.}$=462 nm), fluorescence excitation (dotted blue, $\lambda_{DET.}$=544 nm); **Panel B)** in buffer solution, pH 6.5, containing 50 % glycerol, 298 K, fluorescence blue ($\lambda_{EXC.}$=398 nm) and green ($\lambda_{EXC.}$=477 nm, fluorescence excitation (dotted blue, $\lambda_{DET.}$=509 nm); **Panel C)** in buffer solution, pH 6.5, containing 50 % glycerol, 150 K, fluorescence blue ($\lambda_{EXC.}$=381 nm) and green ($\lambda_{EXC.}$=447 nm, fluorescence excitation (dotted blue, $\lambda_{DET.}$=510 nm); **Panel D)** in PVA, 298 K, fluorescence blue ($\lambda_{EXC.}$=380 nm) and green ($\lambda_{EXC.}$=450 nm, fluorescence excitation (dotted blue, $\lambda_{DET.}$= 530 nm); **Panel E)** in PVA, 150 K, fluorescence blue ($\lambda_{EXC.}$=380 nm) and green ($\lambda_{EXC.}$=450 nm, fluorescence excitation dotted blue ($\lambda_{DET.}$=545 nm) and dotted green ($\lambda_{DET.}$=493 nm).

Effects at low temperatures. The most striking observation is, that the relative absorption peak ratios of GFP-WT in PVA scarcely change at 150 K (Figure 4-4 E, Table 4-1). The excitation spectrum of the single fluorescence band still shows the small deviation in the RH band with respect to the absorption spectrum.

Upon lowering the temperature below the glass point to 150 K, the relative peak heights of the two absorption bands of GFP in buffer/glycerol are inverted (Figure 4-4 B). The deprotonated state dominates the absorption spectrum, while the RH state is reduced to a shoulder in blue wing of the spectrum. The fluorescence spectrum of R^-_{eq} is blue-shifted by 19 nm relatively the fluorescence maximum excited in RH. This difference points to a heavily perturbed environment and efficiently suppressed excited-state deprotonation, caused by glycerol.

As shown in the next chapter, the qualitative features of the steady-state spectra in buffer, buffer/glycerol and PVA matrix are also encountered in mutants, which allow for both, protonated and deprotonated species, e. g. RS8/Org18. However, this sensitivity to the environment is not encountered in blue mutants which cannot de-protonate in the excited state (Chapter 4.4).

4.3.2 GFP-RS8/Org 18 in buffer, glycerol and PVA

At room temperature the dominant low energy absorption band of the mutant GFP-RS8/Org18 in aqueous solution is red-shifted by 25 nm with respect to GFP-WT (Figure 4-5 A). The relative intensity of the absorption bands (Table 4-2) indicates, that the ground state equilibrium favors the deprotonated species. Excitation in RH and R^- leads to a single fluorescence band. The fluorescence excitation spectrum follows the absorption spectrum.

The addition of 50 % glycerol scarcely affects the positions of absorption and fluorescence maxima in GFP-RS8/Org18. It favors the R^-

absorption (Table 4-2), but causes at the same time a decrease of the fluorescence quantum yield of R^-_{eq}, indicated by the deviation from the fluorescence excitation spectrum (Figure 4-5 B).

Cooling to 150 K shifts the ground state equilibrium almost completely towards RH (Figure 4-5 C). In contrast with measurements at room temperature, the fluorescence excitation spectrum at 150 K differs strongly from the absorption spectrum, exhibiting two bands with nearly the same amplitude (Table 4-2). [Kum00b] The R^- band is red-shifted with respect to the corresponding absorption band. Thus only a minority of the chromophores contributes to the green fluorescence.

These results show that addition of glycerol perturbs the environment of the chromophore in GFP-RS8/Org18 heavily, especially at low temperatures, resulting in massive hindrance of RH deprotonation.

GFP-RS8/Org18 in PVA. When GFP-RS8/Org18 is immobilized in a PVA matrix, the features of the room temperature absorption and fluorescence spectra of the mutant in buffer are conserved (Figure 4-5 D). Yet the fluorescence excitation spectrum favors strongly the deprotonated state and deviates from the corresponding absorption spectrum in the RH band, indicating an increase of the fluorescence quantum yield of R^-_{eq} immobilized in PVA.

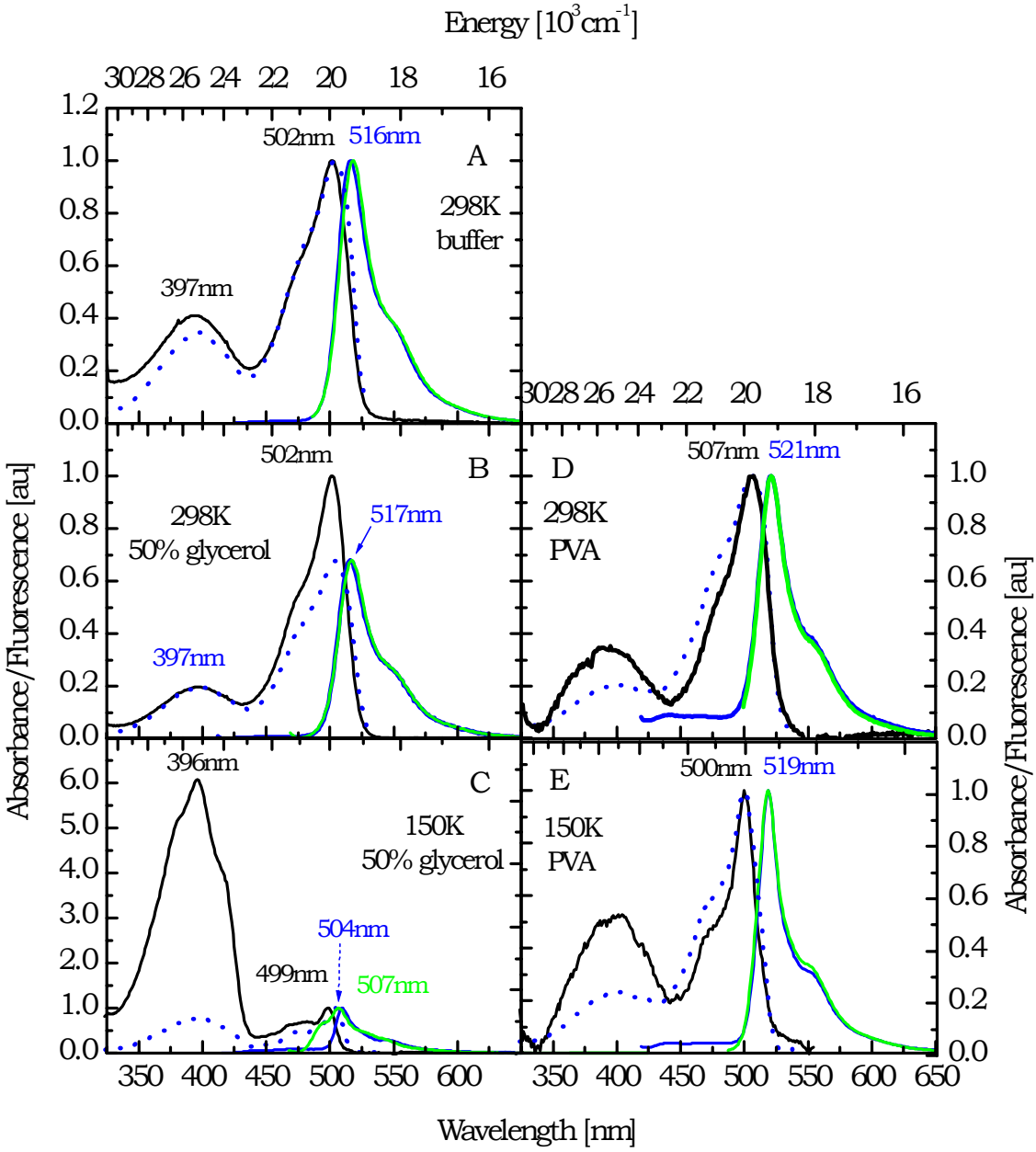

Figure 4-5: Steady-state spectra of RS8/Org18

Absorption (black), fluorescence (blue, $\lambda_{EXC.}$=397 nm) and fluorescence excitation (dotted blue); **Panel A)** in buffer solution, pH 6.5, 298 K, fluorescence (green, $\lambda_{EXC.}$=472 nm), fluorescence excitation ($\lambda_{DET.}$= 539 nm); **Panel B)** in buffer solution, pH 6.5, containing 50 % glycerol, 298 K, fluorescence (green, $\lambda_{EXC.}$=460 nm, fluorescence excitation ($\lambda_{DET.}$= 544 nm); **Panel C)** in buffer solution, pH 6.5, containing 50 % glycerol, 150 K, fluorescence (green, $\lambda_{EXC.}$=459 nm, fluorescence excitation ($\lambda_{DET.}$= 544 nm); **Panel D**) in PVA, 298 K, fluorescence (green, $\lambda_{EXC.}$=475 nm, fluorescence excitation ($\lambda_{DET.}$= 554 nm); **Panel E)** in PVA, 150 K, fluorescence (green, $\lambda_{EXC.}$=468 nm, fluorescence excitation ($\lambda_{DET.}$= 555 nm)

At 150 K the RH absorption increases at the expense of the low energy absorption band (Figure 4-5 E), but a dramatic change like in buffer/glycerol cannot be observed. The fluorescence excitation spectrum is not affected by low temperatures, even the ratio of RH and R^- remains unchanged. Thus the deviation between the absorption and fluorescence excitation bands of RH grows, pointing to reduced deprotonation (Table 4-2).

	in buffer 298 K	with 50 % glycerol 298 K	with 50 % glycerol 150 K	in PVA 298 K	in PVA 150 K
Absorbance	0.4	0.2	5	0.3	0.5
Fluorescence excitation	0.3	0.3	0.8	0.2	0.2

Table 4-2: Relative peak ratios RH/R^- of GFP-RS8/Org18

The results of the low temperature measurements confirm our expectations, as they do not show any pronounced changes upon cooling the GFP-WT and the mutant RS8/Org18 immobilized in PVA to 150 K. This is in contrast to the spectral behavior of both samples in aqueous solution containing 50 % glycerol, where the ground state equilibrium is strongly shifted upon freezing the sample, in case of GFP-WT towards R^-, in GFP-RS8/Org18 to the opposite direction.

4.3.3 Conclusions

In GFP-WT the well known green emission originates from the deprotonated state R^{-*}_{neq} after excited-state proton transfer from the protonated chromophore RH^*. Both states are characterized by an identical environment of the chromophore (Figure 4-2). The subsequent rearrangement of the hydrogen bonding network leads to a blue-shifted fluorescence from the relaxed state $R^{-}_{eq}{}^*$. In buffer solution the ground-state equilibrium between RH and R^- favors the deprotonated species R^-_{eq}. Addition of glycerol leads even at room temperature to massive

changes in the chromophore environment, resulting in a disturbed ground state equilibrium between RH and R^-. In contrast, these perturbations of the protein binding pocket are far less pronounced when the protein is immobilized in a solid polymer matrix. This allows for the conclusion, that PVA disturbs the protein structure less than glycerol, making it a more suitable material for low-temperature experiments. Therefore, when the protein is immobilized in PVA, the drastic change of the steady-state spectra at low temperatures observed in samples containing glycerol should not be detected. This assumption was proved by steady-state spectra, where the features of GFP-WT in buffer solution are conserved upon cooling the sample in PVA to 150 K.

Further confirmation of these findings is provided by the mutant GFP-RS8/Org18, which is capable of ESPT. In this mutant the ground-state equilibrium is at room temperature on the side of R^-. At low temperatures the equilibrium in buffer/glycerol is completely reversed and the fluorescence spectra show two distinct species as a consequence of the disturbed environment. Immobilized in PVA, no pronounced temperature dependency can be observed.

In summary the addition of glycerol seems to affect the structure of GFP and mutants much stronger than immobilization in a PVA matrix. As most hole-burning experiments are performed in PVA, the assumption of a temperature independent protein structure is reasonable. However, the protein structure especially at low temperatures is heavily perturbed by the addition of glycerol in GFP-WT and mutants, which exhibit RH/R^- equilibria. These structural changes certainly complicate the interpretation of Stark effect measurements and excited state kinetics. [Cha96] They may also contribute to the large deuterium effect, for which so far no quantitative explanation has been offered. As theoretical calculations of this effect are based on the assumption, that no large-scale changes in the structure, the flexibility of the protein and the environment of the chromophore are induced by exchanging hydrogen

for deuterium, the drastic difference between theory and experimental results contradict the validity of this assumption. [Los98] It rather confirms the results of this work, that glycerol affects the protein structure in a drastic way. Thus, the application of the primary isotopic effect theory on proteins is questionable as evidently secondary isotopic effects induced by structural changes have a dominant role in glycerol-containing GFP-samples. [Los98]

Fazit. PVA might be a better medium for investigations at low temperatures. Yet this accounts only for systems in which ESPT can occur. Mutants like Y66H and Y66F, in which ESPT is inhibited by substitution in the chromophore, are not affected by addition of glycerol (Figure 4-7). [Kum00b] These systems can be investigated in a buffer glycerol mixture without problems.

4.4 Picosecond Time-Resolved Fluorescence from Blue Emitting Chromophore Variants Y66F and Y66H of the Green Fluorescent Protein

If the excited state proton transfer from the chromophore's hydroxy group is prevented, e.g. upon replacement of the tyrosine by a phenylalanine or a histidine, blue fluorescence around 450 nm is observed. [Cub95, Hei94, Los96, Hei95] These so-called blue fluorescent proteins (BFPs) were among the first GFP mutants with sufficiently altered spectral characteristics to permit double labeling of protein expression [Riz96] and FRET experiments [Hei96, Mit96] solely based on this class of proteins. However, the usefulness of BFPs is tempered by their low fluorescence intensity and photobleaching, especially in the case of the single-site mutants. [Cub95, Hei94, Hei95] Based on crystallographic findings for variants containing Y66F or Y66H in a multiply mutated environment, it was proposed that increased flexibility of the active site

may cause this loss of quantum yield [Pal97, Wac97, Pal99, Web99] rather than inefficiency of protein folding or chromophore formation as suggested earlier for Y66W. [Hei94] The GFP-Y66H chromophore and its immediate environment is depicted in Figure 4-6.

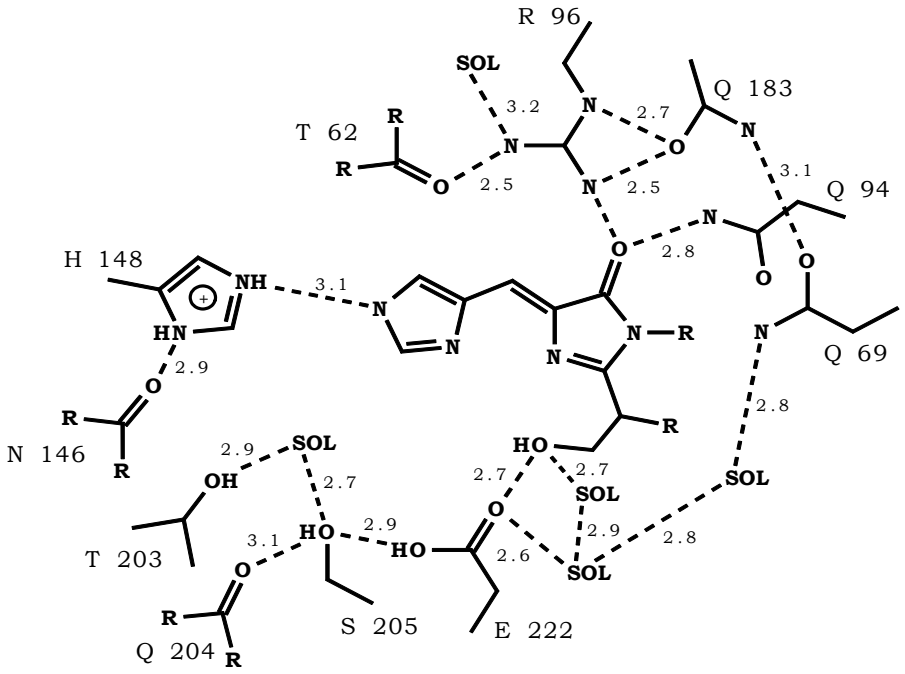

Figure 4-6: Structure of GFP-Y66H chromophore

and parts of its surroundings. [Wac97] SOL=crystal water

4.4.1 Y66H

Steady-state absorption and fluorescence emission spectra of the single-site mutant Y66H at 298 K are depicted in Figure 4-7. They are invariant to the addition of cryoprotector (50 % glycerol) and temperature as shown in [Kum00b].

The absorption spectrum shows one band, which pertains to the chromophore's $S_0 \rightarrow S_1$ transition. Except for a small red shift of less than 4 nm when excited in the red wing of the absorption band, shape and position of the corresponding fluorescence spectra are almost invariant with respect to excitation wavelength and are more structured than the absorption spectrum. The excitation spectrum of this blue fluorescence follows the absorption band of the chromophore closely.

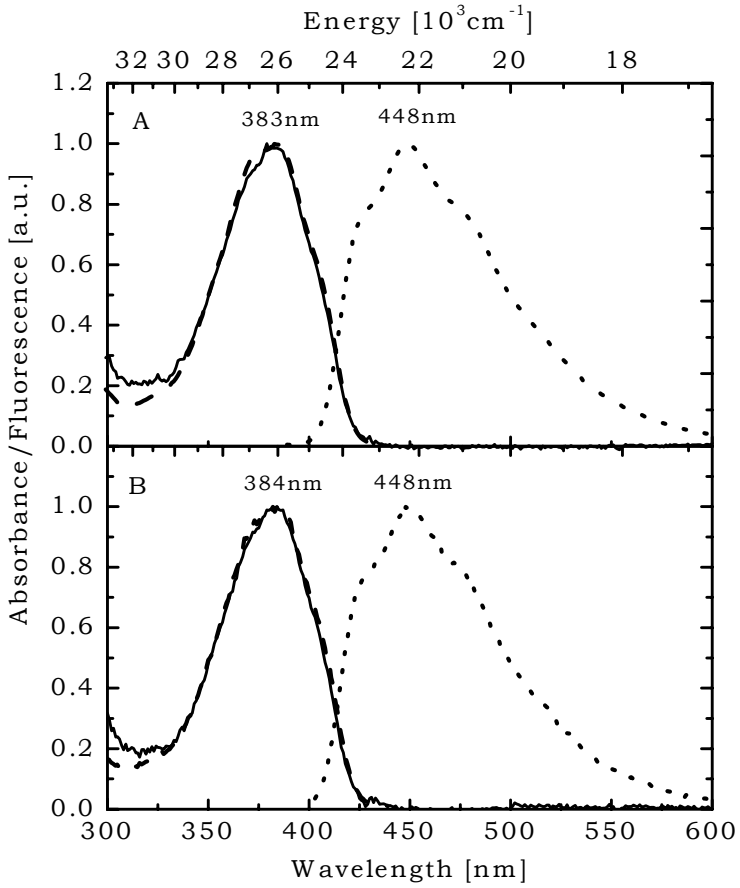

Figure 4-7: Steady-state spectra of GFP-Y66H, 298 K

Absorption (—) and fluorescence (···, $\lambda_{EXC.}$=379 nm) and fluorescence excitation (---, $\lambda_{DET.}$=448 nm). A) in PBS buffer solution, pH 7.4, B) with 50 % glycerol

In general, the spectra become more structured with decreasing temperature while no essential change in peak positions is observed apart from a slight blue shift of a few nanometers. The fluorescence intensity increases significantly when the sample is cooled to 150 k.

In the mutant Y66H the dependence of fluorescence lifetime on temperature is pronounced (Figure 4-8 and Table 4-4).

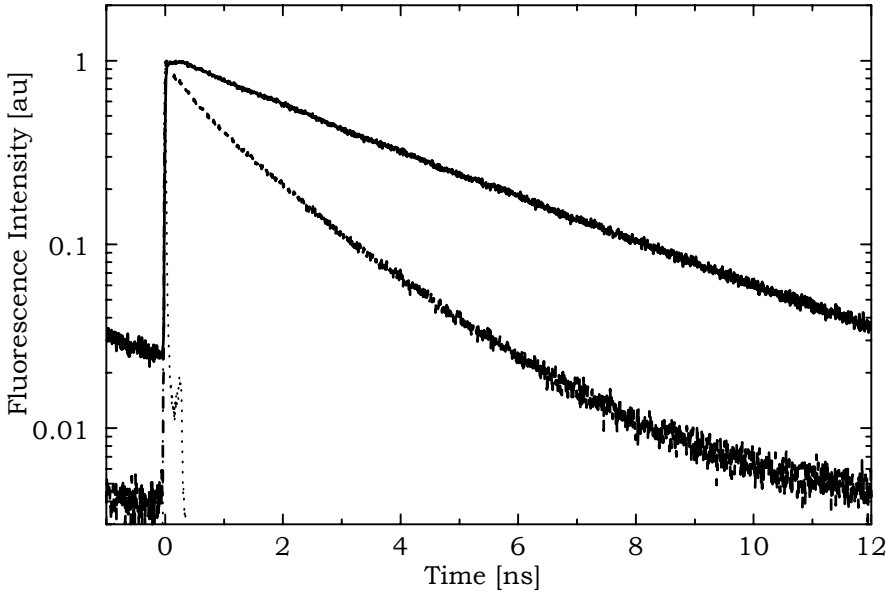

Figure 4-8: Fluorescence decay traces of GFP-Y66H

$\lambda_{EXC.}$=370 nm, $\lambda_{DET.}$=450 nm at 298 K (—) and 150 K (---). IRF (⋯,30 ps FWHM)

At room temperature an average lifetime <t> of 1.1 ns is measured for the S_1-state. Cooling to 150 K only causes a deceleration by a factor of ~3.

		298 K	250 K	150 K
τ1	320 [ps]	41 [%]	6 [%]	10 [%]
τ2	1.6 [ns]	57 [%]	44 [%]	2 [%]
τ3	3.4 [ns]	2 [%]	49 [%]	88 [%]
<t> [ns]		1.1	2.4	3.1

Table 4-3: Fit results of selected fluorescence measurements for Y66 H

$\lambda_{EXC.}$=370 nm, $\lambda_{DET.}$=450 nm. Amplitudes are normalized to 100%. The averaged lifetime is calculated as $\langle t \rangle = \Sigma A_i t_i$

Similar mutants carrying His66 have been subjected to crystallographic studies by different groups. [Pal97,Wac97, Pal99] On the basis of pH 7.4 in our experiments we refer to the X-ray analysis of the mutant Ala1b/F64L/Y66H/Q80R. [Pal97] The mutant chromophore with Tyr66 of GFP-WT replaced by an imidazolyl group is planar and superimposes well on the native one. The structure reveals that at physiological pH

the smaller chromophore and its lack of a hydroxy group at residue 66 leave room for an additional water molecule. This water molecule topologically replaces the phenol oxygen and apparently hydrogen bonds to the N2 atom of the chromophore, to His148, and to another water molecule. In contrast to the Y66F mutant these hydrogen bonds might fix residue 66 in the binding pocket, thus slowing down IC which is reflected in an increase of the excited state lifetime of the chromophore by a factor of more than 15. This large difference might indicate that a rotational motion around only one of the exocyclic bonds (presumably C_γ - C_β) plays the central role in the process leading to the fast radiationless losses: the so-called hula-twist motion, i.e. a concerted and simultaneous rotation around both exocyclic C-C bonds [Web99] should be less sensitive to changes in the fixing of residue 66, since in this case both aromatic moieties of the chromophore are assumed to undergo only small amplitude motions.

Another interesting feature of this mutant is the characteristic rise of the fluorescence signal at low temperatures. This rise could be explained by a conformational change (e.g. a rearrangement of the hydrogen bond network) which favors planarity and thus fluorescence at the expense of IC. Excited-state proton transfer from/to His66 as an alternative mechanism is less probable, since at room temperature an instantaneous rise characteristics has been confirmed even on the femtosecond time scale by fluorescence up-conversion spectroscopy on the double mutant Y66H/Y145F. [Wac97]

4.4.2 Y66F

The steady-state absorption and fluorescence emission spectra of GFP-Y66F are blue-shifted by ~20 nm with respect to GFP-Y66H. The absorption spectrum at 298 K is structured and peaks at 355 nm. The fluorescence spectrum exhibits a structured band at 430 nm,

respectively. The fluorescence excitation spectrum follows the absorption spectrum closely.

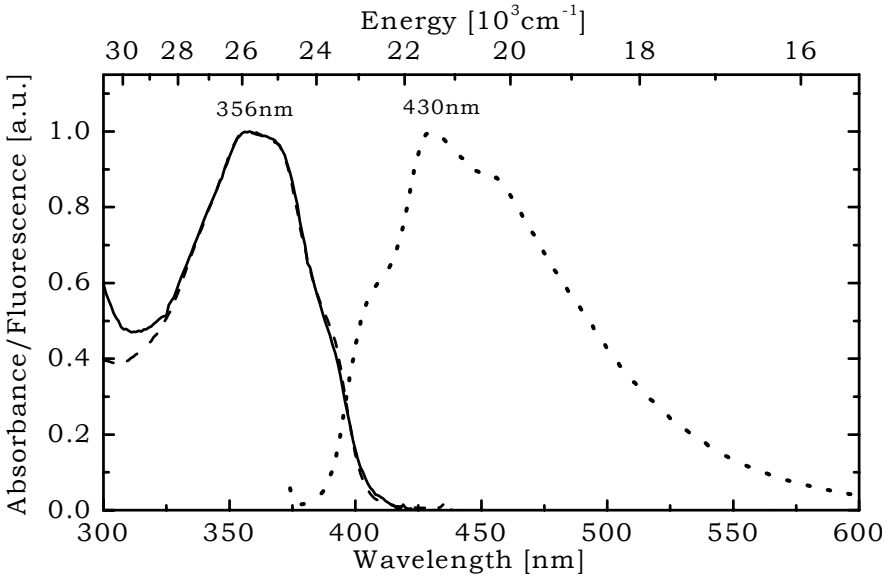

Figure 4-9: Steady-state spectra of GFP-Y66F, 298 K

Absorption (—) and fluorescence (···, $\lambda_{EXC.}$=350 nm) and fluorescence excitation (---, $\lambda_{DET.}$=460 nm).

While at 298 K Y66F fluoresces only weakly, at 80 K a strong blue emission is obtained. Picosecond time-resolved fluorescence measurements (Figure 4-10 and Table 4-4) reveal a fluorescence signal which occurs instantaneously within our time resolution (FWHM of the IRF ~35 ps) and decays non-exponentially at all temperatures (≥ 80 K) with time constants spanning the picosecond to nanosecond range.

Even at 80 K where comparatively longer time components predominate, in most cases a time constant of less than 50 ps is necessary to achieve a good fit.

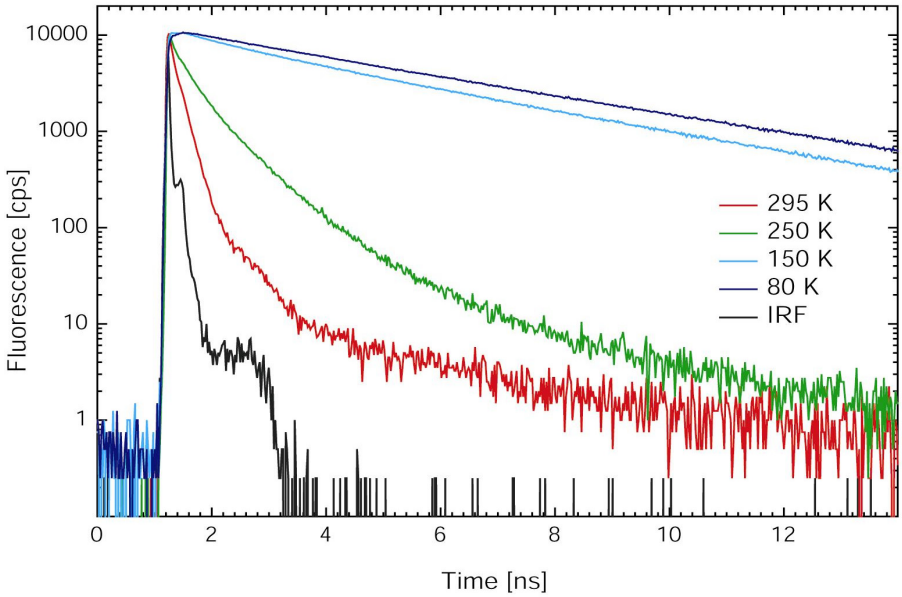

Figure 4-10: Fluorescence decay traces of GFP-Y66F

$\lambda_{EXC.}$=359 nm, $\lambda_{DET.}$=430 nm at selected temperatures. IRF=40 ps

The averaged lifetime <t> = $\Sigma A_i t_i$ of the S_1-state is increased by a factor of >60, i.e. from ~60 ps at 298 K to ~3.7 ns at 80 K. This averaging procedure may overestimate the contribution of the longer time components in contrast to a stretched exponential treatment in which the amplitudes of the shorter components are more pronounced. In addition, the fluorescence kinetics seem to be slightly faster when detected in either wing of the emission band than in the spectral maximum (data not shown).

T [K]	$\lambda_{DET.}$ [nm]	τ_1	A_1 [%]	τ_2	A_2 [%]	τ_3	A_3 [%]	τ_4	A_4 [%]	<t>
295	430	14 ps	47	86 ps	35	200 ps	17	1.3 ns	0.2	74 ps
250	430	43 ps	43	214 ps	31	636 ps	25	1.8 ns	1	272 ps
150	430	14 ps	47	288 ps	6	1.5 ns	13	4.2 ns	33	1.6 ns
80	430	15 ps	12			1.5 ns	12	4.6 ns	75	3.6 ns

Table 4-4: Fit results of selected fluorescence measurements for Y66F

$\lambda_{EXC.}$=359 nm/370 nm, respectively. Amplitudes are normalized to 100%. The averaged lifetime is calculated as <t> = $\Sigma A_i t_i$

Since in the mutant Y66F the hydroxy group at position 66 is replaced by hydrogen, the origin of the picosecond fluorescence decay at high temperatures is expected to differ from wild-type GFP where the fast decay has been shown to be due to excited-state proton transfer to nearby acceptors in the protein environment. [Cha96,Los96] In the case of this mutant we evoke IC to be the process which shortens the excited-state lifetime. This mechanism is supported by a crystallographic structural analysis which reveals that the missing hydroxy group leaves a cavity adjacent to the chromophore. [Pal99] As suspected previously [Pal99] this cavity may indeed allow for an increase of rotational degrees of freedom within the chromophore skeleton.

At all temperatures the fluorescence decay shows dispersive kinetics which is strongly temperature dependent. This feature qualitatively reproduces the temperature dependence of the non-exponential fluorescence decay of a model compound of the chromophore solved in glycerol, which has been demonstrated to depend predominantly on the macroscopic viscosity of the solution rather than on thermal activation of the rotational motion within the chromophore. [Kum02] The non-exponential decay pattern as well as its spectral dependence of the fluorescence reflect structural dispersion. The observation that the shortest picosecond time constant is maintained down to the lowest temperature (80 K) with relatively modest attenuation of its amplitude characterizes the specific protein configuration which allows for the most efficient rotational motion between the two aromatic moieties of the chromophore.

4.4.3 Conclusions and comments

Picosecond time-resolved fluorescence decay traces and their temperature dependence reveal that the loss of fluorescence quantum yield in the single-site mutants Y66F and Y66H at room temperature is reflected in the shortened lifetimes which approach the 3-4 ns range upon lowering the temperature. The fast radiationless decay in these

mutants points to internal conversion favored by motional degrees of freedom around the exocyclic bonds of the chromophore. The feasibility of this decay channel is supported by X-ray structural data on similar blue variants which show specific changes in the hydrogen bond network and the free volume of the chromophore brought about by the mutations.

5 Picosecond Time-resolved FRET in the Fluorescent Protein from *Discosoma Red* (DsRed-WT)

5.1 Introduction

In the red fluorescent protein first isolated from the coral *Discosoma sp.'Red'* (DsRed-WT), the long-wavelength emission maximum is shifted by 57 nm towards the red in comparison to the most red-shifted mutant of GFP (commonly named 10C Q69K), which emits at 529 nm [Pal99] with a quantum yield of 0.7. [Bai00] The mechanism of chromophore maturation is depicted in Figure 5-1.

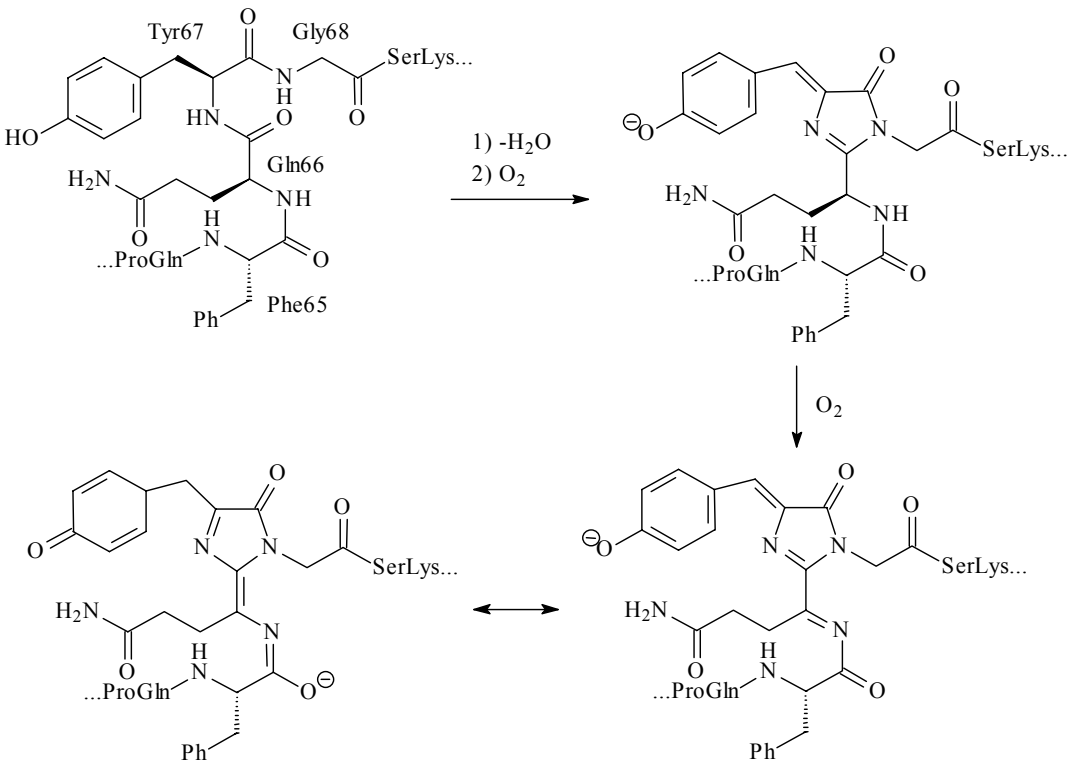

Figure 5-1: Maturation process of the DsRed chromophore

Spectroscopic evidence for oligomerization in DsRed-WT has been recently derived from 1) steady state and 2) time-resolved phenomena:

1) the breakdown of FRET from the immature green emitting to the mature red emitting chromophore upon photobleaching of the latter, [Bai00] and 2) the slow (50 ns) rotational motion indicative for tetramer formation.[Hei00] Moreover, these picosecond time-resolved measurements of fluorescence anisotropy (FWHM 60 ps) also revealed rapid de-polarization (~200 ps) which has been attributed to intra-oligomer FRET between neighboring chromophores exhibiting non-parallel transition dipoles. Further support for FRET has been provided by fluorescence excitation spectra of DsRed-WT and several of its mutants. [Wie01]

This spectroscopic information on the structure of DsRed-WT as well as on the molecular nature of its chromophore was beautifully confirmed in the recently reported 1.9 Å crystal structure analysis. [Wal00, Yar01]

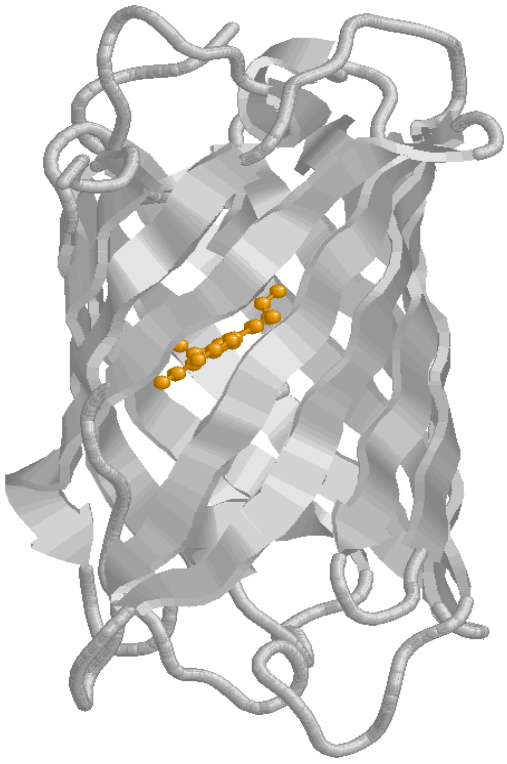

Figure 5-2: X-ray structure analysis of DsRed [Yar01]

The red emitting chromophore shows the expected extension of the conjugated π-system of the GFP-like precursor chromophore through an additional dehydrogenation reaction as concluded from mass spectrometry. [Gro00] The X-ray structure analysis confirmed the previous conclusion, [Bai00] that DsRed-WT assembles into a tetramer. In fact, tetramer formation is driven by two chemically distinct protein interfaces which are not conserved in GFP-WT; GFP is known to have only a weak tendency for dimerization. [Pal97]

5.2 Experimental

5.2.1 Protein expression and purification of drFP583

Expression and purification of DsRed-WT and the double mutant T21S/T217S was carried out as described in [Wie01] with overnight expression at 37°C. The protein was buffered in PBS (4 mM KH_2PO_4, 16 mM Na_2HPO_4, 115 mM NaCl, 0.02 mM NaN_3, pH 7.4).

5.2.2 Estimation of the energy transfer rate

The energy transfer rate $k_{FRET} = r^{-6}\ \kappa^2\ J\ n^{-4}\ k_{FL}$ [Str78] between two FRET-partners within the protein tetramer has been estimated to be in the range of a few picoseconds.

Assumptions: Center-to-center distance of the FRET-partners r = 41 Å; [Wal00] angle between the transition dipole moments of the energy donor and acceptor of 21°[Wal00] (represented in the orientational factor κ); maximal extinction coefficient of the red chromophore $\varepsilon_{max} = 75000\ M^{-1}\ cm^{-1}$, [Bai00] contributing to the spectral overlap integral J between the emission spectrum of the energy donor and the absorption spectrum of the acceptor in a linear manner; a refractive index for a protein environment of n = 1.3; fluorescence decay rate of the green chromophore $k_{FL} = (3.3\ ns)^{-1}$ as in GFP-WT.

Uncertainties in this estimate arise from the unknown distribution of the red and green chromophores in the tetramer and the orientation of their transition dipole moments as well as the unknown fluorescence decay rate of the unquenched green chromophore in DsRed-WT. It should be kept in mind that the deprotonated chromophore species in a yellowish GFP mutant showed a remarkable decrease in fluorescence lifetime from 3.3 ns to ca. 170 ps due to IC induced by rotational motion. [Kum98]

5.3 Results and Discussion

5.3.1 Steady-state spectroscopy

The steady-state absorption, fluorescence excitation and emission spectra of DsRed-WT are depicted in Figure 5-3 A. To facilitate comparison, the corresponding spectra of the DsRed-mutant T21S/T217S and the well-studied GFP-WT are included (Figure 5-3 B and C).

The most prominent feature of DsRed-WT is the predominant red fluorescence with its maximum at 586 nm. Apart from this strong emission band a weak one is found peaking at 498 nm in the green. The absorption spectrum reaches its maximum at 559 nm and exhibits two shoulders at 525 nm and 485 nm. The Stokes shift between the first the maximum and the first shoulder at 525 nm is 1158 cm^{-1}. The shift of the high energy shoulder with respect to the shoulder at 525 nm is 1570 cm^{-1} and therefore considerably larger. As for vibronic progression the energy gaps are to be equidistant, the high-energy shoulder at 485 nm and the corresponding weak green emission at 498 nm were attributed to the immature precursor chromophore. [Bai00, Gro00, Wie01] Its spectral features coincide with the absorption and emission bands of the chromophore in GFP-WT in its anionic state. This leads to the

conclusion that maturation of the red species is incomplete [Bai00, Gro00] and that a certain amount of molecules retains a green emitting chromophore structurally similar to the deprotonated one in GFP-WT.

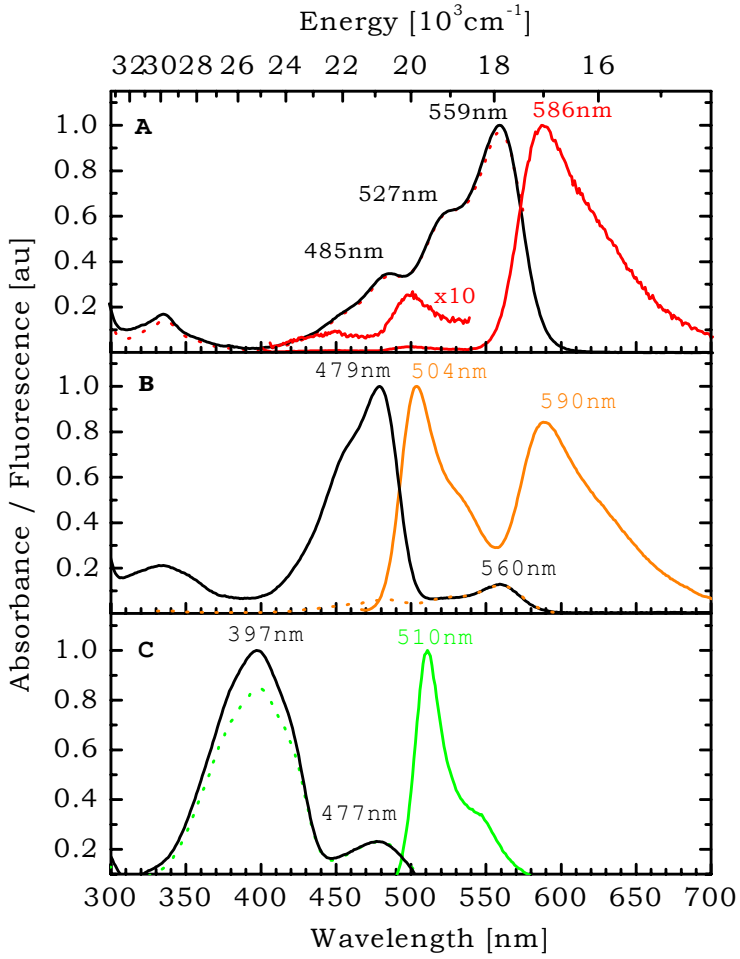

Figure 5-3: Steady-state spectra of DsRed and GFP-WT, 298 K

Absorption (—, black), fluorescence excitation (···) and emission (—) spectra of fluorescent proteins in buffer containing 50 % glycerol (pH 7.4): **(A)** DsRed-WT (red); emission $\lambda_{EXC.}$=390 nm, The emission spectrum from 400 nm to 540 nm is shown magnified by a factor of 10. Fluorescence excitation $\lambda_{DET.}$=585 nm, **(B)** DsRed-mutant T21S/T217S (orange); fluorescence excitation $\lambda_{DET.}$=638 nm, emission $\lambda_{EXC.}$=455 nm, **(C)** GFP-WT (green); emission $\lambda_{EXC.}$=397 nm, fluorescence excitation $\lambda_{DET.}$=553 nm

Since the excitation spectrum of the red fluorescence closely follows the absorption spectrum in the entire spectral range and excitation in the blue wing of the absorption band leads almost entirely to red emission, the observed quenching of the green in favor of the red fluorescence

could be interpreted in terms of FRET (as predicted in [Bai00, Wie01]) between the immature precursor state and the mature red emitting chromophore, coexisting in hetero-oligomers of the protein.

In the DsRed double mutant T21S/T217S, [Wie01] due to incomplete maturation, the green absorption of the GFP-like chromophore dominates the absorption spectrum (Figure 5-3 B). Applying the FRET scenario here, the pronounced increase of green fluorescence relative to the red one with excitation at 479 nm is in accordance with the notion that a relatively large portion of oligomers exists in this mutant with little or no occupancy by red emitting chromophores.

5.3.2 Picosecond to nanosecond time-resolved fluorescence measurements.

To confirm and characterize FRET occurring in DsRed-WT oligomers, time-resolved fluorescence measurements were performed. Investigating the lifetime of the red emitting species, the sample was first excited at 570 nm. The decay of the fluorescence monitored at 587 nm can be fitted bi-exponentially (3.9 ns, 91 % and 0.85 ns, 9 %; Table 5-1). The average lifetime of 3.6 ns is very close to the one obtained for the excited deprotonated chromophore species in GFP-WT (3.3 ns, 100 %; Figure 5-4 A). [Los96] In terms of structure, the observation of minimal non-radiative losses in both proteins is certainly the fingerprint of a tight protein environment which keeps the chromophore planar and does not allow for rotational motions prone to induce internal conversion processes. [Kum98, Kum00]

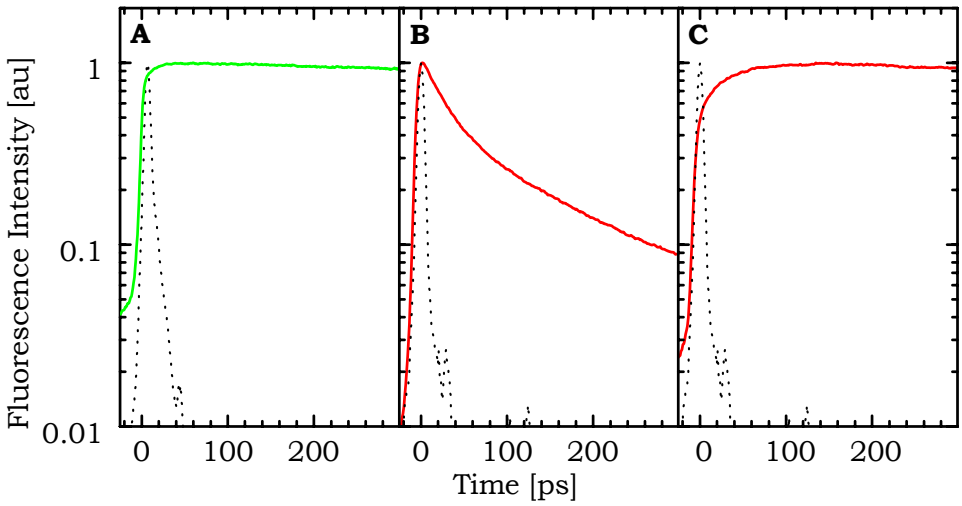

Figure 5-4: Fluorescence decay traces of GFP-WT and DsRed-WT, 298 K

in buffer containing 50 % glycerol (pH 7.4), IRF (blue, 6 ps FWHM): **(A)** GFP-WT; $\lambda_{EXC.}$=462 nm, $\lambda_{DET.}$=530 nm, **(B)** DsRed-WT; $\lambda_{EXC.}$=445 nm, $\lambda_{DET.}$=500 nm, **(C)** DsRed-WT; $\lambda_{EXC.}$=445 nm, $\lambda_{DET.}$=600 nm.

Excitation of the immature GFP-like chromophore in the blue wing of its absorption band ($\lambda_{EXC.}$ = 445 nm) leads to both green and red emission. The green fluorescence monitored at 500 nm (Figure 5-4 B) decays highly multi-exponential and can be fitted with three time components of 14 ps (53 %), 51 ps (32 %) and 285 ps (15 %, Table 5-1). This is much faster than the corresponding excited state of the deprotonated chromophore species in GFP-WT (Figure 5-4 A). The red fluorescence detected at 600 nm is now showing a significant time delay in the onset of the signal which mirrors the fast decay of the green emission (Figure 5-4 C, Table 5-1).

Excitation [nm]	Detection [nm]	τ_1 [ps]	A_1 [%]	τ_2 [ps]	A_2 [%]	τ_3 [ps]	A_3 [%]	τ_4 [ps]	A_4 [%]
570 [a]	587					845	9	3890	91
445 [b]	500	14	53	51	32	285	15		
445 [b]	500	**14**	**55**	**57**	**34**	**466**	**11**		
	600	**14**	**-31**	**57**	**-33**	**466**	**38**	**3890[c]**	**62**

Table 5-1: Fit results of time-resolved fluorescence measurements on DsRed-WT.

Decay amplitudes are normalized to 100%. Negative values indicate rise components. (Figure 5-4). Bold letters represent results from a global fit with shared time constants. Due to the narrow time window of the streak camera the ns-time constant was taken from the TCSPC measurement and kept fixed. We interpret the time constant of 466 ps as the shorter decay component of 845 ps (derived from the TCSPC-measurement) influenced by a third rise component of 285 ps, that is expected from the decay trace of the 500 nm measurement (single fit). [a] measured using TCSPC. [b] measured using synchroscan streak camera. [c] fixed.

These phenomena of similar time constants for the decay in the green and the rise in the red region of the fluorescence spectrum are interpreted by FRET between the anionic states of immature green and mature red chromophores. This interpretation is supported by arguments from steady state spectra and also from X-ray structure analysis. [Wal00] The discovery of a formally charged ε-nitrogen atom of lysine at position 162 forming a salt bridge to the phenolic oxygen of the chromophore [Wal00] supports the stabilization of the anionic species in the green and red emitting chromophores. However, since in GFP-WT, the origin of such antibatic excited state decay and rise dynamics is due to excited state proton transfer (ESPT) [Los96, Cha96] deuteration and low temperature experiments have been performed. These studies show that in contrast to GFP-WT, neither deuteration nor cooling to 80 K has any effect on the absorption spectra or fluorescence kinetics of DsRed-WT. Thus, on the basis of the missing "fingerprint features" ESPT is excluded as the origin of the red emission following blue excitation of DsRed-WT.

The fast decay of the green fluorescence together with the mirror-like rise of the red emission confirms FRET from the excited immature green emitting chromophore to the mature red emitting chromophore. On the basis of distances and angles between the different chromophores in the tetramer, [Wal00] and in consideration of the spectral overlap of green emission and red absorption we calculated an approximate lifetime of 10 ps for the green emitting chromophore which is in good agreement with the experimental data (Table 5-1). Due to its short range nature FRET is not expected to be efficient in complexes arising solely from random diffusional encounters. Therefore, FRET is an excellent tool for probing the oligomerization status of fluorescent proteins- and is indispensable whenever hetero-oligomers are involved.

6 The Novel Phenomenon of Light-Induced Increase of Fluorescence in the Coral Protein AsFP595

6.1 Spectral Properties of the Protein AsFP595

The chromoprotein from the sea anemone *Anemonia sulcata* investigated in this work has a sequence homology of 20 % with GFP. It absorbs at 565 nm (extinction coefficient ~120 000 $M^{-1}cm^{-1}$ [Chu03a]). The emission maximum is found at 596 nm, a 12 nm red-shift compared with DsRed. Therefore it should suit excellently as a gene marker, especially when more proteins, labeled in different colors should be observed in parallel, if it did not suffer from an extremely low fluorescence quantum yield (<0.001). [Luk00] Very surprisingly it offers the unexpected possibility to change the intensity of its fluorescence upon excitation with high intensity light. This Light Induced Fluorescence Enhancement – LIFE – effect, first reported by Lukyanov et al. [Luk00] is reversible and when the intensive irradiation is switched off, the protein returns into the initial non-fluorescent state. [Luk00] LIFE can even be reversed by a flash of intensive blue light, which quenches the strong fluorescence immediately. [Luk00] Recently Chudakov et al. described the relaxation of a fluorescent state of asFP595-WT and mutants to a "dark" state with a halftime of <10 s. [Chu03a,b]

On the basis of mutagenesis data it is assumed that this phenomenon results from cis-trans isomerization of the chromophore in the excited state. [Chu03a] Unfortunately, the detailed structure of the asFP595 chromophore has not yet been determined by X-ray structure analysis. An assumption based on mass spectral data proposes a 6-membered heterocycle, i.e. an 2-(4-hydroxybenzylidene)-6-hydroxy-2,5 dihydro-pyrazine to be formed from the chromophore motive Met-Tyr-Gly and to be responsible for the unusual spectroscopic behavior. After complete

maturation the protein is proposed to split due to hydrolysis in two fragments with 8 kDa and 20 kDa. [Mar01] Another approach based on sequence alignment and a putative structure obtained from comparative protein modeling, predicts a cracked β-can constructed from 6 β-strands to be the structure of asFP595. [Wie00]

Anyhow, as long as the detailed three-dimensional structure of the chromophore is not known, the exact molecular processes on illumination of the protein can only be guessed. Comparison with fluorescent and non-fluorescent protein may give a clue, which processes are essential for a high fluorescence quantum yield in red colored proteins. Two recent X-ray structural analysis of a practically non-fluorescent pigment from the coral *Montipora efflorescence* (pocilloporin Rtms5, 2.2 Å resolution) [Pre03] and a highly fluorescent protein from the sea anemone *Entacmaea quadricolor* (eqFP611, 2.0 Å resolution [Pet03]) show, that both chromophores adopt trans conformation, in contrast to DsRed, which possesses a chromophore in cis configuration (Figure 6-1).

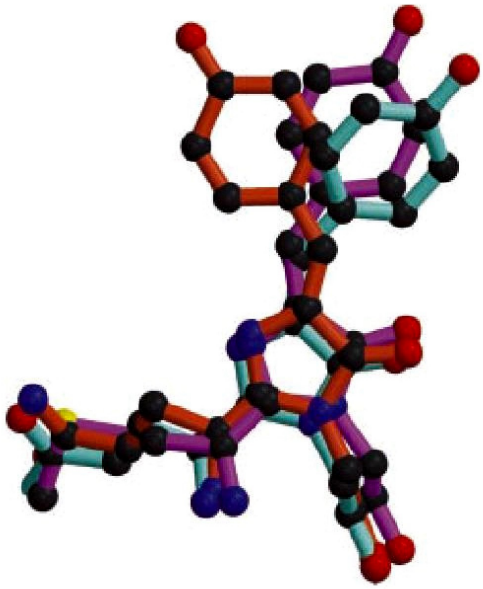

Figure 6-1: Comparison of the chromophores of eqFP611 (magenta), DsRed (orange) and Rtms5 (green)

The superposed chromophores highlight the trans coplanar conformation of the EqFP611 chromophore, the cis coplanar conformation of the DsRed chromophore and the non-coplanar chromophore conformation of Rtms5. Taken from [Pet03].

While the tyrosyl group of RTMS5 is non-coplanar to the plane of the isoalloxazine moiety, the corresponding group in eqFP611 is stacked between a histidine and a phenylalanine, providing coplanar conformation. This hints to a strong influence of the individual environment of the chromophore on fluorescence lifetime, especially if surrounding amino acids restrict the motional freedom by stacking interactions, while the conformation of the chromophores plays a minor role for the fluorescence quantum yield of the protein in question.

6.2 Experimental

6.2.1 Protein expression and purification of asFP595

The asFP595 protein is obtained as described in [Luk00]. The full-length coding region of asFP595 is cloned into a pQE30 vector (Qiagen). The wild type protein as well as its mutant variants are expressed in *E. coli*

with a 6xHis tag at the N-terminus and purified using TALON metal-affinity resine (Clontech). All preparations of the heterologous expression products are at least of 95 % purity according to electrophoresis.

6.2.2 Sample preparation

The protein is dissolved in a mixture of 60 % glycerol and 40 % 50 mM glycine buffer, pH 8. For steady-state measurements at low excitation intensities the protein concentration is adjusted to yield an $OD_{MAX.}$ of 0.3 in a 1 mm quartz cuvette. For the high intensity measurements $OD_{MAX.}$ is 0.22 in a quartz cuvette with 1 cm path length.

Immobilization of asFP595-WT in a solid PVA matrix is carried out as described in Chapter 4.2.2.

6.2.3 High and low intensity steady-state spectroscopy

Low intensity fluorescence spectra are measured using a spectrofluorometer (Spex Fluorolog-2 Model F212I). In order to overcome the negligible fluorescence quantum yield, a 4 mm path-length quartz cuvette is used and the entrance/exit slits of the monochromators are set to 5 mm limiting the spectral resolution to about 7 nm. Low-temperature experiments were performed in a continuous-flow cryostat (Leybold VSK 3-300) cooled with liquid nitrogen.

High intensity fluorescence spectra were taken after excitation with an Ar^+-laser system operated in cw-mode at 514 nm, reaching a maximal power P_{LASER} ~100 mW. Since the excitation beam (~10 mm diameter) was focused onto the sample using a f = 200 mm lens, the minimal radius of the excitation beam was ~1.5 µm. Taking into account the width of the cuvette (10 mm), an effective average beam width of the order of 0.1 mm should be accurate. Thus, the excitation intensity is given by $P_{LASER}/100\ mm^2$. For the maximal power of ~100 mW this

corresponds to a photon flux $3*10^{19}$ Photons/(sec mm²). The fluorescence emission spectrum was recorded using a CCD-matrix array with attached polychromator (InstaSpec IV) with a spectral resolution of 1 nm or better.

6.3 Results and Discussion

6.3.1 Steady-state spectra at low and high excitation intensity

Assignment of photoactive states. The room temperature absorption spectrum of the chromoprotein asFP595 in its non-fluorescent state shows a maximum peaking at 565 nm and a shoulder at 510 nm (Figure 6-2).

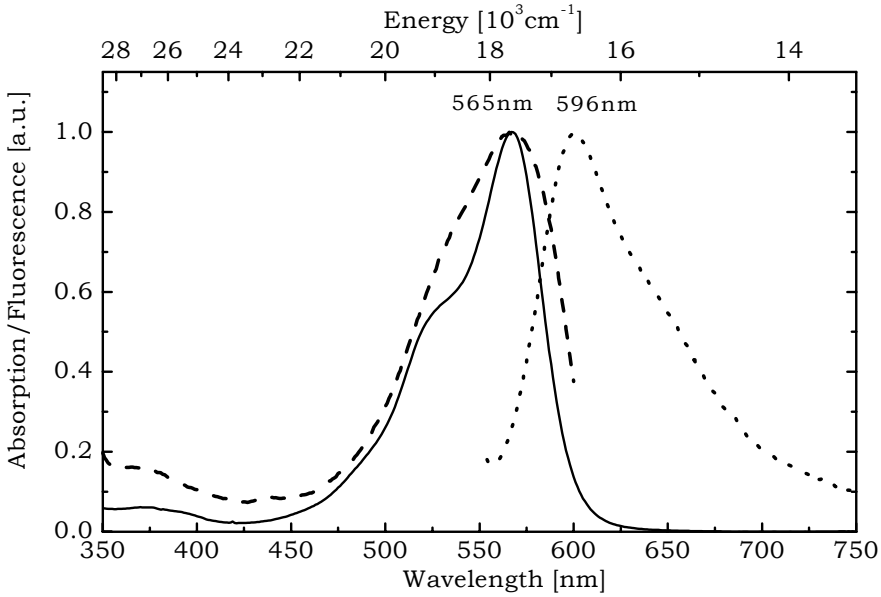

Figure 6-2: Steady-state spectra of asFP595-Wt, 298 K

Absorption (—), fluorescence (···, $\lambda_{EXC.}$=475 nm) and fluorescence excitation (---, $\lambda_{DET.}$=525 nm) spectra, in buffer solution pH 8 and low intensity.

The fluorescence spectrum is hardly measurable due to its low quantum yield (< 0.001 [Luk00]) and exhibits a maximum at 596 nm. The peak of the fluorescence excitation spectrum coincides with the one of the absorption spectrum, its broadening being caused by the decreased

spectral resolution due to the wide entrance/exit slits of the monochromators.

Determination of the protonation state of the chromophore. The Stokes shift, estimated to be in the range 800-1000 cm^{-1}, is slightly smaller than the Stokes shift of the deprotonated state R^- in GFP-WT (1280 cm^{-1}). The Stokes shift of the protonated state RH is 3760 cm^{-1} for GFP-WT and 2500 cm^{-1} for the blue mutant Y66H with tyrosine replaced by phenylalanine causing the inhibition of deprotonation. In case of ESPT the fluorescence maximum is red-shifted by 5600 cm^{-1}, because emission occurs from the deprotonated state R^- upon excitation in the protonated state RH. Therefore the small Stokes shift observed in asFP595 is certainly a fingerprint of the chromophore bearing a negative charge at the tyrosyl moiety.

This assumption is confirmed by adjuvant studies of the pH dependence of the denatured protein asFP595 in comparison with its trypsine-derived chromopeptide in aqueous solution. [Mar01] Under acidic conditions (pH 3.0) the absorption spectra of the chromopeptide and the denatured protein are similar, both showing an absorption maximum at 430 nm. In case of the chromopeptide the absorption spectrum is dominated by different absorption bands depending on the acidity; at pH 3.0, the absorption maximum is at 430 nm, at pH 8.0, the band centered around 535 nm is dominating and at pH 14.0 the maximum is at 380 nm. The corresponding pKa has a value of 6.8. This feature is very similar to the one observed for the chromophore isolated from GFP-WT. [Niw96, Kum02] By changing the pH of the solvent and thus decreasing the proton concentration, the peak position moves from 380 nm for the protonated species to the characteristic 445 nm band for the stabilized anionic, deprotonated state R^-. Based on these established assignments of the GFP absorption bands to its protonated and deprotonated chromophore, it can surely be assumed, that the deprotonated state R^- prevails in the protein asFP595, which is possibly related to the

presence of a deprotonated tyrosyl group being a component of the chromophore. This is assumption is consistent with the similarity of the features of the absorption spectra between the intact asFP595 and the chromopeptide at neutral pH.

Pumping of the Fluorescent State by High Intensity Irradiation. Based on the observation of LIFE described in [Luk00], the dependence of both, intensity and spectral characteristics of fluorescence on excitation intensity, and duration is observed. Low intensity irradiation in the absorption band for several hours induces no detectable increase of the fluorescence quantum yield, even when the pigment is immobilized in a PVA matrix to exclude diffusion phenomena (see Chapter 6.5).

Illumination of the sample by a CW-Ar^+ laser (514 nm) at 298 K with increasing excitation intensity in several steps leads to a red shift of the fluorescence spectrum of ~3 nm (Figure 6-3).

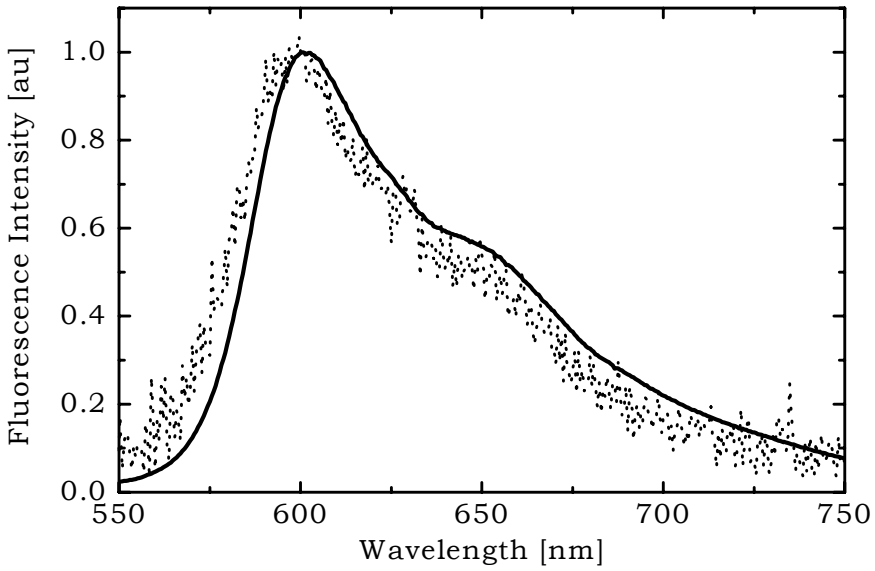

Figure 6-3: Steady-state fluorescence of asFP595-WT, detected at different excitation intensities.

0.04 W/mm² (···) and 10.5 W/mm² (—), $\lambda_{EXC.}$=514 nm by a Ar^+ laser working in CW-mode.

Simultaneously a superlinear dependence of the fluorescence intensity on the excitation intensity can be observed (Figure 6-4). The fluorescence quantum yield increases with excitation intensity by a factor of 30 (Figure 6-5) in the superlinear regime, indicating, that the absorption of two photons is necessary to reach the photoconverted fluorescent state.

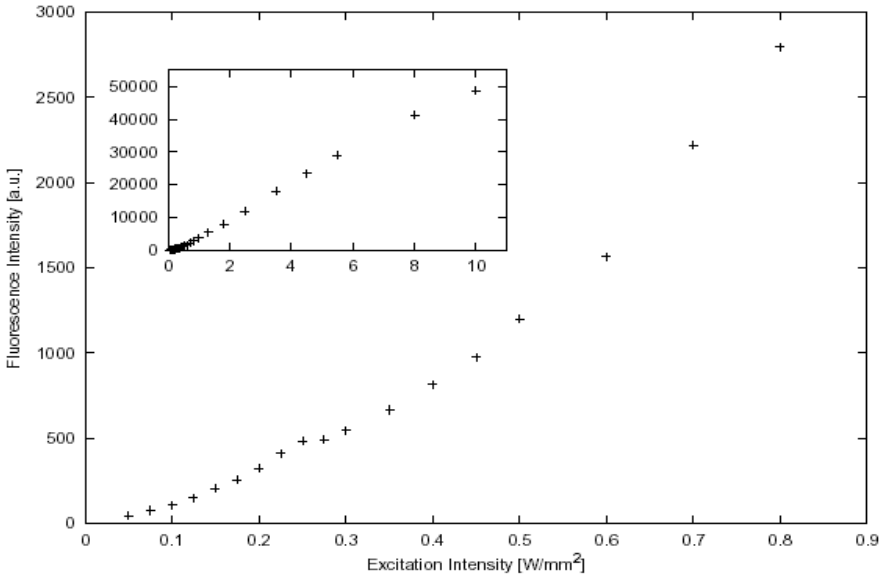

Figure 6-4: Fluorescence intensity versus excitation intensity

$\lambda_{EXC.}$=514 nm by an Ar^+ laser working in CW-mode

The superlinearity is leveling off into a linear dependence at high excitation intensities. Here the fluorescence quantum yield does not depend on the excitation intensity.

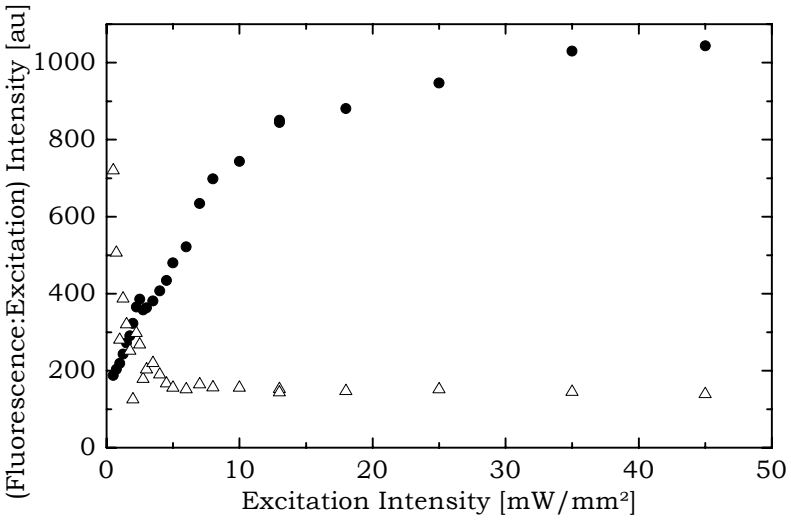

Figure 6-5: Quantum yield versus excitation intensity

• ($\lambda_{EXC.}$=600 nm), Δ ($\lambda_{EXC.}$=500 nm), $\lambda_{EXC.}$=514 nm,

In contrast to the experiments at 298 K, it is easily possible to populate the fluorescent state by illumination at low temperatures even at low excitation intensities. As depicted in Figure 6-6 the fluorescence intensity is increased by a factor of ~16 during a 15 hour exposure to green light (560 nm, 14 µW/mm²).

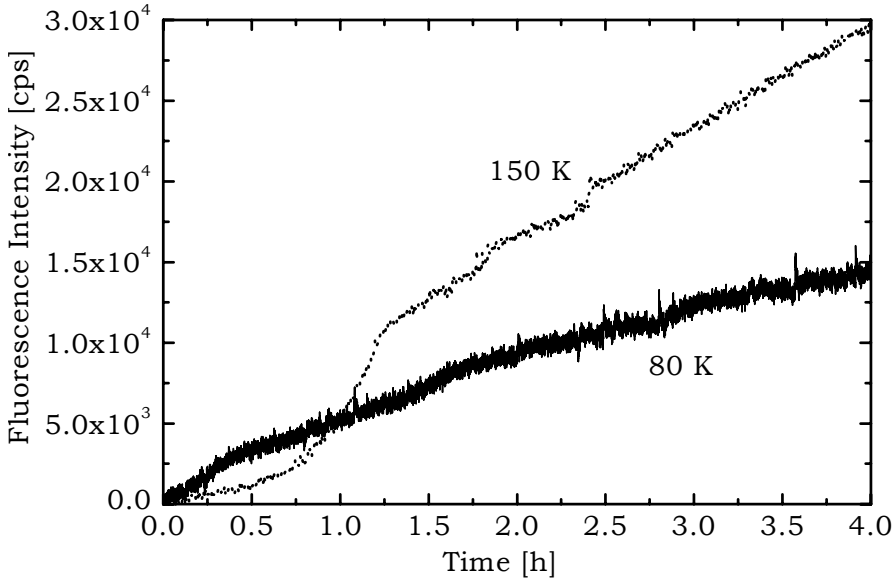

Figure 6-6: Pumping of the fluorescent state

$\lambda_{EXC.}$=514 nm, 150 K (···) and 80 K (—)

Interestingly, the increase of fluorescence is less pronounced at 80 K than at 150 K, independent on the excitation wavelength. Emission and fluorescence excitation spectra are taken before and after illumination (Figure 6-7 A and B).

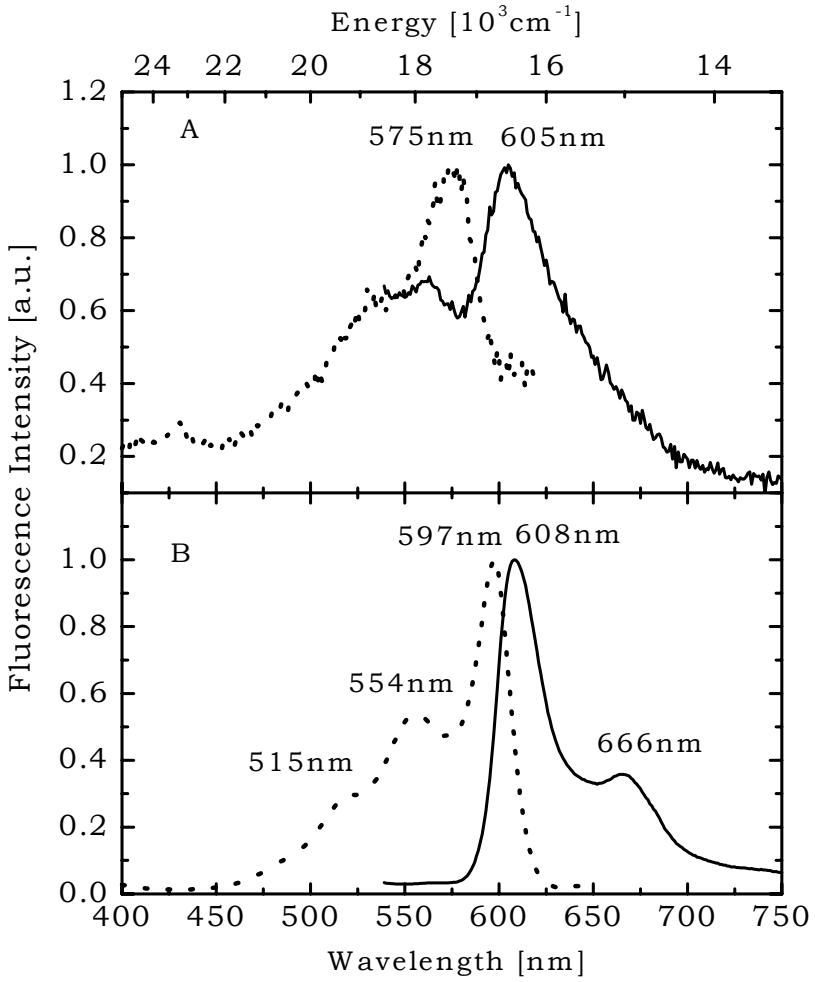

Figure 6-7: Steady-state spectra of asFP595-Wt, 150 K

Emission (—, $\lambda_{EXC.}$=514 nm) and fluorescence excitation (···, $\lambda_{DET.}$=675 nm), 150 K. A) before illumination, B) after 15 h illumination

After 18 h of illumination with 560 nm light at 150 K the fluorescence excitation spectrum shows its maximum at 597 nm with vibronic progression identical to GFP-WT (~1300 cm^{-1}) [Los96]. The emission mirrors the excitation spectrum and peaks at 608 nm. The fluorescence

quantum yield in this fluorescent state is higher by a factor of 20 than in the ground state. The Stokes shift is reduced to 440 cm^{-1}. The corresponding absorption spectrum at 150 K is still dominated by the non-fluorescing flexible state. This points to a very inefficient process leading to increased fluorescence and population of a state with a long lifetime.

The fluorescence and fluorescence excitation spectra of the dark state are still broad and unstructured at low temperatures (Figure 6-7 A). The absorption spectrum is shifted by 12 nm into the red with a vibronic progression of 1100 cm^{-1}.

6.3.2 Fs- and ps- time-resolved absorption and fluorescence spectroscopy

To confirm the result from the steady-state experiments, namely the necessity of a two photon absorption to populate the fluorescent state, femtosecond pump/probe experiments (pulse duration 130 fs, 0.1 μJ) were performed. Probing the population of the excited state as stimulated emission at 595 nm and as ground state depletion at 550 nm, both measurements show similar traces following non-exponential kinetics (Figure 6-8). Global fitting yields three time constants τ_1=319 fs (78 %), τ_2=2.6 ps (19 %), τ_3=12.1 ps (3 %).

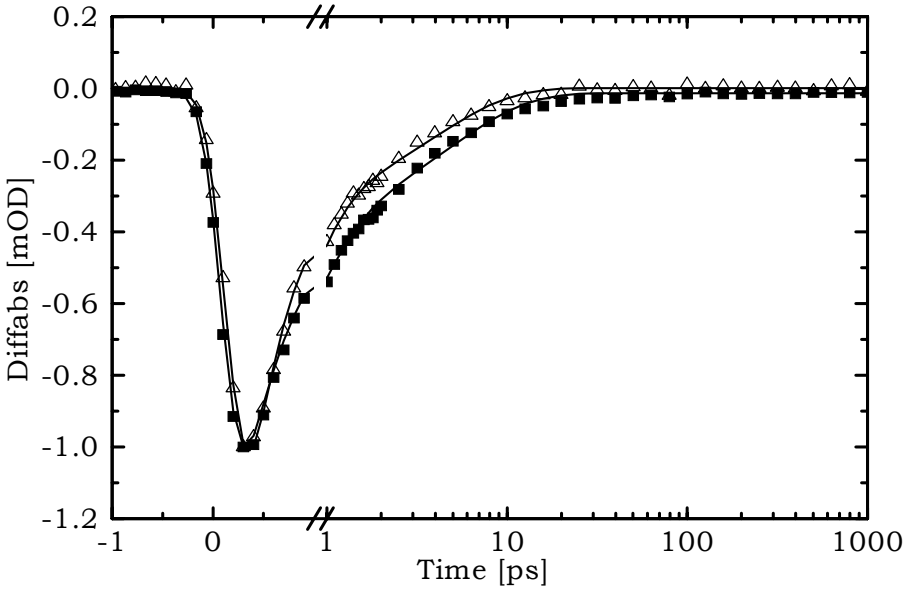

Figure 6-8: Transient absorption spectra of asFP595-WT, 298 K

Evolution of stimulated emission (■ , $\lambda_{DET.}$=590 nm) and ground state recovery (Δ, $\lambda_{DET.}$=550 nm). $\lambda_{EXC.}$= 565 nm. Time resolution 200 fs.

Increasing the excitation intensity by a factor of 10 leads to the presence of a very small ns-component. The time traces for excited state decay and ground state recovery can be fitted globally with the time constants τ_1=532 fs (48 %), τ_2=3.4 ps (39 %), τ_3=35.0 ps (10 %) and τ_4=1.1 ns (3 %). This result proves, that the fluorescent state can hardly be reached upon excitation with a short pulse, even with high excitation power. If a simultaneous absorption of two photons was sufficient to populate this state efficiently, the photon flux of these excitation pulses should be high enough to trigger the conversion. As the amplitude of the ns-component, which can be ascribed to the fluorescent state is extremely small, a consecutive two photon absorption must be required to populate the fluorescing state. Hence the setup was modified to provide a second excitation pulse, which can be delayed in reference to the first one. In such a setup, the LIFE effect was expected to be detectable, if a consecutive two-photon absorption is sufficient to populate the fluorescent state to a detectable amount. Yet the kinetic

traces yield no higher amplitude of the nanosecond component. This implies, that conversion rate into the fluorescent state is very small under the conditions of the experiment.

In order to focus on the increase of the nanosecond component considered to be responsible for LIFE, picosecond time-resolved fluorescence measurements are performed. When the sample is excited at 570 nm with an excitation intensity of ~70 nJ/mm² and a pulse duration of 10 ps, its fluorescence decays exponentially with three time constants τ_1=150 ps (45 %). τ_2=0.8 ns (30 %) , τ_3=2.2 ns (25 %) (Figure 6-9).

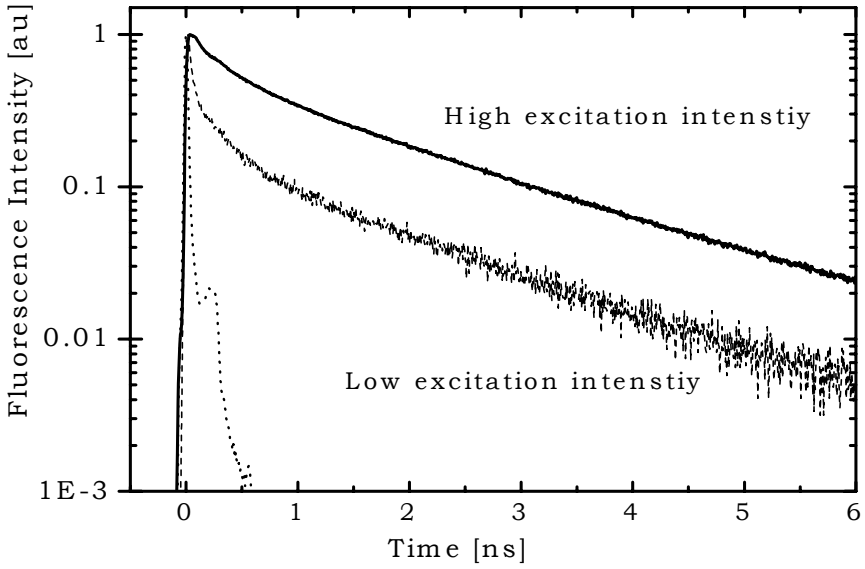

Figure 6-9: Fluorescence decay traces of asFP595-WT, 298 K

With high excitation intensity (—) and low excitation intensity (---, ~30 times lower). $\lambda_{EXC.}$=570 nm, $\lambda_{DET.}$=595 nm, IRF (···, 27 ps FWHM)

For comparison the measurement performed with low excitation intensity is also depicted. The absence of the short time constant on strong illumination can be clearly observed.

6.4 Conclusions

At room temperature the sample is dominated by a species absorbing at 565 nm. It fluoresces at 595 nm with a lifetime of 319 fs resulting in a very low fluorescence quantum yield. Illumination with high excitation intensity leads to photoconversion of the sample, i.e. population of a fluorescent species with a fluorescence maximum at 610 nm and a lifetime of 2.2 ns. As the fluorescence quantum yield of the sample in its original state is only 0.001, [Luk00] a very fast decay channel must lead to efficient fluorescence quenching (k_1), competing with the channel populating the fluorescent state (k_2, Figure 6-10).

If the main deactivation channel of the first excited state of asFP595-WT (k_1) competing with photoconversion (k_2) and fluorescence was either ET, ESPT or ISC, this would lead to population of a metastable intermediate state detectable in transient absorption measurements, on condition that the back reaction is slower than the forward reaction. This is reasonable for such a short lifetime as 319 fs. Furthermore, the excited state decay and ground state depletion signal coincide very well. Hence such a intermediate state can be excluded. This leaves fast IC as the competing dark pathway.

The phenomenon of fluorescence quenching by ultrafast IC has been observed earlier by Kummer et al in GFP bearing the T203Y mutation. [Kum98] In this work average lifetimes at room temperature of 6 ps for RH and 170 ps for the R^- state were reported. Since in transient absorption measurements no intermediate state could be detected and ground state recovery and fluorescence dynamics yield identical time constants, this fast quenching of fluorescence was ascribed to IC. In the single mutant GFP-T203Y the lifetime of the protonated state is even shorter yielding τ_1=1.6 ps (~50 %). [Kum00] As the chromophore in this mutant is known to be tightly bound, [Wac98] rotational motions around one of the bonds cannot lead to such fast decay. As in this mutant the

N2 of the heterocyclic ring is protonated. As a consequence the activation energy for the so-called hula-twist motion with minimized spatial requirements for rotational motion [Web99] is lowered to such an amount, that this concerted simultaneous rotation around both exocyclic C-C bonds becomes very fast. [Voi98] Although ESPT still competes with IC in these mutants, the lifetime of RH* is still in the picosecond range, i.e. an order of magnitude slower than the lifetime measured in asFP595.

Possible mechanisms for the cyclic process of photoconversion (k_2) are ET, ESPT, IC and formation of a triplet state. The kinetic scheme derived from the spectroscopic information is depicted in Figure 6-10.

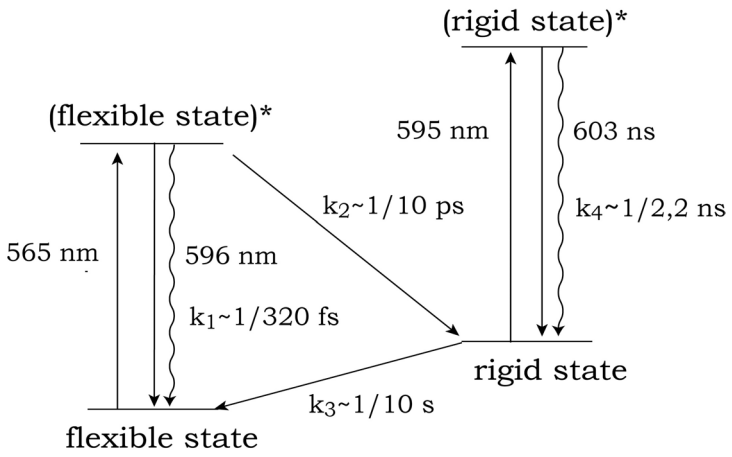

Figure 6-10: Kinetic scheme of the asFP595 photoconversion

As IC is very fast at 298 K, only a small fraction of chromophores can undergo photoconversion. These exhibit fluorescence with a lifetime of 2.2 ns after absorption of a second photon. The following decay to the original weakly fluorescent ground state is slow. [Chu03a,b]

The finding that at 150 K, after more than 20 h illumination with green light, no measurable effect on the absorption spectrum of asFP595 could be observed indicates, that although fast IC is surely slowed, it is still efficient. The formation of the fluorescent state is heavily facilitated at 150 K, as can be concluded from the illumination experiments. At

80 K formation of the fluorescent state is less efficient than at 150 K. This points to a thermally activated photoconversion process. The rate for populating the fluorescent state is temperature dependent and slowed to such an amount, that either the depopulation (k_3) or IC (k_1) of the initial ground state can compete again.

The correlation between fluorescence lifetime, chromophore conformation and environment is displayed in the two recent 3-dimensional structures of the coral pigments Rtms5 [Pre03] and eqFP611 [Pet03]. Both proteins exhibit the well-known 11-stranded β-barrel structure. RTMS5 adopts a markedly different chromophore conformation in comparison to DsRed despite identical chromophore sequences (Gln-Tyr-Gly), [Yar01] resulting in its low fluorescence quantum yield (< 0.0001). The tyrosine ring of the RTMS5 chromophore is non-coplanar and in trans configuration. EqFP611 is fluorescent with a fluorescence quantum yield of 0.45 and a lifetime of 2.5 ns, [Wie02] despite the chromophore motif Met-Tyr-Gly being identical to asFP595. Its chromophore adopts coplanar and trans configuration, with the hydroxyphenyl group sandwiched between His197 and Phe174. As this stacking provides the coplanarity of the tyrosyl group to the imidazolinone ring, the coplanarity seems to be crucial for a high fluorescence quantum yield. A second reason for the stronger fluorescence is, that the sandwiched tyrosyl group has restricted motional freedom. Therefore IC is hindered, resulting in a longer lifetime of the first excited state. In Rtms5 the guanidinium group of Arg197 seems to prevent coplanar orientation of the hydroxyphenyl ring. The pigment has therefore higher motional freedom, which is not restricted by stacking of the hydroxyphenyl ring. This leads to a large IC rate and a low fluorescence quantum yield.

As long as structural evidence is missing, the nature of the drastic increase of fluorescence quantum yield is subject to speculation. Nevertheless, the obvious presence of a fast internal conversion

channel, which implies enough structural freedom of the chromophore to rotate around one of the exocyclic bonds or the presence of a protonated N2 resulting in a hula-twist motion, supports the argument, that restriction of structural freedom is responsible for the increase of fluorescence quantum yield. In case of motion around the exocyclic bonds either the transition to a different conformational state or change of the environment of the chromophore after first excitation could restrict the motion. In case of the hula-twist motion, changing the protonation state by disturbing the hydrogen bridges around the chromophore would enlarge the activation energy of this motion and therefore slow it.

6.5 Similar Photophysical Behavior of AsFP595-WT Immobilized in a Solid Polymer Matrix

In order to establish the assumption, that the LIFE dynamics measured at low temperatures are not caused by addition of glycerol to the protein and thereby perturbing the environment of the chromophore, the protein was immobilized in a solid PVA matrix. In GFP-WT it has been shown, that fixing the protein in a polymer matrix conserves the spectral properties of the GFP protein by scarcely influencing the protein structure (Chapter 4).

The steady-state absorption spectrum of asFP595-WT at room temperature is conserved as expected, when the protein is immobilized in a solid PVA matrix. Surprisingly the corresponding very weak fluorescence is red-shifted by ~20 nm. In contrast to the protein in aqueous solution (Figure 6-2) the fluorescence excitation spectrum of the protein in PVA exhibits two maxima showing no similarity with the absorption spectrum, (Figure 6-11).

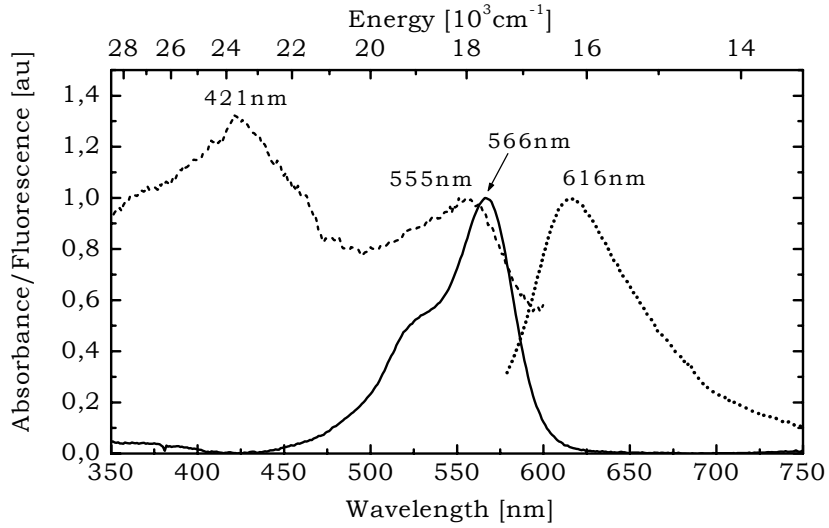

Figure 6-11: Steady-state spectra of asFP595-WT in PVA, 298 K

Absorption (—), fluorescence (···, $\lambda_{EXC.}$=514 nm) and fluorescence excitation (---, $\lambda_{DET.}$=525 nm)

Excitation in the new green band leads to strong blue fluorescence. The red fluorescence is diminished to a small maximum at 625 nm (Figure 6-12).

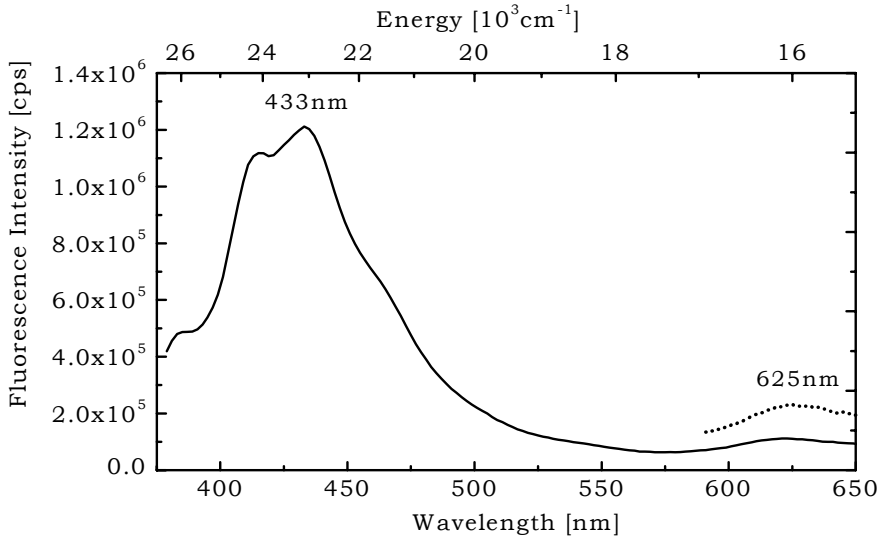

Figure 6-12: Fluorescence spectra of asFP595-WT in PVA, 298 K

$\lambda_{EXC.}$=350 nm (—) and 560 nm (···)

In asFP595-WT in buffer solution also a second fluorescence band can be detected (data not shown). Its maximum is at 492 nm and no trace of the red fluorescence can be detected.

Although the steady-state fluorescence differs from the behavior observed for the protein in solution, the LIFE effect shows similar dynamics, in asFP595-WT in PVA: at room temperature no enhancement of fluorescence is observed, while at 150 K the fluorescent state can be populated easily. Due to immobilization of the protein diffusional artifacts can be excluded. As a consequence, a pronounced temperature dependency of the photoconversion accounts for the differences in LIFE at 298 K and 150 K.

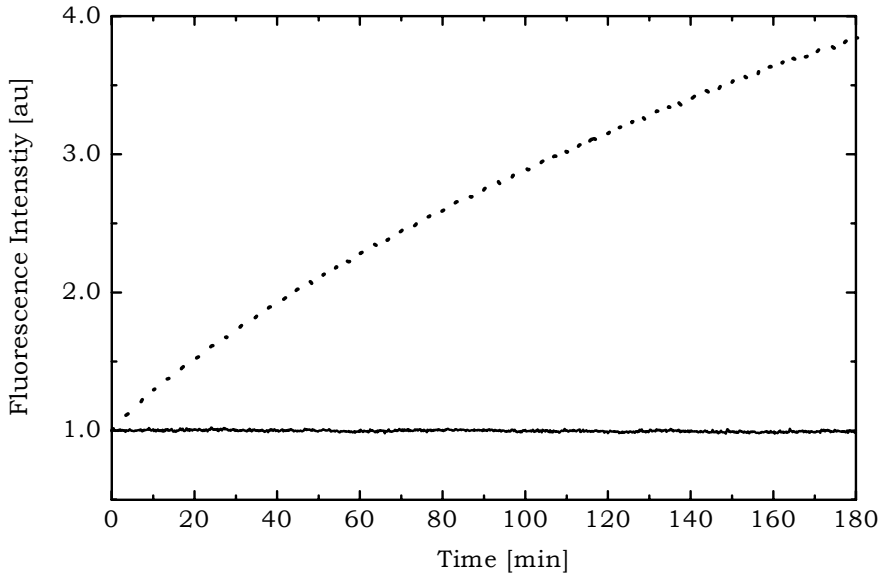

Figure 6-13: 3 h Illumination of asFP595-WT in PVA

$\lambda_{EXC.}$=514 nm, $\lambda_{DET.}$=600 nm, at 298 K (—) and 150 K (···)

Due to technical reasons it was not possible to perform transient absorption measurements on asFP595 protein in PVA. Yet picosecond time-resolved fluorescence measurements yield comparable fluorescence decay kinetics as corresponding measurements of the protein in buffer solution. The decay traces can be fitted by four

exponentials τ_1=17 ps (77 %), τ_2=176 ns (14 %), τ_3=0.9 ns (6 %) and τ_4=3.5 ns (3 %), respectively. The decay of asFP595-WT in buffer solution yields three time constants τ_1=17 ps (84 %), τ_2=230 ns (11 %) and τ_3=1.6 ns (5 %).

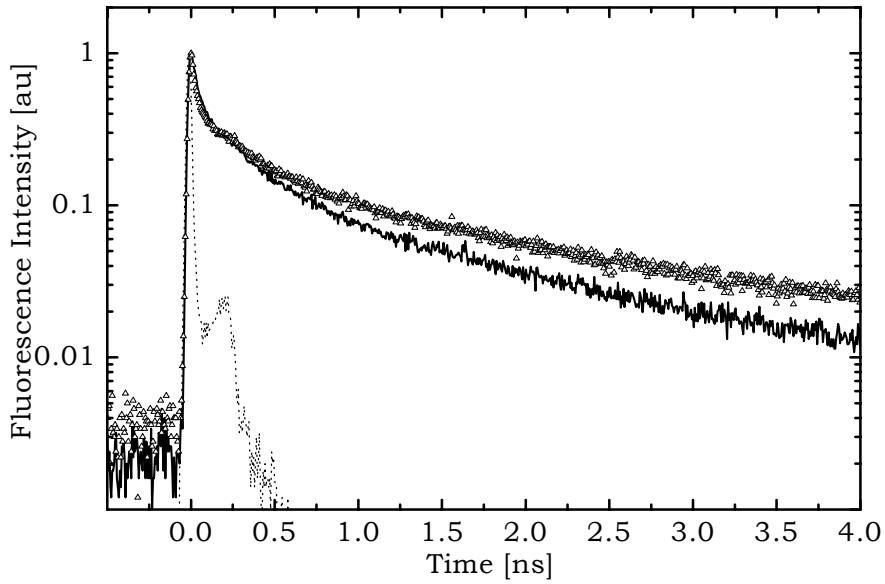

Figure 6-14: Fluorescence decay traces of asFP595-WT, 298 K

In PVA (Δ, $\lambda_{EXC.}$=450 nm) and in aqueous solution, (—, $\lambda_{EXC.}$=390 nm). $\lambda_{DET.}$=595 nm). IRF (···, 27 ps)

Due to the IRF of our TCSPC setup (~25 ps) the system is blind to lifetimes shorter than a few picoseconds, as the fit results for the asFP595 protein in aqueous solution clearly prove. From transient absorption measurements it is known, that the lifetime of the first excited state is <600 fs (Section 6.3.2). The similarity in the fluorescence decay pattern in buffer and PVA leads to the assumption, that the fluorescence lifetime of the protein in PVA is in the range of the protein in buffer, but cannot be resolved in time-resolved measurements.

These results imply, that immobilization of the asFP595 protein has no influence on the LIFE effect and the dynamics required for populating

the fluorescent state, although the steady-state spectra experience a drastic change. This is in contrast to the results of measurements on GFP immobilized in PVA (Chapter 4).

6.6 Drastic Increase of Fluorescence and Observation of FRET in Mutants of the Coral Protein AsFP595

6.6.1 Introduction

The drawback of the low fluorescent quantum yield of asFP595 is subject for several investigations on how to increase fluorescence in such chromoproteins. This goal has been achieved by site-directed and random mutation. With this method Bulina et al. transformed the practically non-fluorescent asFP595-WT into fluorescent variants. [Bul02] They found the positions 148 and 165 to be crucial for high fluorescence quantum yield. As a reference experiment they transformed DsRed into a non-fluorescent form by "proper" mutation. [Bul02] As a side effect, blue and green fluorescent mutants have been created, [Gur01, Luk00] in which the kind of mutation influences the ratio between the fluorescence bands, but scarcely the position of the fluorescence maximum. [Luk00]

The substitution of Ala148 against Ser in asFP595 corresponds to the mutant Rtms5-H146S of pocilloporin from *Montipora efflorescence*, [Pre03] where similar observations have been made. Despite identical chromophore sequences (Gln-Tyr-Gly) in DsRed and RTMS5, the fluorescence quantum yield of the latter protein is smaller by a factor of ~10^3. [Pre03] Interestingly, the fluorescence quantum yield of RTMS5 increases to 0.02 upon replacement of His146 by Ser. [Pre03] The X-ray structure analysis of this mutant (2.4 Å resolution) reveals no large-scale structural changes compared with the wildtype. [Pre03] Yet the possibility cannot be ruled out, that in the fluorescent variant sufficient chromophore mobility has been introduced, allowing the chromophore

in a minority of molecules, which is too small to be observed in the X-ray structure, to adopt a coplanar conformation and consequently lead to an increase in the fluorescence quantum yield. [Pre03]

6.6.2 The single-site mutant asFP595-A148S

This single-site mutant exhibits a higher fluorescence quantum yield (0.012) than asFP595-WT (<0.001). [Luk00] Surprisingly it retains the spectacular possibility of transferring the protein into a fluorescent state by intensive illumination with green light. [Luk00, Chu03a]

Results and Discussion. The steady-state absorption and fluorescence spectra at room temperature resemble the corresponding spectra of asFP595-WT. Although the fluorescence quantum yield in the A148S mutant is larger by almost 2 orders of magnitude compared with asFP595-WT, the fluorescence is still weak. In contrast to the wildtype, its excitation spectrum does not coincide with the absorption spectrum (Figure 6-15). This deviation visible in the arbitrarily normalized steady-state-spectra implies, that the absorbing state is not identical with the emitting state and the low fluorescence quantum yield due to a short lifetime of the first excited state.

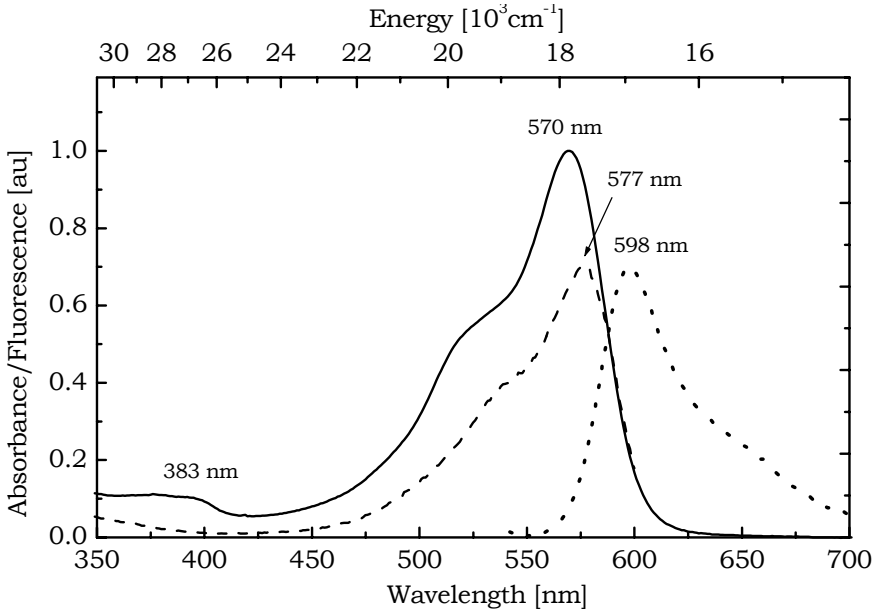

Figure 6-15: Steady-state spectra of asFP595-A148S, 298 K

Absorption (–), fluorescence (···, $\lambda_{EXC.}$=530 nm) and fluorescence excitation (---, $\lambda_{DET.}$=650 nm)

The steady-state fluorescence signal is dominated rather by a minority of molecules fluorescing with a long lifetime, while the majority looses its energy via a fast deactivation channel.

Upon cooling the sample below the glass point to 150 K, the absorption maximum shifts into the red and coincides now with the maximum of the fluorescence excitation spectrum, which is not affected by the low temperature (Figure 6-16). Yet the main absorbing species contributes even at 150 K maximally ~50 % to the red fluorescence.

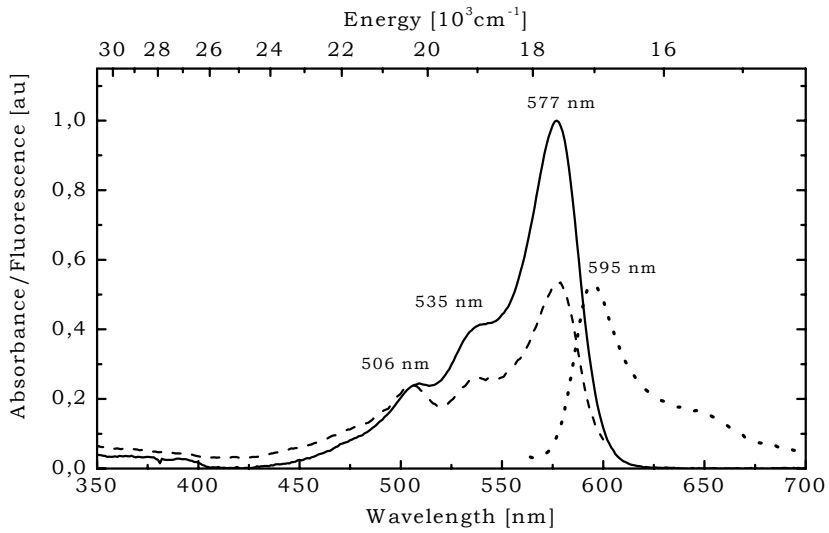

Figure 6-16: Steady-state spectra of asFP595-A148S, 150 K

Absorption (–), fluorescence (···, $\lambda_{EXC.}$=530 nm) and fluorescence excitation (---, $\lambda_{DET.}$=650 nm).

The deviation of the fluorescence excitation spectrum from the absorption spectrum points to the fast decay channel still competing with fluorescence.

In order to investigate, whether the nature of this fast deactivation channel is fast IC as is the case in asFP595-WT, transient absorption measurements are performed. The time traces excited at 532 nm and detected in the range of stimulated emission between 560 nm and 650 nm, are multi-exponential and can be fitted globally with τ_1=243 fs (56 %), τ_2=52 ps (13 %), τ_3=386 ps (13 %) and τ_4=2.4 ns (18 %). It is interesting to note, that these time constants coincide well with the decay kinetics measured in asFP595-WT, pointing to the same deactivation channel, i.e. fast IC, being active in WT and mutant. The amplitude of the ns-component in asFP595-A148S is higher by a factor of six compared to WT. It originates from a species, in which fast IC is inhibited, consequently dominating the steady-state fluorescence spectrum.

Most surprisingly the LIFE effect can be achieved in asFP595-A148S. [Luk00] Therefore the ns-component observed in the transient absorption measurements is investigated further with time-resolved fluorescence measurements. High energy excitation at 570 nm results in a multi-exponential decay, which can be fitted with three time constants τ_1=236 ps (58 %), τ_2=1.5 ns (18 %) and τ_3=3.0 ns (24 %) (Figure 6-17). This decay kinetics are in parallel with the results of the corresponding measurements of asFP595-WT (Chapter 6.3.2).

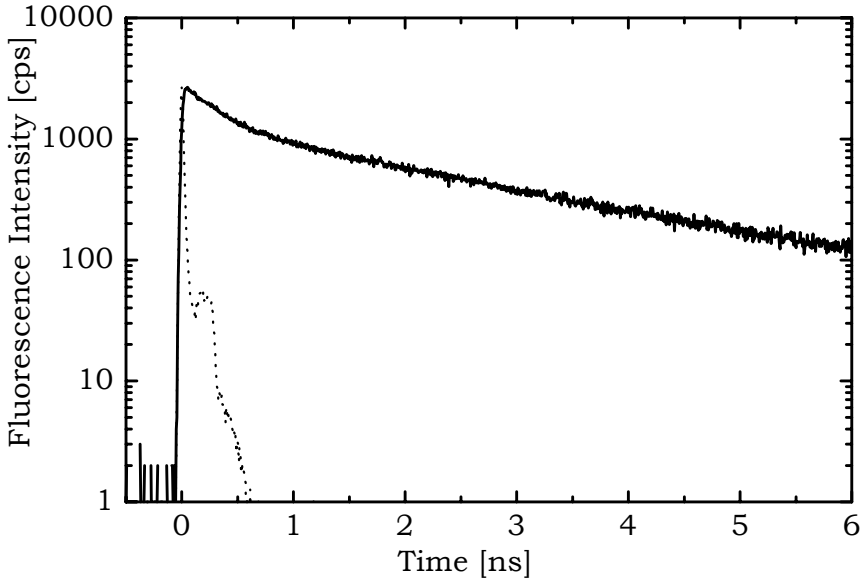

Figure 6-17: Fluorescence decay traces of asFP595-A148S, 298 K

($\lambda_{EXC.}$=570 nm, $\lambda_{DET.}$=595 nm) with high excitation intensity, IRF (···, 27 ps)

Conclusions. The transient absorption measurements show, that fast IC occurs in the single-site mutant asFP595-A148S. The amplitude of the ns-component is higher by a factor of six compared to WT in its fluorescent state, resulting in a higher fluorescence quantum yield.

The shortest decay time here of 236 fs is in the range of the fastest decay time measured in asFP595-WT. This leads to the conclusion, that the mutation does not influence the efficiency of IC. It rather implies, that a higher percentage of the molecules contains a chromophore in a rigid conformation, fluorescing with a ns-lifetime. This conclusion is

confirmed by the shifted fluorescence excitation spectrum, which does not follow the absorption spectrum, hinting to a second species to be responsible for the steady-state fluorescence signal. Consequently it can be said, that it is possible to stabilize a red emitting state by mutation of A148S.

The most interesting result is the proof, that time-resolved measurements of asFP595-A148S, excited with high intensity light show similar decay kinetics as measurements of as asFP-WT under similar conditions. It can be concluded, that this mutation does not influence the processes leading to the LIFE effect.

6.6.3 Population of a green absorbing state with highly quenched fluorescence after substitution in the chromophore

The mutant R6 investigated in this section is a triple mutant bearing the substitutions C64A, M65Q and T70A. Position 148 remains unchanged. Mutation of methionine 65 against gluthamine leads to an identical chromophore motif as in DsRed: Gln-Tyr-Gly. Therefore the photophysical behavior is expected to mimic the spectroscopic features of DsRed.

Results and Discussion. In this mutant a green absorption maximum additionally to the expected red absorption can be detected. The fluorescence maximum of the mutant R6 peaks at 587 nm and resembles strongly the fluorescence spectrum of DsRed ($\lambda_{MAX.}$=586 nm). As no green fluorescence can be observed, it has to be quenched very efficiently (Figure 6-18). The excitation spectrum of the dominant red fluorescence coincides well with the absorption spectrum in the low energy range, but misses the green absorption band completely.

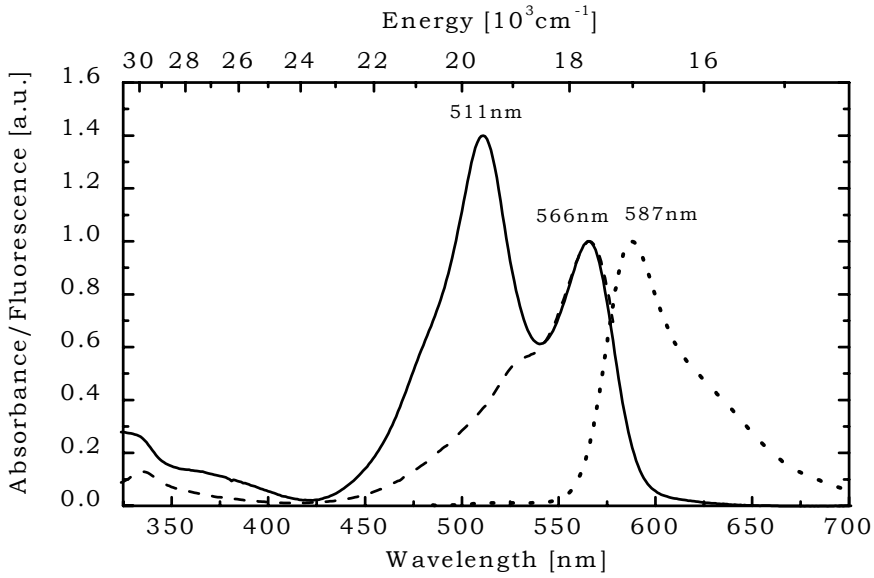

Figure 6-18: Steady-state spectra of asFP595-R6

Absorption (–), fluorescence (···, $\lambda_{EXC.}$=475 nm) and fluorescence excitation (---, $\lambda_{DET.}$=588 nm)

In order to investigate the dynamics of fluorescence quenching, time-resolved fluorescence measurements were performed. Upon excitation at 445 nm the fluorescence decay traces detected between 500 nm and 520 nm yielded four time constants τ_1=15 ps (68 %), τ_2=85 ps (26 %), τ_3=630 ps (5 %) and τ_4=2.5 ns (1 %). The shortest time component is on the verge of the time-resolution, therefore the fit result gives only an upper limit for this time constant. Upon detection in the red wing of the steady-state fluorescence band, the short component presents itself as a rise component by its negative amplitude (Figure 6-19). The fit yields four time constants τ_1=42 ps (-50 %), τ_2=83 ps (29 %), τ_3=1.5 ns (5 %) and τ_4=3.7 ns (17 %).

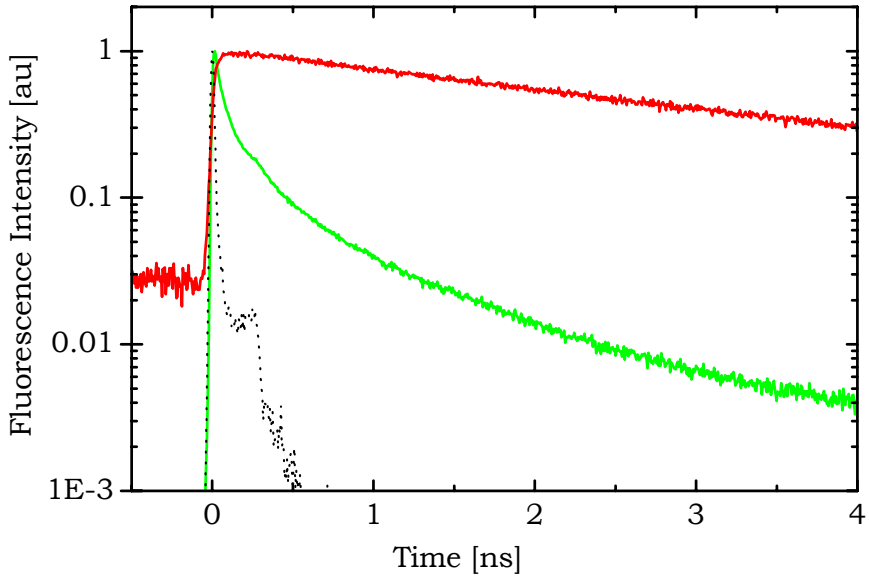

Figure 6-19: Fluorescence decay traces of asFP595-R6

$\lambda_{EXC.}$=445 nm, $\lambda_{DET.}$=500 nm (green) and $\lambda_{DET.}$=630 nm (red), IRF (···, 25 ps)

The shortest decay time of 15 ps of the green fluorescence together with a concomitant rise in the onset of the red fluorescence signal parallels the fluorescence dynamics of DsRed, which is explained by FRET from the green fluorescing precursor chromophore to the maturated red fluorescing chromophore (Chapter 5). [Schüt01] In contrast to DsRed, the rise component in asFP595-R6 (42 ps) does not mirror the short decay time (15 ps), implying that FRET from the green species to the red fluorescing is active, but not the main process for quenching the green fluorescence.

The drastic deviation between fluorescence excitation spectrum and absorption has been observed in several GFP mutants and was explained either by fast IC [Kum98] or by ultrafast ET [Kum00a] as deactivation channel competing with fluorescence. IC, which is also the main process for quenching the red fluorescence in asFP595-WT, would lead to additional shortening of fluorescence lifetime, resulting in a discrepancy of decay and rise components in the time-resolved fluorescence measurements.

The average of the ns-components (3.2 ns) is in the range of the lifetime of the deprotonated state of GFP [Los96] and can be assigned to molecules with a rigid chromophore formation, which does not allow for fast IC. Due to the long lifetime this species dominates the steady-state fluorescence spectrum.

Conclusions. The steady-state spectra experience a dramatic change compared to asFP595-WT, when the chromophoric amino acid Met65 is substituted by Gln. In the absorption spectrum a green species can be observed without exhibiting detectable green fluorescence. In DsRed the existence of a green absorption band is due to hindered maturation of the chromophore. [Wie02] Together with the similar fluorescence spectrum, this green absorption points to the identical chromophore motif to be responsible for similar chromophore formation process as in DsRed.

Time-resolved measurements yield a short lifetime of ~15 ps when detected in the green spectral range. Detection in the red wing of the low energy fluorescence band reveals a ~3 times longer rise component. The wavelength dependence of the short fluorescence decay time together with the presence of a rise component in the red wing of the detection range is certainly a fingerprint of energy transfer between a green emitting and the red emitting species similar to DsRed. (Schüt01] Yet the rise time in the asFP595 mutant does not mirror the decay time, therefore FRET cannot be the only radiationless deactivation channel of the green fluorescence. The most probable explanation for further shortening of the green fluorescence lifetime is fast IC, which has been reported for GFP [Kum02a] and asFP595-WT (Chapter 4.4 and 6) to lead to drastic shortening of the first excited singlet state.

The evidence of FRET in this Ds-Red like mutant indicates, that these mutations further cause a tendency to form dimers or oligomers. This assumption could be confirmed by transient absorption measurements,

but due to technical reasons these measurements had not been performed.

Lukyanov et al reported, that mutation in the surrounding of the chromophore led to additional green fluorescence. The nature of the substitution influences not so much the position of absorption and fluorescence bands as the ratio between green and red fluorescence. [Luk00] Therefore the mutants A148S/T70A/E201x and A148S/S165V are investigated. The position A148 plays a dominant role in quenching the red fluorescence of asFP595-Wt as already observed in the single-site mutant asFP595-A148S (Section 6.6.2).

6.6.4 The triple mutants A148S/T70A/E201x

The first mutation to be examined is Glu201. It is replaced by either alanine, valine or leucine (mutants E201A, E201V, E201L). As a casual mutation threonine 70 is replaced by alanine.

The steady-state absorption and fluorescence spectra of the mutant E201A are depicted in Figure 6-20. Most interestingly, the excitation spectrum of the dominant red fluorescence does not coincide at all with the absorption spectrum. This leads to the assumption, that only a minority of molecules contributes to the steady-state fluorescence spectrum. The majority of pigments possess a chromophore with a high degree of motional freedom in its green absorbing state as well as in its red absorbing state, leading to efficient quenching of both green and red fluorescence by fast IC.

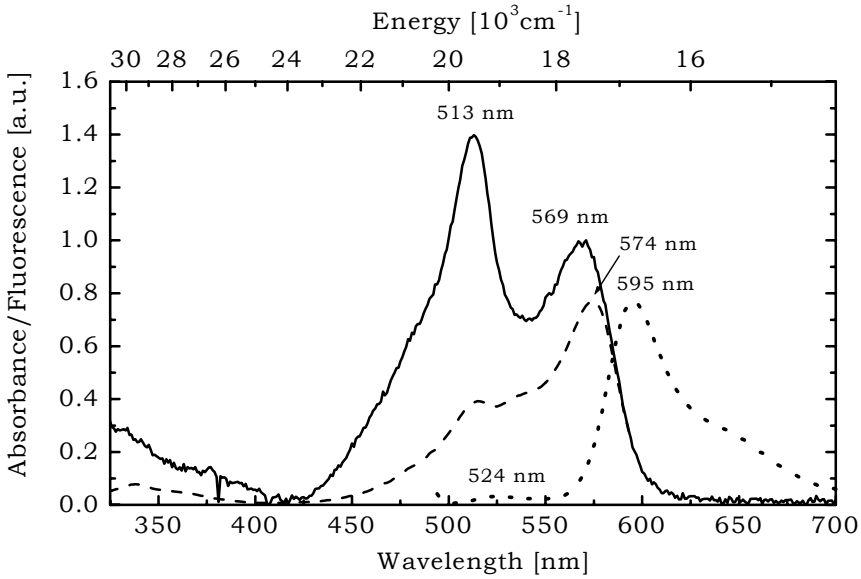

Figure 6-20: Steady-state spectra of asFP595-E201A

Absorption (–), fluorescence (···, $\lambda_{EXC.}$=480 nm) and fluorescence excitation (---, $\lambda_{DET.}$=630 nm)

Further substitution of E201 by either valine or leucine leads to pronounced stabilization of the green absorbing species (Figure 6-21).

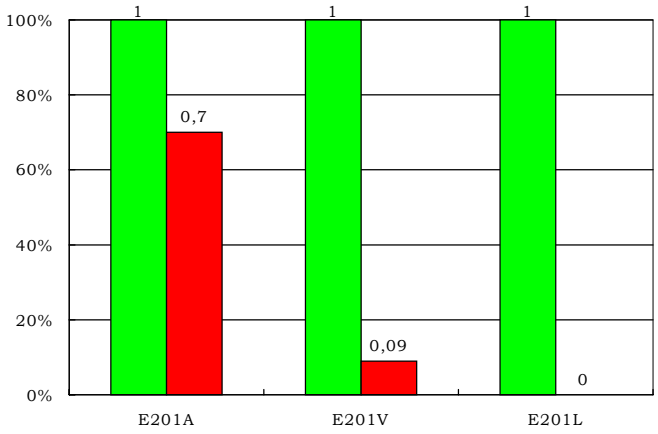

Figure 6-21: Normalized ratios of absorption

E201L could even be called „green-fluorescent“ mutant, since the low energy band is completely missing in its absorption and fluorescence excitation spectrum. Consequently, its fluorescence spectrum is

dominated by a strong fluorescence at 524 nm with only a small shoulder at 595 nm (data not shown).

6.6.5 Stabilization of a blue species by the double mutation A148S/S165V

Additionally to the green and the red state exhibits the double mutation asFP595-A148S/S165V a blue absorbing species (Figure 6-22). Excitation in this band leads to a weak emission signal at 450 nm and two dominant fluorescence bands in the green and red wavelength range. It is interesting to note, that the red fluorescence is red-shifted by 17 nm with respect to asFP595-WT. The excitation spectrum of the red emission follows the absorption spectrum in the low-energy range, but deviates strongly in the high-energy range.

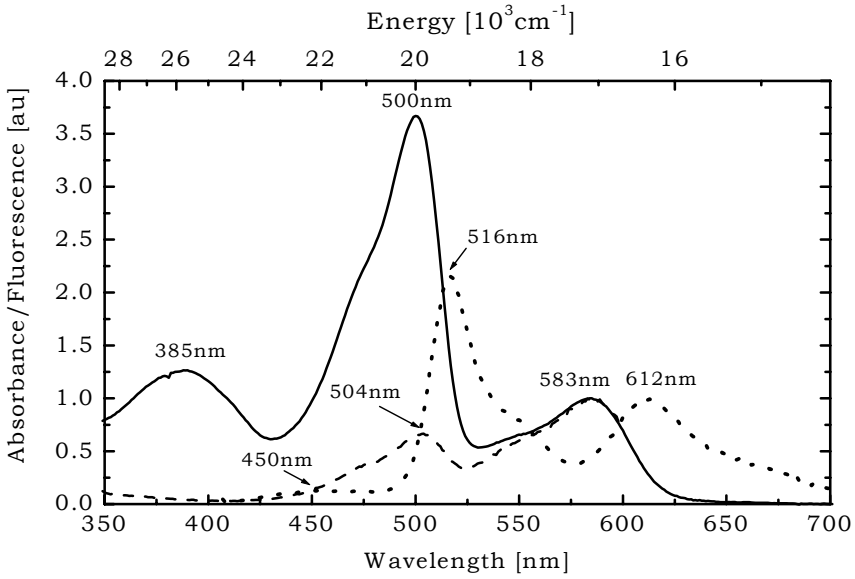

Figure 6-22: Steady-state spectra of asFP595-A148S/S165V

Absorption (–), fluorescence (···, $\lambda_{EXC.}$=390 nm) and fluorescence excitation (---, $\lambda_{DET.}$=670 nm).

In this mutant the green species exhibits strong fluorescence itself and therefore contributes only to ~50 % to the red emission, implying a

chromophore with less motional freedom as in the mutant asFP595-R6 (Figure 6-18).

Time-resolved fluorescence measurements show, that FRET between the green fluorescing and the red fluorescing species occurs in the double mutant A148S/S165V. Upon excitation at 445 nm the decay traces detected in the green emission band (Figure 6-23) can be fitted with the time constants τ_1=28 ps (41 %), τ_2=156 ps (31 %), τ_3=604 ps (21 %) and τ_4=1.6 ns (7 %). Detection in the red fluorescence band leads to the shortest time constant representing a rise component marked by its negative amplitude: τ_1=70 ps (-100 %), τ_2=0.9 ns (60 %) and τ_3=2.2 ns (40 %).

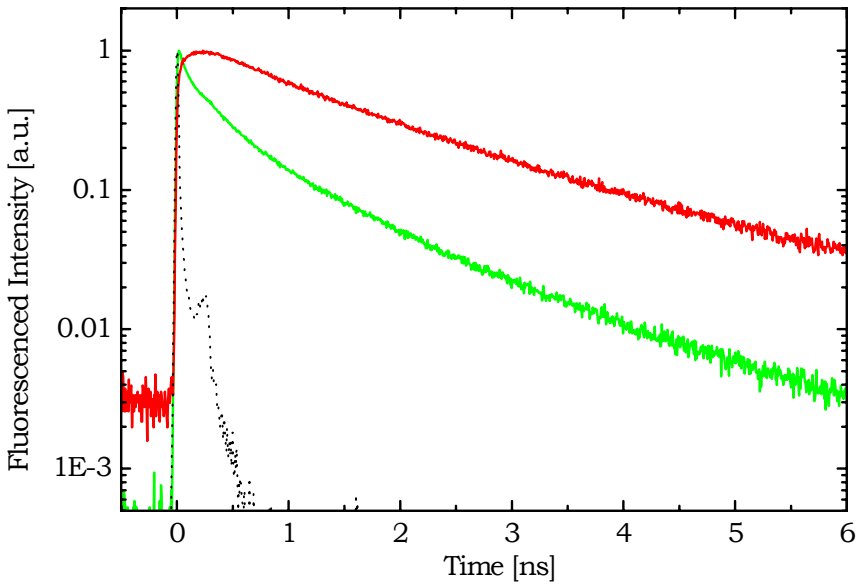

Figure 6-23: Fluorescence decay traces of asFP595-S165V

$\lambda_{EXC.}$=445 nm, $\lambda_{DET.}$=500 nm (green) and $\lambda_{DET.}$=650 nm (red), IRF (···, 25 ps)

Again the rise component is by a factor of ~2 slower than the shortest decay time of the green fluorescence (28 ps). Again FRET is obviously not the only deactivation channel, leading to the quenching of the green fluorescence, but competing with IC. Comparison with the fluorescence decay kinetics of the mutant asFP595-R6 suggests IC being less

efficient in the mutant A148S/S165V. As a consequence, the green fluorescence can be observed in the steady-state fluorescence spectrum.

Conclusions. Mutations in the environment of the chromophore in asFP595 lead to the stabilization of a green and, in case of the mutant A148S/S165V, a blue absorbing species. Comparison with GFP and DsRed indicates, that this species corresponds well to the protonated chromophore RH.

The triple mutation A148S/T70A/E201x leads to increased motional freedom of both green and red absorbing species, as the fluorescence excitation spectrum deviates strongly from the absorption spectrum. In contrast, the mutation A148S/S165V stabilizes the red fluorescing species, which exhibits a lifetime of 3.7 ns in time-resolved fluorescence measurements and consequently dominates the fluorescence spectrum. From the discrepancy in the decay traces of time-resolved measurements detected in the green emission band and the onset of the red fluorescence it can be concluded, that in all investigated mutants the green fluorescence is highly quenched by two competing processes: i) IC and ii) FRET from the green fluorescing to the red emitting species. Applying the FRET scenario derived from DsRed to these mutants points to hindered maturation of the asFP595 chromophores because of mutation in the chromophore or in its vicinity. It furthermore hints to a tendency to form dimers or oligomers with chromophores in different maturation states.

7 Primary Photophysics of the FMN binding LOV2 domain of the plant Blue Light Receptor Phototropin

7.1 Structure and Function of the LOV2 Domain

The LOV domains (molecular weight 12.1 kDa) can be easily bleached under high excitation intensity giving rise to a new absorption band at 390 nm. Comparison with the spectroscopic features of mercuric ion reductase [Mil90] led to the conclusion that the transient product state is a flavin carbon C(4a)-thiol adduct. In LOV2 this metastable adduct is formed within 4 μs from a intermediate which resembles the flavin triplet state on the basis of its absorption spectrum. This adduct recovers spontaneously with a halftime of ~50 s [Swa01] (Figure 7-1).

The observation that the adduct does not form in the mutant LOV2-C39A confirmed independently the decisive role of cysteine at position 39 being the amino acid of central importance for the initiation of the reversible photocycle. [Sal00, Swa01] Instead flavin radical is formed together with irreversible alkylation of the N(5) position of the FMN cofactor, when the cysteine in the LOV 1 domain of *Clamydomonas reinhardtii* is replaced by methionine. M65 builds a bridge to N(5) of FMN causing a large red-shift of the flavin radical spectrum. [Kot03, Bit03]

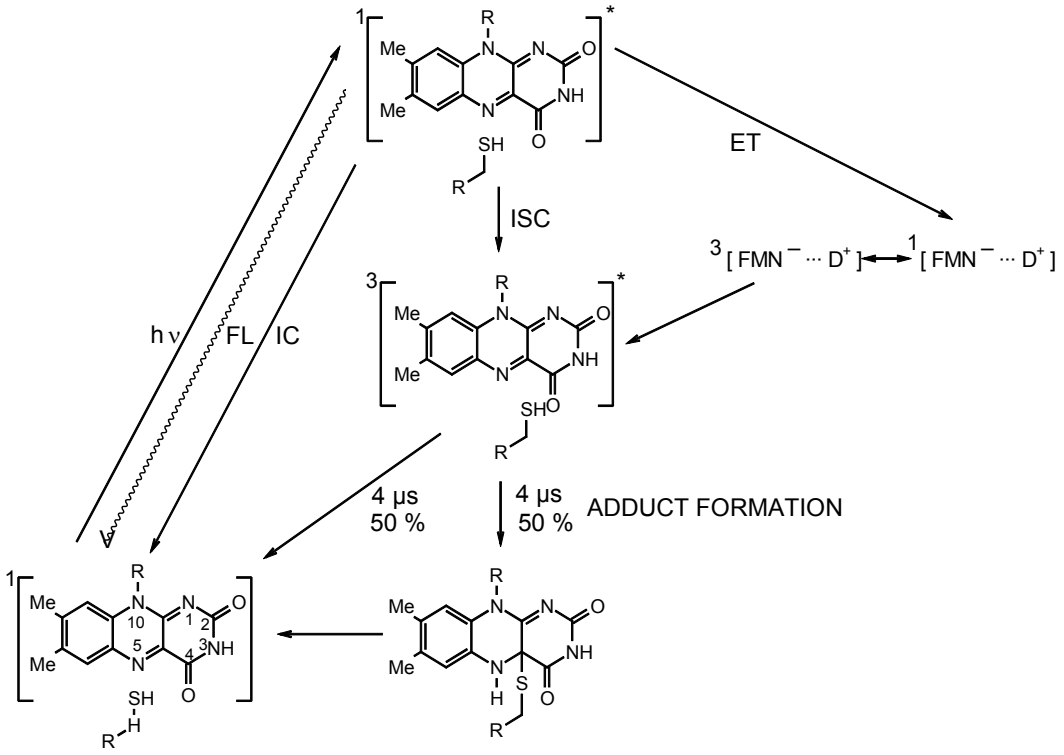

Figure 7-1: Photocycle of the LOV2 domain.

R-SH indicating Cys39. Potential deactivation channels of the singlet excited state ^{1}FMN* are fluorescence (FL), internal conversion (IC), formation of triplet ^{3}FMN* via intersystem crossing (ISC) or radical pair recombination following spin conversion induced by hyperfine interaction. In the latter case the primary process is the reduction of FMN by a nearby donor species (D = tryptophane or tyrosine).

These conclusions on the mechanism are confirmed by the X-ray structural analysis [Cro01] of the LOV2 domain from *Adiantum capillus-veneris* phy3 (at 2.7 Å resolution, Figure 7-2 A). A single molecule of FMN is bound non-covalently in the interior of the protein by a network of hydrogen bonds as well as van der Waals and electrostatic interactions. The flavin-binding pocket is primarily polar on the pyrimidine side of the isoalloxazine ring and non-polar around the dimethylbenzene moiety. There are two buried water molecules, one forming a hydrogen bond to the 2'hydroxyl group of the ribityl chain and the other to the flavin's 3'hydroxyl group; both water molecules form hydrogen bonds to the side chain of asparagine 965.

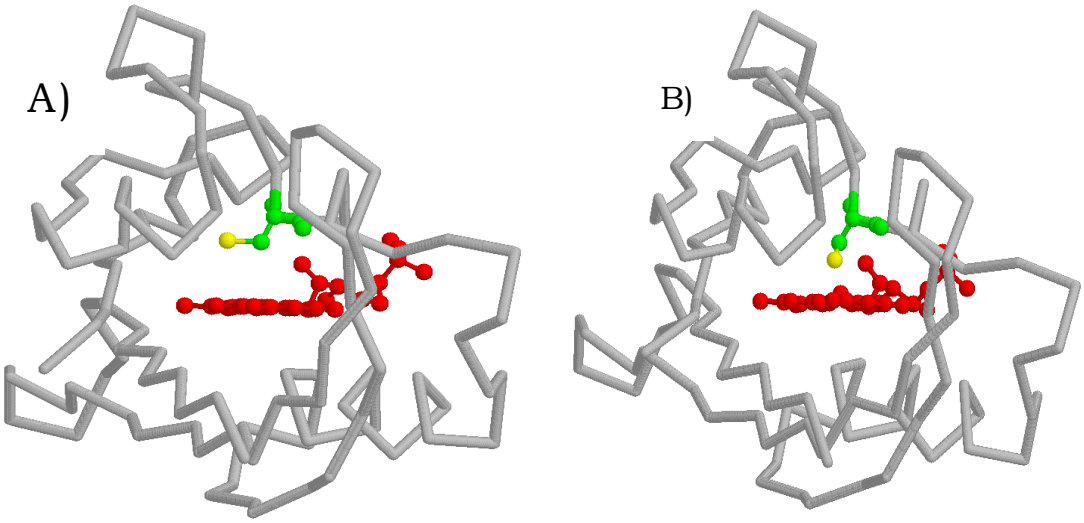

Figure 7-2: X-ray structural analysis of LOV2-WT

In A) its dark state and B) after illumination

Most relevant for the mechanism of adduct formation is the observation that there is no indication of a hydrogen bond to nitrogen 5 of the flavin isoalloxazine moiety. Spectroscopic investigations on LOV1-WT and LOV2-WT domains and mutants of *Avena sativa* Phot1 [Sal00] have shown that cysteine C39 is not essential for flavin binding but is crucial for the reversible photocycle depicted in Figure 7-1. On the basis of dark-light difference absorption spectra and NMR investigations [Sal01] the formation of a C(4a)-cysteinyl adduct has been postulated. [Sal00]

In fact, the X-ray structural analysis of LOV2-WT (*Adiantum capillus-veneris* phy3) in its bleached state revealed a unique photochemical switch in the flavin binding pocket, where the absorption of light drives the formation of a reversible covalent bond between a well conserved cysteine residue and the flavin cofactor at the carbon atom (4a). This structural work provides a highly resolved (2.3 Å) molecular picture of a cysteinyl-flavin covalent adduct which is responsible for phototropin kinase activation and subsequent signal transduction (Figure 7-2 B). These studies show (i) a ~8° tilt of the FMN isoalloxazine ring and (ii) the rotation of the C39 side chain by 100° around the C_{α}-$C_{ß}$ bond [Cro02] which induces a displacement of the sulfur atom by 2.3 Å. This sulfur

atom is now located within covalent bonding distance of the carbon(4a) of FMN. These results were recently confirmed for the LOV1 domain from *Clamydomonas reinhardtii* by the X-ray structural analysis of the dark state and the bleached state at 1.9 Å and 2.8 Å resolution, respectively. [Fed03] This study also revealed the formation of a covalent bond between the flavin C4a and cysteine at position 57.

As indicated in the kinetic scheme (Figure 7-1), triplet formation may in principle proceed via two different mechanisms: singlet-triplet intersystem crossing (ISC) and singlet-triplet spin-conversion in a primary radical pair induced by hyperfine interaction [Mic79, Vol99]. As extensively shown in the recent literature oxidized flavin in its excited singlet state may take up an electron from nearby tyrosine or tryptophane thus forming a singlet phase radical pair. [Zho01, Web02]

In the structure of the LOV2 domain the four potential candidates with electron donor properties are the amino acid residues Y29, Y72 and Y97 and W80, which are located at average center-to-center distance from flavin of ~14 Å. In the context of this work it should be added, that at high light intensities the photo-generated triplet state has been shown to act as a potent oxidant [Kay03] for redox active amino acid residues in a mutant with a triplet lifetime exceeding the one of the native LOV2 domain.

7.2 Experimental

7.2.1 Protein expression and purification of the LOV2 domains

Cloning of the LOV2 domain of the cDNA from *Avena sativa* Phot1 into the bacterial expression vectors pCAL-n-EK as a fusion to the calmodulin binding peptide (CBP) was carried out as described recently [Chr99]. Site directed mutagenesis to generation the mutant LOV2 protein LOV2-C39A was performed according to the Quick Change protocol

from Stratagene. For expression of the fusion proteins the *E. coli* host strain BL21(DE3) pLysS was used. Expression of the LOV proteins was induced by the addition of isopropyl ß-D-galactopyranoside (1 mM, final concentration) when the culture has reached an OD_{600} of 0.2-0.3. Expression was carried out at 30°C in the dark for 3.5 hours. Cells were lysed overnight at -20°C in the presence of 0.2 % Triton-X 100. Purification of the CBP-fusion proteins on calmodulin resin was performed according to the instructions of Stratagene. The purified fusion proteins were stored at 4°C in high-salt elution buffer (1 M NaCl, 50 mM Tris-HCl, pH 8.0, 10 mM ß-mercaptoethanol, 2 mM EGTA).

7.2.2 Fluorescence quantum yields

For determination of the fluorescence quantum yields of LOV2-WT and LOV2-C39A, samples were diluted to an OD of 0.047. As standard a solution of fluorescein in 0.1 M NaOH was used (Φ_{FL} = 0.925) [Mag02]. All measurements were carried out in quartz cuvettes with a path length of 2 mM.

7.3 Results and Discussion

7.3.1 Steady-state spectroscopy

All time-resolved measurements are based on the steady-state absorption, fluorescence and fluorescence excitation spectra of the LOV2-WT domain and LOV2-C39A mutant taken at low light intensity at 298 K. Figure 7-3 shows, that the respective spectra for WT (A) and mutant (B) are nearly identical.

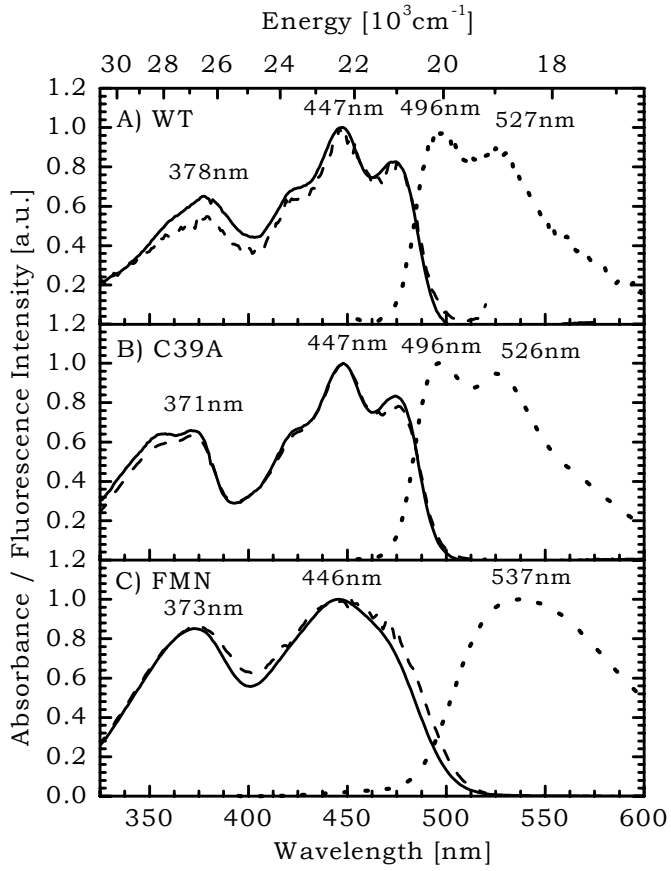

Figure 7-3: Steady-state spectra of (A) LOV2-WT (B) LOV2-C39A, and (C) FMN free in aqueous solution, pH 8

Absorption (—), fluorescence (···, $\lambda_{EXC.}$=475 nm) and fluorescence excitation (---, $\lambda_{DET.}$=525 nm) spectra at 298K and low intensity

In analogy to the spectroscopic features of oxidized flavins the positions of the absorption peaks at 373 nm and 447 nm of both WT and mutant are assigned to the $S_0 \rightarrow S_2$ and the $S_0 \rightarrow S_1$ transitions, respectively. Considering the high sensitivity of the $S_0 \rightarrow S_2$ absorption band of oxidized flavin to the polarity of the environment, [Hee82] it is interesting to note that in both proteins the position of this band resembles the one of FMN free in aqueous solution. This similarity is consistent with the highly polar pyrimidine site of the isoalloxazine ring in the protein pocket. [Cro02] Within the $S_0 \rightarrow S_1$ absorption band a vibronic structure is clearly resolved in the protein. This feature points to a reduction of

inhomogeneous broadening of the flavin chromophore fixed in the protein binding pocket as compared with FMN in solution.

Deconvolution with three Gaussian profiles results in peaks for LOV2-WT/LOV2-C39A at 425 nm/428 nm, 449 nm/450 nm and 475 nm/476 nm with an average Full-Width-Half-Maximum (FWHM) of 600 cm^{-1} exhibiting a relative intensity of 0.3 : 0.4 : 0.3 and a vibronic progression of approximately 1200 cm^{-1}. This progression is in agreement with previous observations on oxidized flavins in non-polar solutions [Mül73, Ewe79]. As to be expected, the fluorescence excitation spectrum follows the absorption spectrum. The fluorescence spectra of both LOV2 samples show also vibronic progression responsible for two maxima, which can be deconvoluted into two vibrational bands peaking at 493 nm and 520 nm. The vibronic progression of 1070 cm^{-1} in the ground state is slightly smaller than for the excited state. Since the relative amplitudes of these emission bands are 0.4 : 0.6, they are not a mirror image of the corresponding absorption spectrum. This effect has been observed previously for free flavins in frozen solution at 77 K [Ewe79] as well as for the flavin fluorescence spectrum of the LOV1 domain of *Clamydomonas reinhardtii* Phot1, for both WT and mutant where cysteine is replaced by serine. [Hol02] If the lifetime of the excited electronic singlet state S_1 is sufficiently long for the excited molecules to attain thermal equilibrium, the fluorescence emission occurs primarily from the zero-point vibrational level of S_1. If the nuclear configurations of the ground and excited electronic states are sufficiently similar, the vibrational wave functions are the same. This assumption is the basis for the empirical mirror symmetry relation between the fluorescence and absorption spectra which is commonly observed in condensed media and also reported for the preparations of the LOV2 domain described in reference [Ken03]. Deviations from mirror symmetry as encountered in the fluorescence spectra of the LOV2 domain in Figure 7-3 as well as the LOV1 protein indicate differences in the nuclear configurations in the electronic ground and excited states, S_0 and S_1.

In contrast to FMN bound to either LOV2-WT or LOV2-C39A, the spectra of free FMN in aqueous solution at pH 8.0 are devoid of vibronic structure. Nevertheless, a similar numerical analysis results in three vibronic absorption bands, peaking at 425 nm, 447 nm and 471 nm. The average FWHM of these bands is 800 cm^{-1} and therefore larger than in LOV2 protein. The vibronic progression is 1150 cm^{-1}. The peak positions and relative amplitudes coincide with the results for the protein samples. Similarly, the fluorescence band of FMN in the protein pocket is composed of two vibronic transitions peaking at 511 nm and 541 nm. (equivalent to a progression of 1100 cm^{-1}). The relative amplitudes of these bands are 0.3 and 0.7.

The comparison of LOV2-WT, mutant C39A and free flavin shows that the Stokes shift of the protein samples ($\Delta E_{Stokes} \approx 770$ cm^{-1}) is considerably smaller than the one of FMN dissolved in aqueous solution ($\Delta E_{Stokes} \approx 1662$ cm^{-1}). This difference clearly points to the enhancement of nuclear relaxation of excited flavin and its aqueous surroundings as compared to flavin bound in the protein pocket of the LOV2 domain. [Gis80, Mül91] Although the main features of the steady state spectra are the same in WT and mutant, the fluorescence quantum yields Φ_{FL} differ for the two species: $\Phi_{FL} = 0.14$ for wildtype and $\Phi_{FL} = 0.26$ for the mutant LOV2-C39A. Since steady state measurements cannot account for contributions of thermally activated delayed fluorescence according to $T_1 \rightarrow S_1$, these contributions can be disregarded on the basis of energetics: ΔE ($S_1 \rightarrow T_1$) ≈ 0.31 eV [Tra81, Cha69] assuming that the $S_1 \rightarrow T_1$ energy gap of oxidized flavin is more or less invariant for FMN in the two proteins and solution.

7.3.2 Time-resolved spectroscopy

The fluorescence decay of LOV2-WT and LOV2-C39A is shown in Figure 7-4. Both traces can be fitted mono-exponentially to a time constant of 2.2 ns for WT and 4.3 ns for the mutant. The fluorescence lifetime of

the mutant is comparable to the lifetime of free FMN in aqueous solution at pH 7 which has been determined to be 4.6 ns. [Hee91]

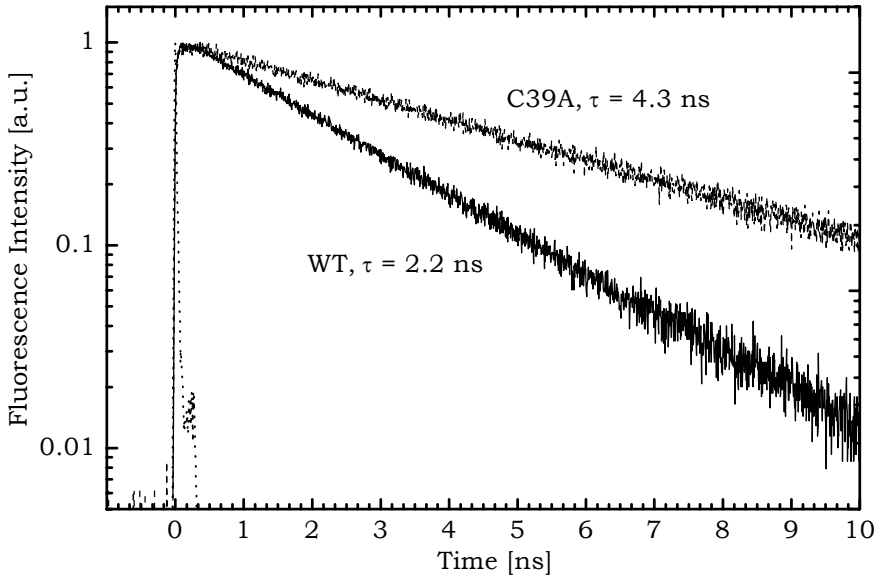

Figure 7-4: Fluorescence decay traces of LOV2-WT and LOV2-C39A, 298 K

$\lambda_{EXC.}$=443 nm, $\lambda_{DET.}$=495 nm, IRF (···, 27 ps)

In order to identify potential decay channels underlying the excited state lifetime, time-resolved absorption spectra with 200 fs resolution were taken in the spectral range between 550 nm and 750 nm (Figure 7-5). Probing at 550 nm allows to follow stimulated emission ($S_1 \rightarrow S_0$) as reflected in negative difference absorbance. This signal decays mono-exponentially culminating in a positive difference absorption, which is assigned to the triplet ($T_1 \rightarrow T_n$) transition. [Hee85] As expected, the intensity of the stimulated emission follows the increase of the FMN triplet concentration and confirms the time constant of the fluorescence measurements (Figure 7-4). The positive difference absorbance monitored at 650 nm grows in with the time constant observed for the decay of the stimulated emission. At times <100 ps the signal reflects the excited state absorption $S_1 \rightarrow S_n$, whereas due to its larger extinction coefficient at longer times the signal increases and the triplet absorption predominates. The identity of these mono-exponential traces

of excited state decay and triplet formation exclude any other photoprocess like charge separation and internal conversion on the sub-ns time scale.

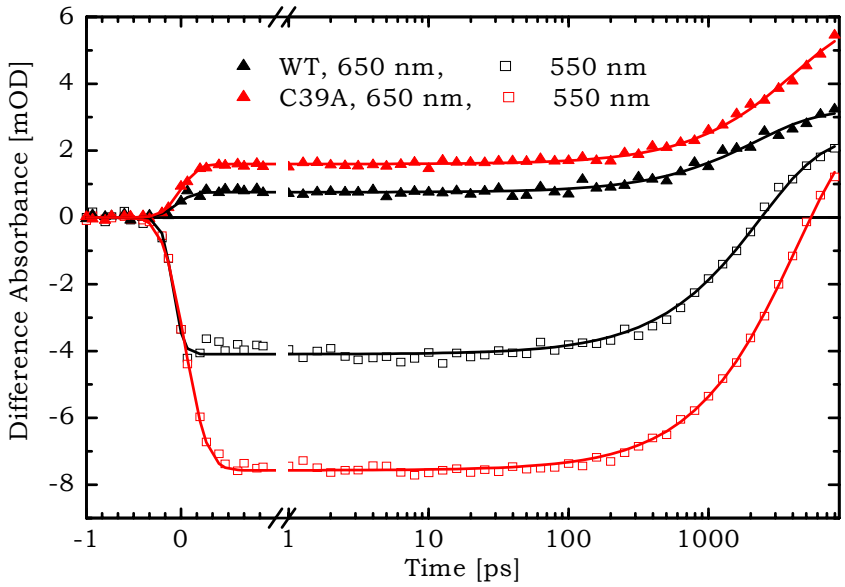

Figure 7-5: Transient absorption of LOV2-WT and LOV2-C39A

Stimulated emission ($\lambda_{DET.}$=550 nm), triplet absorption ($\lambda_{DET.}$=650 nm), IRF=200 fs

Information on the relative efficiency of $S_1 \rightarrow T_1$ ISC is given by the ratio of the absorption signal at long delay times representing the $T_1 \rightarrow T_n$ transition and the initial signals related to the excited singlet state, i.e. the $S_1 \rightarrow S_n$ transition probed at 650 nm and the $S_1 \rightarrow S_0$ transition probed at 550 nm. Since the relative extinction coefficients of FMN in the excited singlet and triplet states are unknown absolute triplet quantum yields cannot be given. However, a global analysis of the transient absorption measurements shows that the quantum yield for triplet formation Φ_{ISC} of LOV2-WT is by a factor of 1.23 ± 0.07 higher as compared to the mutant LOV2-C39A. This increase may be due to the particular electrostatics and/or the external heavy atom effect exerted by the sulfur atom of the nearby C39. With respect to the well known high ISC rate in sulfur containing compounds it should be added that

the cysteinyl-adduct, stable at low temperatures, does not show any fluorescence under steady state conditions. The residual weak fluorescence observed at 80 K is due to a minority of unbleached FMN in LOV2-WT (Figure 7-6).

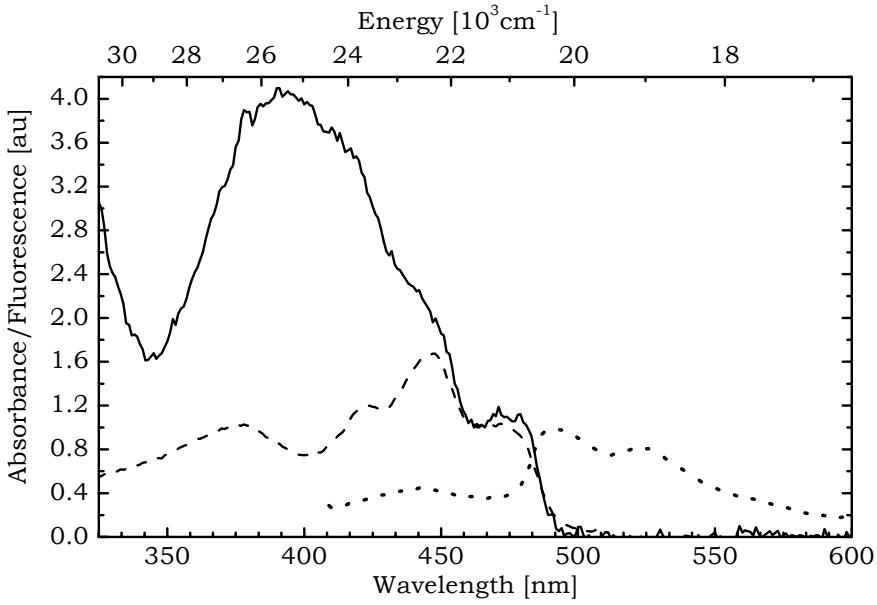

Figure 7-6: Steady-state spectra of LOV 2, 150 K, high intensity

Steady state absorption (—), fluorescence (···, $\lambda_{EXC.}$=390 nm), and fluorescence excitation (---, $\lambda_{DET.}$=525 nm) spectra

Because of the similarity of the steady state spectra with their pronounced vibronic structure it can be assumed, that in WT and mutant the FMN chromophore is immobilized in the protein binding pocket in a similar way. Assuming that motional freedom of the chromophore correlates with the IC rate, it is probable that these rates are similar. In the following we put this assumption to test by comparing its consequences on the background of the absolute triplet yield Φ_{ISC} = 0.88 [Swa01], which has been independently determined.

The resulting data set for LOV2-WT, LOV2-C39A and FMN in solution is given in Table 7-1. All rates and quantum yields rest on the assumption that k_{IC} (WT) = k_{IC} (C39A) and the experimental data of this paper: fluorescence quantum yields and lifetimes. And derived from the

transient absorption measurements $\frac{\Phi_{ISC}(\mathrm{WT})}{\Phi_{ISC}(\mathrm{C39A})} = 1.23 \pm 0.07$. This enhancement corresponds to an increase of the ISC rate in LOV2-WT by a factor of 2.4 leading to an absolute quantum efficiency of triplet formation in LOV2-WT of 0.83 ± 0.05 in agreement with the literature. [Swa01]

	τ [ns]	Φ_{FL}	Φ_{RAD} [ns]	Φ_{IC}	k_{IC} [ns^{-1}]	Φ_{ISC}	k_{ISC} [ns^{-1}]
LOV2-WT	2.2	0.14	16.4	0.03	67.1	0.83	2,7
LOV2-C39A	4.3	0.26	17.0	0.07	67.1	0.68	6.5
FMN	4.6	0.26	18.1	0.09	52.2	0.65	7.2

Table 7-1: Lifetimes, quantum yields and rates of LOV2-WT, LOV2-C39A and FMN free in solution

Fluorescence lifetime τ, radiative lifetime τ_{RAD} , quantum yields Φ for fluorescence (FL), internal conversion (IC) and triplet formation (ISC) and rates k for IC and ISC.

While the increased ISC rate is still consistent with the recent results of Kennis et al. [Ken03], the measurements represented in this paper provide clear evidence that the most important primary reaction in the LOV2 domain is intersystem crossing and that this process leads to a substantial increase of the triplet yield in LOV2-WT as compared to the mutant. This result is in contrast to corresponding study [Ken03] where no increase in the triplet yield is reported. Instead the main effect of the protein environment in LOV2-WT as compared to FMN free in solution is an increase of IC rate by a factor of 5 in the protein. This discrepancy cannot be explained but may be related to the differences in the sample preparation. This latter issue may be reflected in the different relative amplitudes of the vibronic fluorescence bands of the LOV2-WT domain in this work and the paper by Kennis et al. [Ken03]

In contrast to FMN in the C39A mutant and FMN free in solution the increase of the ISC rate and of the respective triplet yield are the most relevant characteristics of the primary photophysics of the wild type

LOV2 domain. The triplet states thus formed trigger the formation of the cysteine-adduct which is the key photoproduct responsible for the sensoric function of the LOV2 protein. The general relevance of these primary photophysics is also borne out by the comparative ps time-resolved fluorescence study on the LOV1 domain, WT and mutant C57S. [Hol02]

8 Observation of Excited Energy Transfer in (6-4) Photolyase by Picosecond Time-Resolved Fluorescence

8.1 About Photolyases

Cyclobutane Pyrimidine Dimer (CPD) and pyrimidine-(6-4)-pyrimidone photoproduct are lesions in DNA, which are induced by UV-light. Each of these lesions is repaired specifically by a photolyase enzyme. Both CPD-photolyase [San94] and (6-4) photolyase [Tod99] have similar sequences and most likely similar structures and reaction mechanisms. Several reviews on photolyases and their properties have been published in the past decade. [San03, Hee95]

The CPD photolyase has been extensively characterized: it is a 55 kDa-65 kDa enzyme and contains two chromophores. The catalytic cofactor is a two-electron reduced Flavin Adenine Dinucleotide (FAD) while the second, either a methenyltetrahydrofolate (MTHF) or a 8-hydroxy-7,8-didemethyl-5-deazariboflavin (8-HDF) [San94, San00b], functions as a photo-antenna, increasing the catalytic efficiency of the enzyme. [Pay90a] In order to repair a DNA lesion, the enzyme locates the damage in a light-dependent manner and forms a Michaelis complex with the substrate. Upon exposure of this complex to light, the second chromophore absorbs a photon and transfers the excitation energy to the flavin, which in turn transfers an electron to the DNA lesion; the cyclobutane ring of the CPD damage breaks and generates two pyrimidines. [Zha97b, San94] Consecutive back transfer of the electron restores the neutral flavin radical to the catalytically competent FADH-form and the enzyme dissociates from DNA to enter new cycles of catalysis. [San94, Kim94] It was proposed, that (6-4) photolyase functions in a similar manner. Yet recently the neutral flavin radical was found to be a long-lived intermediate of two consecutive single-electron reductions

under participation of redox-active amino-acid residues. As final electron donor acts a neutral tyrosine radical. These findings, obtained by time-resolved electron paramagnetic resonance contrast the CPD photolyase, which yielded remarkable different signals. [Web02]

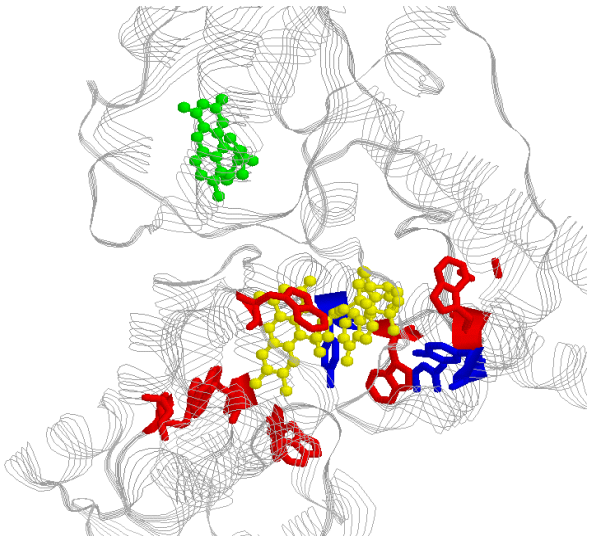

Scheme 8-1: Section of the X-ray structural analysis of CPD photolyase from *Anacystis nidulans*

FAD (yellow), trp (red and tyr (blue) within 10 Å distance from FAD. The antenna pigment is marked green.

The X-ray structural analysis of the CPD photolyase from *Anacystis nidulans* shows, that there are multiple tryptophanes and tyrosines present in the neighborhood of the flavin. Therefore in can be assumed, that multiple electron transfer from these amino acids is still competing with energy transfer from the 8-HDF antenna pigment. [Tam97]

8.2 Experimental

The (6-4) photolyase protein was provided by A. Sancar, Department of Biochemistry and Biophysics, University of North Carolina, School of Medicine, Chapel Hill, North Carolina 27599

Purification of (6-4) Photolyase. The recombinant *Xenopus* (6-4) photolyase was expressed in *E. coli* as a fusion protein with glutathione-S-transferase, GST-(6-4)PL (5) and purified through a glutathione column followed by chromatography on heparin-agarose. The enzyme was >90% pure as tested by SDS-PAGE and Coomassie blue staining. The enzyme was stored at -80°C in storage buffer containing 50 mM Tris-HCl, pH 8.0, 1 mM EDTA, 100 mM NaCl, 1 mM DTT and 50 % glycerol.

8.3 Results and Discussion

8.3.1 Steady-state spectroscopy

The steady state absorption spectrum at room temperature shows a single maximum at 412 nm (

Figure 8-1). If corrected for scattering, the maximum is at 423 nm, and a second very small one becomes visible at ~560 nm.

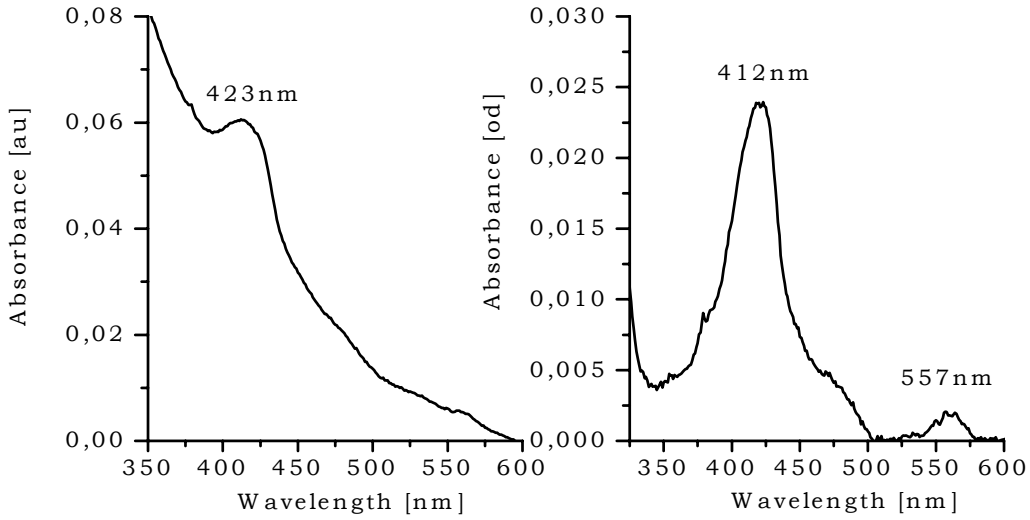

Figure 8-1: Steady-state absorption of 6-4 photolyase, 298 K

The fluorescence spectrum excited in the absorption band resembles the broad unstructured fluorescence spectrum of oxidized flavin free in solution (Figure 8-2). The corresponding fluorescence excitation spectrum shows a dominant band at 354 nm, where the signal of the antenna molecule is expected. [Kim91] The fluorescence spectrum, excited in the range of MTHF absorption exhibits a maximum at 445 nm, which can be ascribed to MTHF fluorescence [San94, Hit97] in addition to the FAD signal.

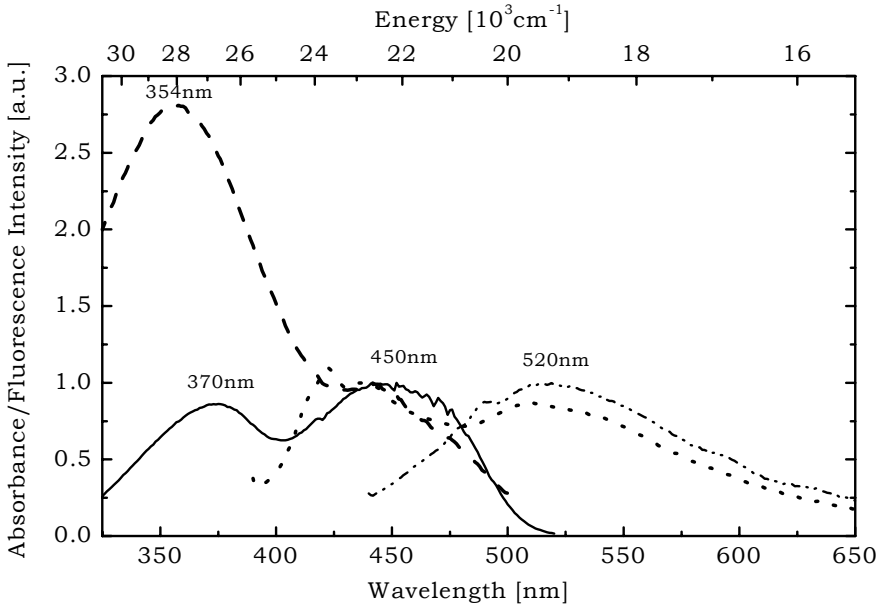

Figure 8-2: Steady-state fluorescence and fluorescence excitation of (6-4) photolyase

Fluorescence (···, $\lambda_{EXC.}$=370nm/-···-, $\lambda_{EXC.}$=420nm), fluorescence excitation (---, $\lambda_{DET.}$=520nm), fluorescence excitation of FMN (—, $\lambda_{DET.}$=520nm)

In Figure 8-2 the excitation spectrum of FMN free in neutral aqueous solution is included. This excitation spectrum rules out FAD as the sole origin of this high energy band. Consequently its predominance can be attributed to EET from excited MTHF to FAD. MTHF in protein is known to absorb maximally at 437 nm [Eke90] and exhibits its fluorescence at 463 nm. [Mal95] In CPD photolyase the absorption peak of the pterin cofactor is found in the range between 377 nm and

415 nm. [San87, Eke94, Mal94] Yet in aqueous solution the absorption maximum of MTHF shifts to 354 nm. [Kim91, Hit97] From the fluorescence excitation spectrum depicted above we may therefore assume, that the protein provides a highly polar environment for the antenna pigment.

It is surprising, that neither the fluorescence excitation spectrum of FMN free in solution nor of (6-4) photolyase resembles the absorption spectrum (

Figure 8-1) measured in this photolyase sample, as it does not show traces of oxidized flavin or MTHF. Despite this discrepancy it is consistent with absorption spectra published for flavoproteins still containing their second chromophore. [Zha97a, Sel98, Oka98, Mal95] It exhibits more resemblance to the absorption of reduced flavin but for the position of the shoulder on an otherwise by scattering dominated curve, which would be expected at ~360 nm. [Hit97] This leads to the conclusion, that the absorption spectrum does not represent the photoactive protein as the fluorescence excitation spectrum deviates strongly from the absorption spectrum. Even after the scattering correction the expected bands can not be observed. Thus no comment is possible on the polarity of the FAD environment, which can be determined by the position of its high energy absorption band originating from the S_2 transition. [Hee82] As a consequence only the fluorescence and fluorescence excitation spectra will be considered in the following sections. Even more as for *Xenopus laevis* (6-4) photolyase as well as *Arabidopsis thaliana* cryptochrome1 (Chapter 9.2) it has been shown, that the recombinant protein lacking its antenna exhibits the structured absorption spectrum of fully oxidized flavin tightly bound in a protein matrix. [Tod97, Lin95]

The slight blue-shift of the flavin fluorescence excited in the MTHF absorption band with respect to the one obtained for directly excited FAD can be explained in terms of equilibrated or not equilibrated environmental conditions. This can be clearly observed upon freezing

the sample to 150 K. The fluorescence maximum at 510 nm becomes structured exhibiting now two peaks at 495 nm and 520 nm (Figure 8-3). This effect is due to different transitions favored at different temperatures. [Ewe79]

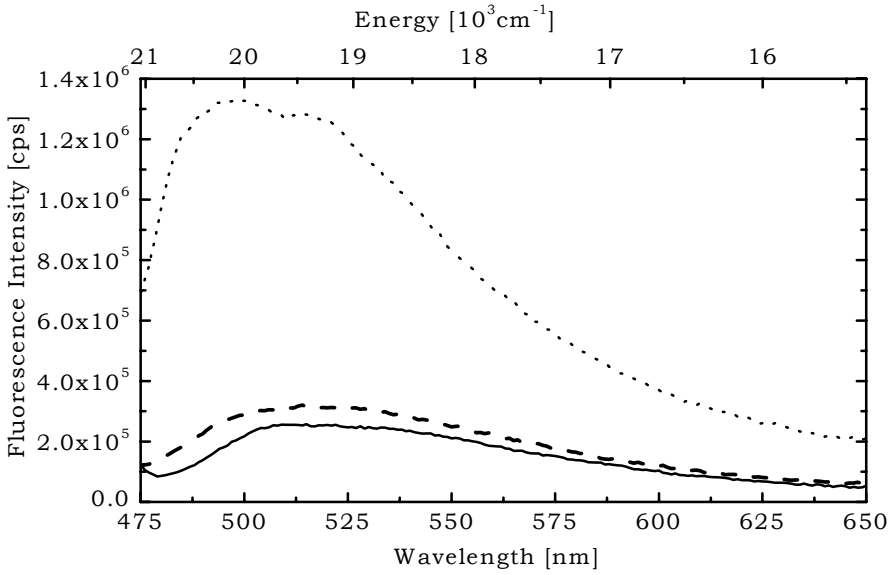

Figure 8-3: Steady-state fluorescence spectra at low temperatures of (6-4) photolyase

298 K (—), 240 K (---) and 90 K (···), $\lambda_{EXC.}$=450nm

8.3.2 Time-resolved fluorescence measurements

In order to further establish EET as the mechanism underlying its excitation spectrum, the steady-state fluorescence data were completed with fluorescence decay kinetics measured at 275 K and 90 K. After excitation at 430 nm, the global fit of the fluorescence decay kinetics yields four decay times (Table 8-2). The relative amplitude of the short time component (29 ps) decreases from 94 % (470 nm, MTHF fluorescence) to 7 % (546 nm, FAD fluorescence) (Figure 8-4).

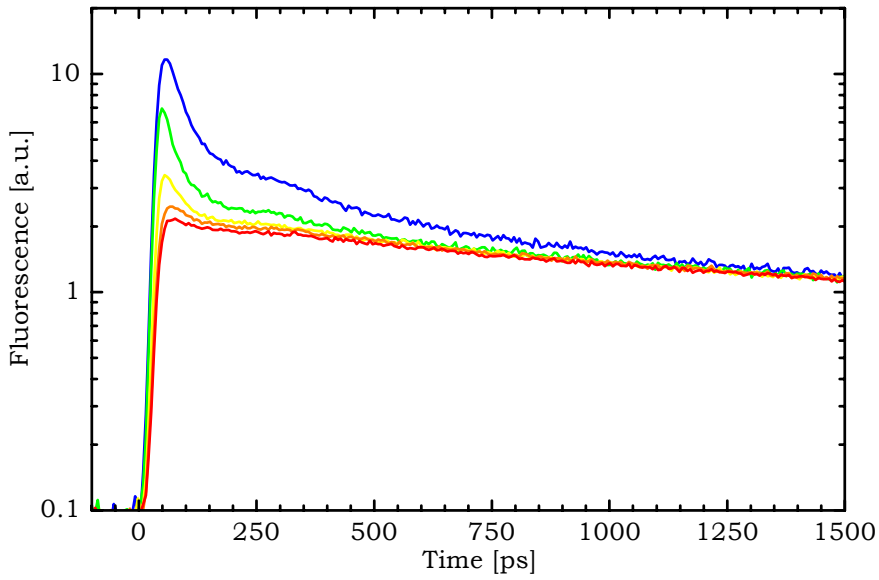

Figure 8-4: Fluorescence decay traces of (6-4) photolyase, 270 K

$\lambda_{DET.}$=485 nm (blue), 500 nm (green), 515 nm (yellow), 530 nm (orange), 546 nm (red), $\lambda_{EXC.}$ = 430 nm

The relative amplitudes of the other three components increase when the detection wavelength is tuned from blue to red. Therefore they can be assigned to FAD fluorescence (Table 8-1).

	470 [nm]	485 [nm]	500 [nm]	515 [nm]	530 [nm]	546 [nm]
τ_1 29 [ps]	94	81	83	55	21	7
τ_2 87 [ps]	3	11	5	20	38	44
τ_3 0.8 [ns]	2	5	5	9	13	15
τ_4 4.3 [ns]	1	4	8	16	28	35

Table 8-1: Time constants τ and relative amplitudes [%] of (6-4) photolyase TCSPC measurements, 270 K

$\lambda_{EXC.}$=430 nm

Upon cooling to 90 K, the short component (24 ps) still dominates the decay kinetics. Its amplitude shows values between 78 % (470 nm) to 23 % (546 nm) (Table 8-2).

		470 [nm]	500 [nm]	515 [nm]	530 [nm]	546 [nm]
τ_1	24 [ps]	78	59	38	30	23
τ_2	172 [ps]	11	17	28	30	30
τ_3	1.7 [ns]	8	10	17	18	17
τ_4	6.7 [ns]	3	13	18	22	30

Table 8-2; Time constants τ and relative amplitudes [%] of TCSPC measurement of (6-4) photolyase, 150 K

$\lambda_{EXC.}$=430 nm

This wavelength dependency of the short time constant can be interpreted in terms of a nearly activationless EET between the MTHF cofactor and the FAD chromophore.

8.3.3 Discussion and conclusions

The most relevant feature at all temperatures in the context of EET is the wavelength dependency of the fluorescence decay time constants. At 275 K the contribution of the short component (29 ps) decreases from dominating 94 % in the blue edge (470 nm, MTHF emission) to less than 10 % in the red edge of the steady-state emission band (546 nm, FAD emission). Due to that wavelength dependence the short component can not be ascribed to the decay of FAD but is rather interpreted as residual fluorescence from MTHF. Due to its large extinction coefficient this chromophore is still excited to a certain extent at 432 nm, and within 30 ps the excitation energy is then transferred to FAD. Although no rise in the red region can be observed, the contribution of MTHF fluorescence with the resulting energy transfer dominates these decay kinetics in the blue region.

Such an interpretation is consistent with the literature data [Kim91, Jor90] where fluorescence of MTHF in CPD photolyase has been reported to peak around 470 nm with lifetimes of 134 ps (EET to $FADH^-$) and 30 ps (EET to FADH°), respectively. It further excludes reduced flavin to be the origin of the absorption spectrum, as it exhibits a long lifetime of 1.4 ns

in the absence of its photoproduct, when it is fixed in a protein like in *E. coli* CPD photolyase. [But99] The average of the longer components is comparable to the lifetime of oxidized flavin (3.5 ns) in CPD photolyase. [Kim91, Kim,92] They contribute to more than 90% to the emission quantum yield.

Finally, at 150 K no remarkable change of the fluorescence kinetics could be observed. This is again consistent with the interpretation that MTHF is the dominant fluorophore in photolyase which transfers energy to FAD by the Förster mechanism.

9 Cryptochromes

Cryptochromes have high sequence homology to photolyases. [Ahm93, Lin95, Cas99] Despite this similarity, they do not show any signs of DNA repair activity. [Hsu96] Instead they function as photoreceptors for synchronizing the circadian clock with the daily light-dark cycles in animals [Hsu96, Zha97a, Thr98, Miy98, Vit99] and regulate some of the blue-light responses in plants such as growth and development. [Cas99, San00a] Cryptochromes are widespread in nature and have been found in many plants, animals and bacteria. [San03]

They exhibit 25-40% sequence identity to photolyase with higher degrees of homology to (6-4) photolyase than to CPD photolyase. [Tod96, Tod99, Cas99, San00a] Cryptochromes also contain both MTHF and FAD as cofactors. [Mal95] A significant structural feature of cryptochromes is that many of them, especially those of plant origin, have a 50-250 amino acid C-terminal extension with no homology with photolyase and very little homology among themselves. [San00a, Ahm96] It is thought that this extension mediates the effector function of cryptochrome, and indeed, over expression of this extension in *Arabidopsis* conferred a phenotype of continuous blue-light exposure, even when the plant was kept under red light. [Yan00, Sha02] The reaction mechanism of plant cryptochromes is not known yet. The only X-ray structural analysis available at present identifies an new cryptochrome class (Cry DASH) from *Synechcystis*. Like in photolyase the FAD binds non-covalently in a U-shaped conformation with close proximity of the solvent-accessible adenine and isoalloxazine rings at the bottom of a cavity formed between two distinct lobes of the helical domain. The electron transfer chain from the protein surface to FAD for activation of oxidized FAD is also conserved in comparison to *E. coli* photolyase [Li91, Aub00] (Trp320, Trp373 and Trp396, respectively).

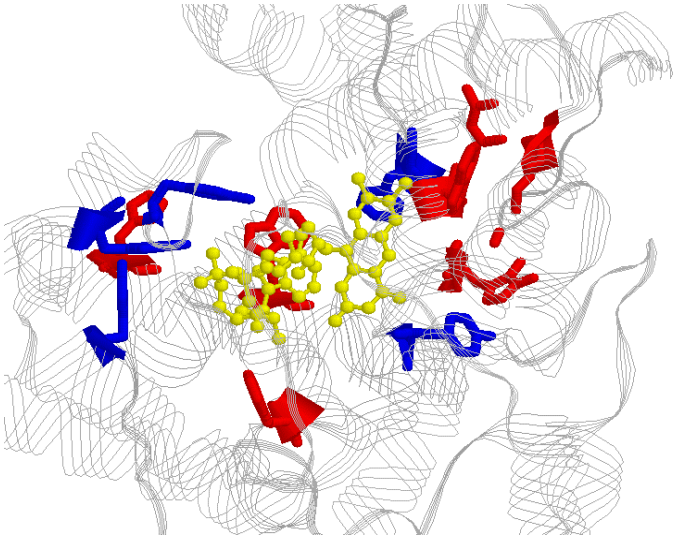

Figure 9-1: Section of the X-ray structural analysis of Cry DASH from *Synechcystis*.

Trp (red) and tyr (blue) within 10 Å distance from FAD (yellow). [Bru03]

Cryptochromes are not available from their natural sources in quantities required for photochemical characterization. Hence, we used recombinant proteins produced in heterologous systems to perform our studies. These proteins have certain drawbacks; the flavin cofactor becomes oxidized and they lose all or the majority of the pterin cofactor during purification. Animal cryptochromes contain substochiometric amounts of FAD when expressed in and purified from *Escherichia coli*. [Hsu96, Hit97, Zha97a]

9.1 Experimental

The cryptochrome proteins were provided by A. Sancar, Department of Biochemistry and Biophysics, University of North Carolina, School of Medicine, Chapel Hill, North Carolina 27599

Overproduction and Purification of MBP-HY4 (atCry1). The fusion proteins were purified by affinity chromatography on an amylose resin. *E. coli* UNC523F'lacI^q/pKM1995 or UNC523F'lacI^q/pKM1996 were

grown in Luria broth to A_{600}=0.6 and induced with 0.1 mM IPTG for 8 h. Cells were harvested and resuspended in 10 ml of lysis buffer (50 mM Tris-HC1, pH 7.5, 100 mM NaCl, 1 mM EDTA, and 10 % sucrose) per liter of culture. After a freeze-thaw cycle, the cells were sonicated 10x10 s with Branson sonicator. The cell debris was removed by centrifugation at 32000 g for 30 min, followed by a spin at 120000 g for 60 min. The cell-free extract was dialyzed against buffer B (100 mM Tris-HC1, pH 7.5, 1 mM EDTA, 10 mM β-mercaptoethanol, 20% glycerol) +0.1 M KCl and loaded onto an amylose column equilibrated with the same buffer (30 ml of resin for cell-free extract from 10-15 l culture). The column was washed with six column volumes of buffer B +0.1 M KC1, and the bound proteins were eluted with buffer B +0.1 M KC1 +10 mM maltose. 3 ml-fractions were collected, and the fusion proteins were located by SDS-PAGE and coomassie staining. Fractions containing the photoreceptor proteins were combined, concentrated by ultrafiltration, and dialyzed against storage buffer (50 mM Tris-HC1, pH 7.5, 100 mM NaC1, 1 mM EDTA, 5 mM dithiothreitol, and 50 % glycerol) and stored at -80°C. [Mal95]

Overproduction and Purification of hsCry2. The sequence of the HsCry2 gene was first identified by searching a database containing approximately one million human ESTs. Hybridization screening yielded the clone SO5. An MBP fusion of the SO5 clone was constructed by ligating an *Eco*RI/*Bgl*II fragment containing the entire open reading frame of SO5 into the *Eco*RI/*Bam*HI site of pMalc2. This construct, which contained the carboxy terminal 381 amino acids of hsCry2, was named pDH1996-2. [Hsu96] Attempts to overproduce these proteins in *E. coli* as non-fusion forms failed. Therefore, MBP fusion CRY2 were constructed and the protein was purified by amylose affinity chromatography as described previously. [Mal95]

9.2 Cryptochrome1

The *Arabidopsis thaliana* cryptochrome1 (AtCry1) protein is expected to possess no antenna pigment, as cryptochromes readily loose the MTHF molecule during the purification procedure.

9.2.1 Results

Steady-state spectroscopy. At room temperature, the steady-state absorption spectrum shows two main bands (Figure 9-2). The low energy band, peaking at 446 nm with vibronic progression (~1380 cm^{-1}) is assigned to the S_1-state of the oxidized flavin. The high energy band, originating from the S_2 state, shows two maxima at 356 and 369 nm. Such structured spectra are known for free flavin in unpolar solution [Ewe79] or, more likely in this case, for flavins fixed in a protein binding site. As discussed already in Chapter 7, the S_2 state is very sensitive to the polarity of the environment. Its position at 369 nm hints to a flavin surrounded by polar amino acids. The fluorescence spectrum of AtCry1 exhibits a broad unstructured band, which is shifted by more than 10 nm to the red in comparison with cryptochrome1 from *Drosophila melanogaster* (520 nm) [Oka98]. Taken into account, that the fluorescence excitation spectrum is identical to the unstructured one of flavin free in aqueous solution, it can be assumed that the fluorescence is caused by a minority of FAD not tightly bound in the protein pocket. The majority of the molecules fixed in the protein pocket do not contribute to the steady state fluorescence spectrum.

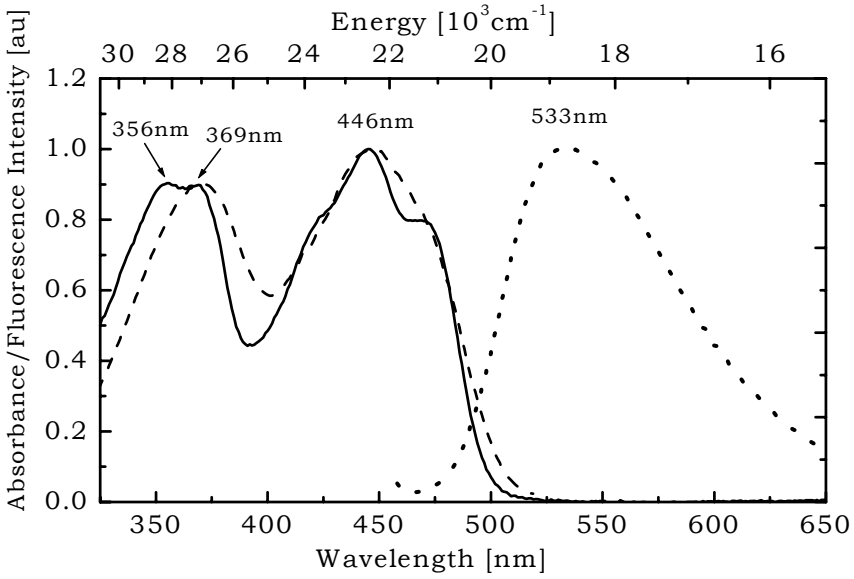

Figure 9-2: Normalized steady-state spectra of AtCry1, 298 K

Absorption (—), fluorescence (···, $\lambda_{EXC.}$=444 nm) and fluorescence excitation (---, $\lambda_{DET.}$=535 nm). In buffer solution, pH 8

Upon cooling to 90 K, the fluorescence intensity increases by two orders of magnitude. The spectrum becomes structured and the maximum shifts by more than 30 nm into the blue (Figure 9-3). It does not mirror the low energy absorption band. This effect has been observed previously for free flavins in frozen solution at 77K [Ewe79]. Upon freezing flavin free in aqueous solution the $S_1^0 \rightarrow S_0^1$ (λ_{DET}=525 nm) transition, dominant at room temperature, becomes less probable in favor of the $S_1^0 \rightarrow S_0^0$ transition (λ_{DET}=495 nm). [Hee82, Ewe79] This effect causes a large blue shift of the emission maximum. At the same time vibronic bands can be clearly resolved. The absorption spectrum does not change its shape upon cooling below the glass point (data not shown). At these low temperatures the fluorescence excitation spectrum is structured and resembles the absorption spectrum with only a slight difference in the high energy band missing the second maximum.

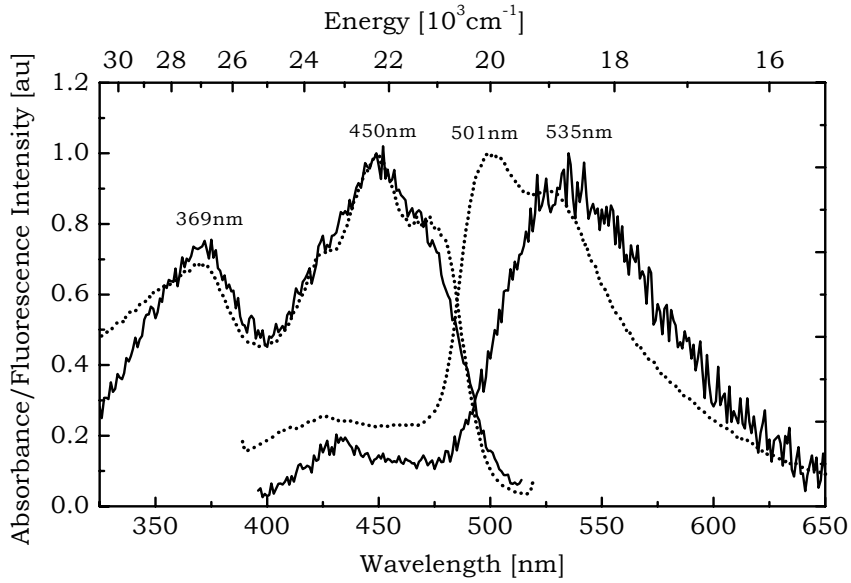

Figure 9-3: Steady-state spectra of AtCry1, low temperatures

Fluorescence ($\lambda_{EXC.}$=370 nm) and fluorescence excitation ($\lambda_{DET.}$=535 nm) at 298 K (—) and 90 K (···), containing 50 %glycerol.

Time-resolved fluorescence measurements. At room temperature the fluorescence decay kinetics of AtCry1 in buffer solution, excited either into the low or the high energy band of the oxidized FAD and detected in the wavelength range between 485 nm and 560 nm, can be fitted by a sum of four exponentials. The global fit yields the time constants 13 ps (75 %), 103 ps (13 %), 1.0 ns (2 %), and 4.8 ns (10 %), respectively (Figure 9-4). The relative amplitudes show no pronounced wavelength dependency.

Upon cooling to 150 K, the 13 ps component disappears completely. The shortest decay time is now 156 ps (63 %). τ_2 = 1.7 ns (10%) and τ_3 = 5.2 n (27%). The absence of the short decay time at low temperatures can be easily observed (Figure 9-4).

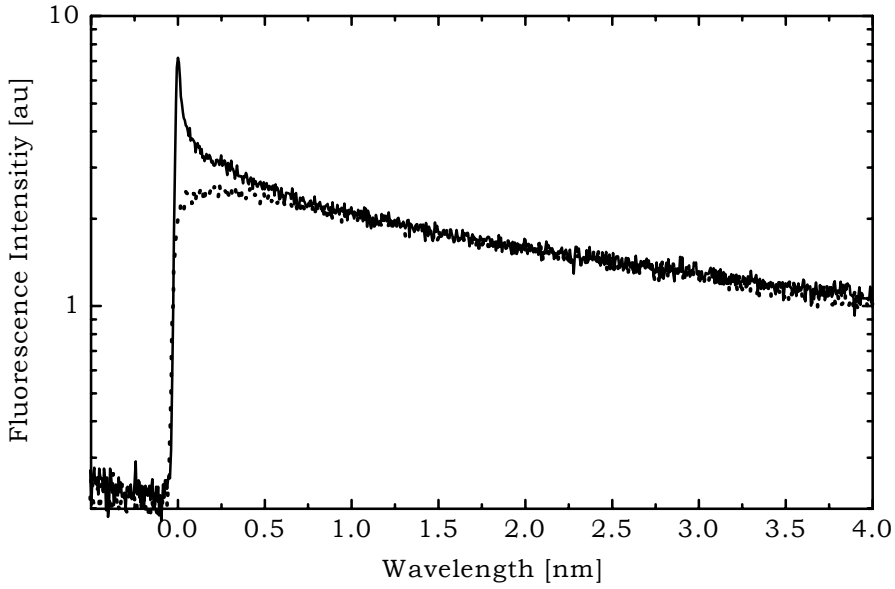

Figure 9-4: Fluorescence decay traces of AtCry1

$\lambda_{EXC.}$ =450 nm, $\lambda_{DET.}$=530 nm, at 250 K (—), 150 K (···)

9.2.2 Discussion and conclusions

The steady state absorption spectrum of AtCry1 showing vibronic progression leads to the conclusion that the flavin is tightly bound in the protein pocket. Its fluorescence is strongly quenched at room temperature as the steady-state fluorescence and fluorescence excitation spectrum are dominated by a minority of FAD either free in solution or just loosely bound in the protein pocket in a way, that it is exposed to the surrounding buffer. Upon freezing the sample, the fluorescence intensity increases by a factor of ~100, indicating that the processes of fluorescence quenching can not operate when the sample is cooled below the glass point.

These findings are confirmed by time-resolved fluorescence measurements. They yield at room temperature a short time component of 13 ps. This is on the verge of the instrumental time resolution. Therefore this value gives an upper limit for the lifetime of the first excited state. The high amplitude of this short component (75 %) is the reason, that this species dominates the absorption spectrum but does scarcely contribute to the steady state fluorescence spectrum.

EET from an MTHF antenna pigment cannot account for this shortening of the lifetime of the first excited state, as steady state spectra give no hint of the presence of an antenna molecule in agreement with the fact, that these recombinant proteins readily loose the pterin chromophore after a 2-3 column purification procedure. [Mal95, Hsu96]

The only X-ray structural analysis so far shows several tyrosines and tryptophanes in the neighborhood of the flavin. [Bru03] These aromatic amino acids are possible candidates for ET to the flavin. Similar multi-exponential fluorescence quenching dynamics –partly with even shorter decay times– have been reported for a large number of "non-fluorescent" flavoproteins such as the riboflavin binding protein, glucose oxidase [Mat98], mercuric ion reductase [Kal91], lipoamide dehydrogenase, glutathione reductase [Kok87, Bas92, Ber98] and flavodoxin [Vis87]. They are frequently ascribed to ET from a nearby aromatic amino acid, in particular from a tryptophane or a tyrosine, a conclusion that is generally supported, where available, by X-ray structural data. [Mon97, Hec93] The dispersive kinetics are a common feature of ET in proteins and may be explained in terms of conformational heterogeneity, which inevitably exists in recombinant cryptochromes produced in heterologous hosts. This is in strong contrast with recent results, reporting ET on a millisecond time-scale for atCry1. [Gio03]

The lifetime of FAD free in aqueous solution at neutral pH is 2.3 ns [Hee82] due to self-quenching of the fluorescence caused by the adenine moiety. But addition of glycerol prevents stacking and causes a more complete shift towards an open, non-quenched conformation. [Ber02] This is consistent with earlier spectroscopic studies showing that non-polar solvents prevent stacking interactions [Pen67] and the corresponding lifetime of FAD varies from 3 ns to 5 ns. [Vis87, Lee90] The amount of 60 % glycerol in our sample is sufficient to explain the measured lifetime of 4.8 ns caused by FAD not bound in the protein pocket.

9.3 Cryptochrome 2

In our studies we used human cryptochrome 2 (HsCRY2) [Hsu96]. It shares homology with cryptochrome1 but lacks the C-terminal extension. [Bat93] HsCry2 is readily degraded by blue or red light, i.e. all wavelengths which activate the enzyme, in a phytochrome-dependent manner. [Guo99, Lin98]

9.3.1 Results and discussion

Steady-state spectroscopy: At room temperature, the steady state absorption spectrum shows only a shoulder at 420 nm on an otherwise by scattering dominated curve. It resembles closely the spectrum shown in

Figure 8-1 and is therefore not shown. But this similarity hints to an antenna molecule being present in the HsCry2-sample. Consequently it is not surprising, that the steady-state fluorescence depends on the excitation wavelength (Figure 9-5). Excitation in the main absorption band of MTHF at 350 nm leads to a dominant blue fluorescence. When HsCry2 is excited at 450 nm, the resulting fluorescence shows a broad band with maxima at 495 nm and 510 nm (Figure 9-5). The fluorescence excitation spectrum does not depend on the detection wavelength. It shows a dominant band originating from MTHF. The fluorescence and fluorescence excitation spectra at room temperature show clearly, that MTHF is present in this sample. The excitation spectrum detected in the fluorescence band of FAD exhibits scarcely a trace of oxidized flavin and consequently points to energy transfer from MTHF to FAD being active. Obviously it is not as efficient as in (6-4) photolyase: excitation at 350 nm yields dominantly blue fluorescence originating from unquenched antenna molecules.

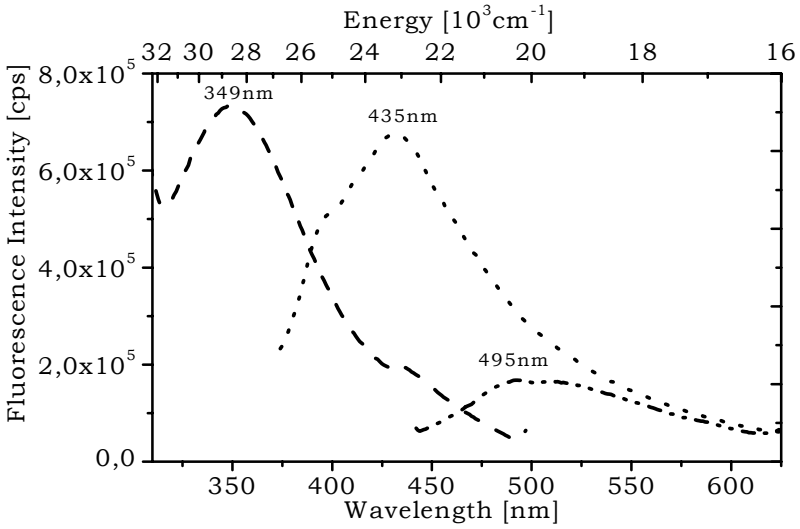

Figure 9-5: Steady-state fluorescence and fluorescence excitation of HsCry2, 298 K.

Emission (···, $\lambda_{EXC.}$=350 nm/-·-·-, $\lambda_{EXC.}$=420 nm), fluorescence excitation (---, 535 nm)

Time-resolved fluorescence measurements. The fluorescence decay kinetics of HsCRY2 at 275 K excited in the MTHF absorption band and detected in a wavelength range between 440 nm and 546 nm yield four exponentials in a global fit (Table 9-1). The shortest time constant is 24 ps and exhibits a wavelength dependent amplitude.

$\lambda_{DET.}$ [nm]		440	455	500	515	530	546	560
τ_1	24 [ps]	45	44	27	28	30	27	27
τ_2	62 [ps]	24	26	29	27	26	28	28
τ_3	0.9 [ns]	19	19	28	27	26	26	26
τ_4	3.5 [ns]	11	12	17	18	18	19	19

Table 9-1 Time constants τ and relative amplitudes [%] of HsCry2 TCSPC measurement, 270 K

$\lambda_{EXC.}$=370 nm

The amplitude of the short component is highest at 440 nm and can be ascribed to MTHF fluorescence. The amplitude consequently decreases as the detection wavelength is tuned into the range of flavin emission

(500 nm). Upon further tuning of the detection wavelength the amplitude does not change anymore. This leads to the assumption, that the flavin fluorescence itself is quenched by another fast deactivation channel, leading to short lifetimes in whole detection range of the FAD fluorescence.

This assumption is confirmed by time-resolved fluorescence measurements excited in the low energy absorption band of FAD: the global fit yields four time constants τ_1=56 ps (36 %), τ_2=336 ps (30 %), τ_3=1.4 ns (23 %) and τ_4=4.4 ns (11 %). The two shortest time components (56 ps and 336 ps) are larger by a factor of 2 as compared to direct excitation of the antenna molecule. The relative amplitudes show no wavelength dependence. These findings lead to the conclusion that energy transfer from the antenna to FAD occurs, additionally to electron transfer from a nearby aromatic amino acid.

Spectroscopic features at low temperatures. In HsCry2 the addition of glycerol once again causes a tremendous change in the steady-state fluorescence excitation spectrum (Figure 9-6). While the fluorescence spectrum remains unaffected the fluorescence excitation spectrum experiences a red-shift by 27 nm with a concomitant broadening. Therefore time-resolved measurements were carried out in front-face geometry, which allows measuring without addition of glycerol in a snowy sample.

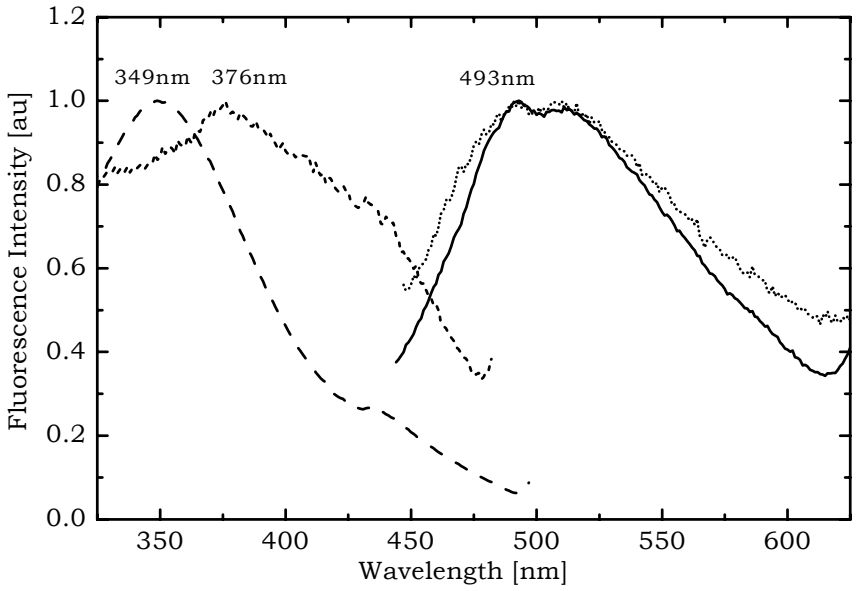

Figure 9-6: Steady-state fluorescence and fluorescence excitation of HsCry2 without glycerol: fluorescence (—, $\lambda_{EXC.}$=420 nm) and fluorescence excitation (---, $\lambda_{DET.}$=513 nm), **containing 50 % glycerol**: fluorescence (···, $\lambda_{EXC.}$=420 nm) and fluorescence excitation (---, $\lambda_{DET.}$=509 nm) at 298 K

Upon cooling to 150 K the short component of 24 ps (270 K) is absent and the fluorescence decay traces yield three time constants τ_1=133 ps (35 %), τ_2=1.1 ns (28 %) and τ_3=4.0 ns (37 %). Further cooling to 90 K results in the loss of the 133 ps component. The decay kinetics consists of two components in the ns-range: τ_1=1.0 ns (39 %), τ_2=4.0 ns (61 %). The vanishing of the short components can be clearly observed in Figure 9-7

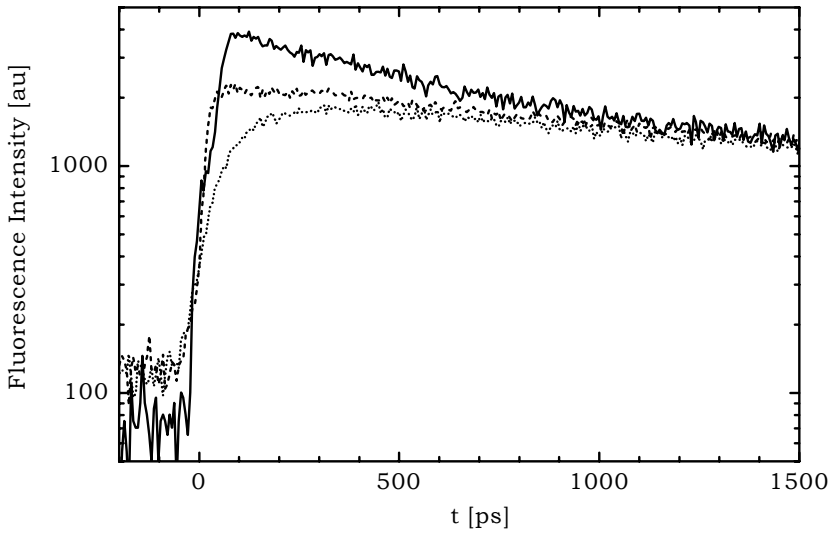

Figure 9-7: Fluorescence decay traces of HsCry2

$\lambda_{EXC.}$=432 nm, $\lambda_{DET.}$=530 nm. 275 K (—), 150 K (---), 90 K (···)

If the sample is excited at 430 nm at 150 K, the short time component is again absent: τ_1 = 319 ps (30 %), τ_2 = 2.0 ns (45 %) and τ_3 = 5.9 ns (25 %). The time constants are larger by a factor of 2 as compared to the respective measurement excited at 370 nm

9.3.2 Conclusions

The short fluorescence lifetime together with the wavelength dependence of its relative amplitude when excited at 370 nm, suggests that energy transfer from MTHF to FAD is active in HsCry2. Although the antenna pigment in HsCry2 should have been lost during the purification process, the steady-state spectra clearly show the presence of MTHF in the sample, i.e. the dominant maximum of the excitation spectrum at 350 nm.

Anyhow, it is not as efficient as in (6-4) photolyase as can be concluded from i) steady-state spectra, ii) the comparison of time-resolved fluorescence measurements with corresponding decay kinetics of (6-4) photolyase) and iii) the temperature dependence of the fluorescence decay kinetics.

i) In HsCry2 the MTHF fluorescence peaking at 439 nm dominates the emission spectrum in contrast with the corresponding spectrum of (6-4) Photolyase (Figure 8-2 and Figure 9-5).

ii) The global fit of the (6-4) photolyase decay kinetics yielded as shortest time component 29 ps (94 %). With similar decay times is this amplitude is larger by a factor of 2 as compared to HsCry2.

iii) In contrast to (6-4) photolyase containing MTHF, where the time-resolved fluorescence showed no temperature dependence, the loosing of the short time constant in HsCry2 upon cooling accounts for an activated process.

The fact, that excitation in the main FAD absorption band yields a short decay time and its relative amplitude showing no wavelength dependence points to a dark deactivation pathway competing with flavin fluorescence. In AtCry1 it has been shown, that multiple ET from nearby tyrosines and tryptophanes leads to such an effect (Section 9.2). It is convincing, that in HsCry2 this process competes with EET from MTHF and therefore leads to a shortening of the fluorescence lifetime upon excitation into the low-energy absorption band of FAD.

10 Conclusions

Green and Red Fluorescent Proteins

Influence of the solvent on the absorption spectra of wildtype GFP and mutants. Comparison of steady-state measurements of wildtype GFP and a mutant, which is still capable of ESPT shows, that addition of glycerol leads to massive changes in the ground-state equilibrium between the protonated state RH and the deprotonated state R^-, disfavoring R^-. If both proteins are immobilized in a solid polymer matrix (PVA), these changes are negligible and the spectral characteristics at room temperature are conserved at low temperatures in contrast corresponding spectra measured in buffer/glycerol matrix.

Origin of low quantum yield in blue fluorescent proteins. Picosecond time-resolved fluorescence decay traces and their temperature dependence reveal that the loss of fluorescence quantum yield in the single-site chromophore mutants Y66F and Y66H at room temperature is accompanied by short lifetimes which approach the 3-4 ps range. Upon lowering the temperature to 150 K these lifetimes approach the ns-range. The underlying mechanism is internal conversion to the electronic ground state, which is favored by motional degrees of freedom of the chromophores. The feasibility of this decay channel is supported by X-ray structural data on similar blue variants which show specific changes in the hydrogen bonding network and the free volume of the chromophores brought about the mutations. [Pal97, Wac97, Pal99] These results indicate that the predominant loss channel depends in a sensitive way on hydrogen bond interactions between the chromophore and its immediate protein environment.

Intra-oligomer excitation energy transfer in the Red Fluorescent Protein DsRed. Picosecond time-resolved fluorescence spectroscopy on the novel red fluorescent protein wildtype DsRed reveals ultrafast, intra-oligomer Fluorescence Resonance Energy Transfer (FRET) from an immature

green emitting GFP-like chromophore to the mature red emitting chromophore. Since FRET is by its very nature a short range process, it represents a highly suitable method to probe oligomerization, preferentially applicable to efficient screening of protein variants with mutagenetically altered surface docking sites.

Excited state processes in a specific red protein from corals (asFP595-WT and mutants). Time-resolved fluorescence and absorption measurements establish fast IC as the main process for quenching the red fluorescence in asFP595-Wt exhibiting a lifetime of ~400 fs. A fluorescent state can be pumped by consecutive two-photon absorption. The absorption of the second photon leads to a reversible photoconversion populating a state with ns-lifetime and a relative amplitude, which depends on the intensity of the excitation light, resulting in a higher fluorescence quantum yield. This long-lived emission is red-shifted by 10 nm with respect to the residual fluorescence of the main absorbing state. Mutations of this protein lead to two classes of mutants. In class 1 mutants the structure of the binding site is heterogeneous, partially stabilizing the chromophore in a more rigid conformation, partially allowing for fast IC (236 fs). The latter species shows the same behavior as WT in the sense that the fluorescent state can be formed upon illumination. The class 2 mutants shows a close resemblance to DsRed in the sense that oligomers containing mature and non-mature chromophores are existing, therefore allowing for FRET.

Proteins Containing Flavin in its Oxidized State

ISC as the predominant primary process in the Light- Oxygen- and Voltage- sensitive domain (LOV). In the LOV2-WT protein of *Avena sativa* singlet-triplet intersystem crossing proceeding within 2.3 ns is the primary process which increases the triplet yield by a factor of 1.23 as

compared to a mutant where cysteine 39 is replaced by alanine. This flavin triplet state is responsible for the formation of a cysteinyl-flavin adduct which triggers the unique photocycle of the LOV2 domain and thus the sensoric function of the blue light receptor phototropin.

Identification of an antenna pigment in (6-4) photolyase and cryptochrome 2. The steady state excitation spectrum of (6-4) photolyase and cryptochrome 2 shows a predominant peak at 360 nm, indicating the presence of an antenna pigment (methenyltetrahydrofolate, MTHF). The short lifetime of the MTHF fluorescence and its dependence on the detection wavelength establishes excitation energy transfer from MTHF to the flavin, ascribing a photoantenna role to the MTHF pigment in (6-4) photolyase.

Electron transfer in cryptochrome 1. In contrast to (6-4) photolyase the fluorescence lifetime of the oxidized flavin in cryptochrome 1 is short (<20ps). This short lifetime is the fingerprint of this sensoric protein system. It is tentatively attributed to electron transfer from 6 tryptophanes and 4 to the oxidized flavin. According to the X-ray structure analysis of a cryptochrome homologue Cry DASH the average distance of these aromatic amino acids is <10 Å from the chromophore. [Bru03]

11 References

[Ahm93] M. Ahmad, A.R. Cashmore, *Nature* **1993**, *366*, 162.

[Ahm96] M. Ahmad, A.R. Cashmore, *Plant. Mol. Biol.* **1996**, *30*, 851.

[Aub00] C. Aubert, M.H. Voss, P. Mathis, A.P. Eker, K. Brettel, *Nature* **2000**, *405*,0586.

[Bai00] G.S. Baird, D.A. Zacharias, R.Y. Tsien, *Proc. Natl. Acad. Sci. USA* **2000,** *97*, 11984.

[Bas92] P.I. Bastiaens, A. van Hoek, W.E. Wolkers, J.C. Brochon, A.J. Visser, *Biochemistry* **1992**, *31*, 7050.

[Bat93] A. Batschauer, *Plant J.* **1993**, *4*, 705.

[Ber02] P.A. van den Berg, K.A. Feenstra, A.E. Mark, H.J. Berendsen, A.J. Visser, *J. Phys. Chem. B* **2002**, *106*, 8858.

[Ber98] P.A.W. van den Berg, A. van Hoek, C.D. Walentas, R.N. Perham, A.J.W.G. Visser, *Biophys. J.* **1998**, *74*, 2046.

[Bev92] P. Bevington, D. Robinson, *Data Reduction and Error Analysis for the Physical Science*, McGraw-Hill International, **1992**.

[Bit03] R. Bittl, C.W. Kay, S. Weber, P. Hegemann, *Biochemistry*, **2003**, *42*, 8506.

[Bix89] M. Bixon, M.E. Michel-Beyerle, J. Jortner, A. Ogrodnik, *Biochem. Biophys. Acta* **1989**, *997*, 273.

[Bre97] K. Brejc, T.K. Sixma, P.A. Kitts, S.R. Kain, R.Y. Tsien, M. Ormö, S.J. Remington, *Proc. Natl. Acad. Sci. USA* **1997**, *94*, 2306.

[Bri99] W.R. Briggs, E. Huala, *Annu. Rev. Cell. Dev.* **1999**, *15*, 33.

[Bru03] R. Brudler, K. Hitomi, H., Daiyasu, H. Toh, K.-i. Kucho, M. Ishiura, M. Kanehisa, V.A. Roberts, T. Todo, J.A. Tainer, E.D. Getzoff, *Molecular Cell* **2003**, *11*, 58.

[Bru89] G.A. Bruckner, D.F. Kelley, *Chem. Phys.* **1989**, *136*, 213.

[Bub98] G. Bublitz, B.A. King, S. Boxer, *J. Am. Chem. Soc.* **1998**, *120*, 9370.

[Bul02] M.E. Bulina, D.M. Chudakov, N.N. Mudrik, K.A. Lukyanov, *BMC Biochemistry* **2002**, *3*, 7.

[But99] J. Butenandt, L.T. Burgdorf, T. Carell, *Angew. Chem. Int. Ed.* **1999**, *38*, 708.

[Cas99] A.R. Cashmore, J.A. Jarillo, Y.-J. Wu, D. Liu, *Science* **1999**, *284*, 760.

[Cha69] R.W. Chambers, D.R. Kearns, *Photochem. Photobiol.* **1969**, *10*, 215.

[Cha96] M. Chattoraj, B.A. King, G.U. Bublitz, S.G. Boxer, *Proc. Natl. Acad. Sci. USA* **1996,** *93*, 8362.

[Chr99] J.M. Christie, M. Salomon, K. Nozue, M. Wada, W.R. Briggs, *Proc. Natl. Acad. Sci. USA* **1999**, *96*, 8779.

[Chu03a] D. Chudakov, A. Feofanov, N. Mudrik, S. Lukyanov, K. Lukyanov *J. Biol. Chem.* **2003**, *278*, 7215.

[Chu03b] D. Choudakov, V. Belousov, A. Zaraisky, V. Novoselpv, D. Staroverov, D. Zorov, S. Lukyanov, K. Lukyanov, *Nature biotechnol.*, **2003**, *21*, 191.

[Cro01] S. Crosson, K. Moffat, *Proc. Natl. Acad. Sci. USA* **2001**, *98*, 2995.

[Cro02] S. Crosson, K. Moffat, *The Plant Cell* **2002**, *14*, 1067.

[Cub95] A.B. Cubitt, R. Heim, S.R. Adams, A.E. Boyd, L.A. Gross, R.Y. Tsien, *TIBS* **1995**, *20*, 448.

[Dex53] D.L. Dexter, *J. Chem. Phys.* **1953**, 21, 836.

[Dic97] R. Dickson, A. Cubitt, R. Tsien, W. Moerner, *Nature* **1997**, *388*, 355.

[Dop96] J. Dopf, T.M. Horiagon *Gene* **1996**, *173*, 39.

[Duy74] R.P. van Duyne, S.F. Fischer, *Chem. Phys.* **1974**, *5*, 183.

[Eke90] A.P. Eker, P. Koolman, J.K. Hessels, A. Yasui, *J. Biol. Chem.* **1990**, *14*, 8009.

[Eke94] A.P. Eker, H. Yajima, A. Yasui, *Photochem. Photobiol.* **1994**, *60*, 125.

[Eng70] R. Engelman und J. Jortner, *Mol. Phys.* **1970**, 18, 145.

[Ewe79] J.K. Eweg, F. Müller, A.J. Visser, C. Veeger, D. Bebelaar, J.D. van Voorst, *Photochem. Photobiol.* **1979**, *30*, 463.

[Fan99] C. Fankhauser, J. Chory, *Curr. Biol.* **1999**, *9*, R123.

[Fed03] R. Fedorov, I. Schlichting, E. Hartmann, T. Domratcheva, M. Fuhrmann, P. Hegemann, *Biophys. J.* **2003**, *84*, 2474.

[För49] T. Förster, *Naturwissenschaften* **1949**, 36, 186.

[För50a] T. Förster , *Z. Elektrochemie*, **1950**, *54*, 42.

[För50b] T. Förster , *Z. Elektrochemie*, **1950**, *54*, 531.

[För59] T. Förster, *Discuss. Faraday Soc.* **1959**, *27*, 7.

[För65] T. Förster, Delocalized excitation and excitation transfer in Modern Quantum Chemistry, ed. O. Sinanoglu, Academic Press, New York, **1965.**

[Gis80] S. Gishla, *Methods Enzymol.* **1980**, *66*, 360.

[Gio03] B. Giovani, M. Byrdin, M. Ahmad, K. Brettel, *Nature Struct. Biol.* **2003**, *10*, 489.

[Gro00] L.A. Gross, G.S Baird, R.C. Hoffman, K.K. Baldridge, R.Y. Tsien, *Proc. Natl. Acad. Sci. USA* **2000,** *97*, 11990.

[Gro85] R. van Grondelle, *Biochem. Biophys. Acta* **1985**, 811, 147.

[Gro94] R. van Grondelle, *Biochem. Biophys. Acta* **1994**, 1187, 1.

[Guo99] H.W. Guo, H. Duong, N. Ma, C.T. Lin, *Plant J.* **1999**, *19*, 279.

[Gur01] N.G. Gurskaya, A.P. Savitsky, Y.G. Yanushevich, S.A. Lukyanov, K.A. Lukyanov, *BMC Biochemistry* **2001**, *2*, 6.

[Häb95] T. Häberle, *Dissertation*, Technische Universität München, **1995**.

[Har95b] G. Hartwich, M. Friese, A. Ogrodnik, H. Scheer. M.E. Michel-Beyerle, *Chem. Phys*. **1995**, *197*, 423.

[Hec93] H.J. Hecht, H.M. Kalisz, J. Hendle, R.D. Schmid, D. Schomburg, *J. Mol. Biol.* **1993**, *229*, 153.

[Hee82] P.F. Heelis, *Chem. Soc. Rev.* **1982**, *11*, 15.

[Hee85] P.F. Heelis, G.O. Phillips, *J. Phys. Chem.* **1985**, *89*, 770.

[Hee91] P.F. Heelis, in: F. Müller (Ed.) Chemistry and biochemistry of flavoenzymes, Vol. 1, CRC Press, Boca Raton, **1991**, p. 171.

[Hee95] P.F. Heelis, *Chem. Soc. Rev.* **1995**, *24*, 289.

[Hei00] A.A. Heikal, S.T. Hess, G.S. Baird, R.Y. Tsien, W.W. Webb, *Proc. Natl. Acad. Sci. USA* **2000,** *97*, 11996.

[Hei85] H. Heitele und M.E. Michel-Beyerle in *Antennas and Reaction Centers of Photosynthetic Bacteria - Structure, interaction and Dynamics*, M.E. Michel-Beyerle, Springer Verlag, Berlin, **1985**.

[Hei94] R. Heim, D.C. Prasher, R.Y. Tsien, *Proc. Natl. Acad. Sci. USA* **1994**, *91*, 12501.

[Hei95] R. Heim, A.B. Cubitt, R.Y. Tsien, *Nature* **1995**, *373*, 663.

[Hei96] R. Heim, R.Y. Tsien, *Curr. Biol.* **1996**, *6*, 178.

[Hit97] K. Hitomi, S.T. Kim, S. Iwai, N. Harima, E. Otoshi, M. Ikenaga, T. Todo, *J. Biol. Chem.* **1997**, *272*, 32591.

[Hol02] W. Holzer, A. Penzkofer, M. Fuhrmann, P. Hegemann, *Photochem. Photobiol.* **2002**, *75*, 479.

[Hsu96] D.S. Hsu, X. Zhao, S. Zhao, A. Kazantsev, R.-P. Wang, T. Todo, Y.-F. Wie, A. Sancar, *Biochemistry* **1996**, *35*, 13871.

[Hua97] E. Huala, P.W. Oeller, E. Liscum, I.-S. Han, E. Larsen, W.R. Briggs, *Science* **1997**, *278*, 2120.

[Jea88] J.M. Jean, D. Chan, G.R. Fleming, *Isr. J. Chem.* **1988**. *28*, 169.

[Joh88] J.L. Johnson, S. Hamm-Alvarez, G. Payne, G.B. Sancar, K.V. Rajagopalan, A. Sancar, *A. Proc. Natl. Acad. Sci. USA* **1988**, *85*, 2046.

[Jor76] J. Jortner, *J. Chem. Phys.* **1976**, 64, 4860-4867

[Jor80] J. Jortner, *Biochem. Biophys. Acta* **1980**, *594*, 193.

[Jor90] M.S. Jorns, B.Y. Wang, S.P. Jordan, and L.P. Chanderkar, *Biochemistry* **1990**, *29*, 552.

[Jor99] J. Jortner in *Electron Transfer - From Isolated Molecules to Biomolecules*, ed. J. Jortner und M. Bixon, Wiley, New York, **1999**.

[Kal91] B. Kalman, A. Sandstrom, B.A. Johansson, B. Lindskoy, *Biochemistry* **1991**, *30*, 111.

[Kay03] C.W. Kay, E. Schleicher, A. Kuppig, H. Hofner, W. Rüdiger, M. Schleicher, M. Fischer, A. Bacher, S. Weber, G. Richter, *J. Biol. Chem.* **2003**, *278*, 10973.

[Ken03] J.T. Kennis, S. Crosson, M. Gauden, I.H. van Stokkum, K. Moffat, R. van Grondelle, *Biochemistry* **2003**, *42*, 3385.

[Kim91] S.T. Kim, P.F. Heelis, T. Okamura, Y. Hirata, N. Mataga, A. Sancar *Biochemistry* **1991**, *30*, 11262.

[Kim92] S.T. Kim, P.F. Heelis, A. Sancar, *Biochemistry* **1992**, *31*, 11244.

[Kim94] S.T. Kim, K. Malhotra, C.A. Smith, J.S. Taylor, A. Sancar, *J. Biol. Chem.* **1994**, *269*, 8535.

[Koj97] S. Kojima, T. Hirano, H. Niwa, M. Ohashi, S. Inouye, F.I. Tsuji, *Tetrahedron Lett.* **1997**, *38*, 2875.

[Kok87] A. de Kok, A.J. Visser, *FEBS Lett.* **1987**, *218*, 135.

[Kot03] T. Kottke, B. Dick, R. Fedorov, I. Schlichting, R. Deutzmann, P. Hegemann, *Biochemistry* **2003**, *42*, 9854.

[Kum00a] A.D. Kummer, J. Wiehler, H. Rehaber, C. Kompa, B. Steipe, M.E. Michel-Beyerle, *J. Phys. Chem. B* **2000,** *104*, 4791.

[Kum00b] A.D. Kummer, *Dissertation*, Technische Universität München **2000**.

[Kum02a] A.D. Kummer, C, Kompa, H. Niwa, T. Hirano, S. Kojima, M.E. Michel-Beyerle, *J. Phys. Chem.* **2002**, *106*, 7554.

[Kum02b] A.D. Kummer, J. Wieler, T.A. Schüttrigkeit, B.W. Berger, B. Steipe, M.E. Michel-Beyerle, *ChemBioChem.* **2002**, *3*, 659.

[Kum98] A.D. Kummer, C. Kompa, H. Lossau, F. Pöllinger-Dammer, M.E. Michel-Beyerle, C.M. Silva, E.J. Bylina, W.J. Coleman, M.M. Yang, D.C. Youvan, *Chem. Phys.* **1998,** *237,* 183.

[Kun85] T.A. Kunkel, *Proc. Natl. Acad. Sci. USA* **1985**, *82*, 488.

[Lee90] R. Leenders, P. Bastiaens, R. Lunsche, A. van Hoek, A.J. Visser, *Chem. Phys. Lett.* **1990**, *165*, 315.

[Lev66] V.O. Levich, *Adv. Electrochem.* **1966**, *4*, 249.

[Li91] Y.F. Li, P.F. Heelis, A. Sancar, *Biochemistry* **1991**, *30*, 6322.

[Li98] H.B. Li, W.K. Zhang, X. Zhang, J.C. Shen, B.B. Liu, C.X. Gao, G.T. Zou, *Macromol. Rapid Commun.* **1998**, *19*, 609.

[Lin95] C. Lin, D.E. Robertson, M. Ahmad, A.A. Raibekas, M.S. Jorns, P.L. Dutton, A.R. Cashmore, *Science* **1995**, *269*, 968.

[Los96] H. Lossau, A. Kummer, R. Heinecke, F. Pöllinger-Dammer, C. Kompa, G. Bieser, T. Jonsson, C.M. Silva, M.M. Yang, D. Youvan, M.E. Michel-Beyerle, *Chem. Phys.* **1996,** *213*, 1.

[Los98] H. Lossau, *Dissertation,* Technische Universität München **1998**.

[Luk00] K.A. Lukyanov, A.F. Fradkov, N.G. Gurskaya, M.V. Matz, M.L. Markelov, A.G. Zaraisky, X. Zhao, Y. Fang, W. Tan, S.A. Lukyanov, *J. Biol. Chem.* **2000,** *275*, 25879.

[Mag02] D. Magde, R. Wong, P.G. Seybold, *Photochem. Photobiol.* **2002**, *75*, 327.

[Mal95] K. Malhotra, S.-T. Kim, A. Batschauer L. Dawut, A. Sancar *Biochemistry* **1995**, *34*, 6892.

[Mal95] K. Malhotra, S.-T. Kim, A. Sancar *Biochemistry* **1994**, *33*, 8712.

[Mar01] V. Martynov, A. Savitsky, N. Martynova, P. Savitsky, K. Lukyanov, S. Lukyanov, *J. Biol. Chem.* **2001**, *276*, 21012.

[Mar56] R.A. Marcus, *J. Chem. Phys.* **1956**, *24*, 966.

[Mar63] D. Marquardt, *J. Soc. Indust. Appl. Math.* 11, **1963**, 431.

[Mar85] R.A. Marcus und N. Sutin, *Biochem. Biophys. Acta* **1985**, *811*, 265.

[Mat98] N. Mataga, H. Chosrowjn, Y. Shibata, F. Tanaka, *J. Phys. Chem. B* **1998**, *102*, 7081.

[Mat99] M.V. Matz, A.F. Fradkov, Y.A. Labas, A.P. Savitsky, A.G. Zaraisky, M.L. Markelov, S.A. Lukyanov, *Nat. Biotechnol.* **1999**, *17*, 969.

[Mic79] M.E. Michel-Beyerle, H. Scheer, H. Seidlitz, D. Tempus, R. Haberkorn, *FEBS Lett.* **1979**, *100*, 9.

[Mil90] S.M. Miller, V. Massey, D. Ballou, C.H. Williams, M.D. Distefano, M.J. Moore, C. T Walsh, *Biochemistry* **1990** *292*, 831.

[Mit96] R.D. Mitra, C.M. Silva, D.C. Youvan, *Gene* **1996**, *173*, 13.

[Miy98] Y. Miyamoto, A. Sancar, *Proc. Natl. Acad. Sci. USA* **1998**, 95, 6097.

[Mon97] H.L. Monaco, *EMBO J.* **1997**, *16*, 1475.

[Mor74] H. Morise, O. Shimomura, F.H. Johnson, J. Winant, *Biochemistry* **1974**, *13*, 2656

[Mül73] F. Müller, S.G. Meyhew, V. Massey, *Biochemistry* **1973**, *12*, 4654.

[Mül91] F. Müller, Free Flavins: Syntheses, Chemical and Physical Properties in Chemistry and Biochemistry of Flavoenzymes, CRC Press, Boca Raton, **1991**.

[Mut76] M.W. Mutz, M.A. Case, J.F. Wishart, M.R. Ghardiri, G.L. McLendon, *J. Am. Chem. Soc.* **1976**, *121*, 858.

[Niw96] M. Niwa, S. Inouye, T,. Hirano, T. Matsuno, S. Kojima, M. Kubata, M. Ohashi, F. Tsuji, *Proc. Natl. Acad. Sci. USA* **1996**, *93*, 13617.

[Oka98] S. Okano, S. Kanno, M. Takao, A.P. Eker, K. Isono, Y. Tsukahara, A. Yasui, *Photochem. Photobiol.* **1998**, *69*, 108.

[Orm96] M. Ormö, A. Cubitt, K. Kallio, L. Gross, R. Tsien, S. Remington. *Science* **1996**, *273*, 1392.

[Pag99] C.C. Page, C.C. Moser, X. Chen und P.L. Dutton, *Nature* **1999**, *402*, 47.

[Pal97] G.J. Palm, A. Zdanov, G.A. Gaitanaris, R. Stauber, G.N. Pavlakis, A. Wlodawer, *Nat. Struct. Biol.* **1997,** *4*, 361.

[Pal99] G.J. Palm, A. Wlodawer, *Methods in Enzymology* **1999**, *302*, 378.

[Pay90a] G. Payne, A. Sancar *Biochemistry* **1990**, *29*, 7715.

[Pay90b] G. Payne, M. Wills, C. Walsh, A. Sancar, *Biochemistry* **1990**, *29*, 5706.

[Pen67] G.R. Penzer, G.K. Radda, *Rev. Chem. Soc.* **1967**, *21*, 43.

[Pet03] J. Petersen, P. Wilman, T. Beddoe, A. Oakley, R. Devenish, M. Prescott, J. Rossjohn, *J. Biol. Chem.* **2003,** *278*, 44626-44631.

[Pöl93] F. Pöllinger, *Dissertation,* Technische Universität München **1993**.

[Pöl96] F. Pöllinger, C. Musewald, H. Heitele, M.E. Michel-Beyerle, C. Anders, M. Futscher, G. Voit, H. Staab, *Ber. Bunsenges. Phys. Chem.* **1996**, *100*, 2076.

[Pra92y] D.C. Prasher, V.K. Eckenrode, W.W. Ward, F.G. Prendergast, M.J. Gormier, *Gene* **1992**, *111*, 229.

[Pre03] M. Prescott, M. Ling, T. Beddoe, A. Oakley, S. Dove, O. Hoegh-Guldberg, R. Devenish, J. Rossjohn, *Structure* **2003**, *11*, 275.

[Pre92] W. Press, S. Teukolsky, W. Vetterling, B. Flannery, Numerical *Recipes in C*, Cambridge University Press, **1992**.

[Raz80] K. Razi-Naqvi, *Photochemistry and Photobiology* **1980**, 31, 523.

[Riz96] R. Rizzuto, M. Brini, F. De Giorgi, R. Rossi, R. Heim, R.Y. Tsien, T. Pozzan, *Curr. Biol.* **1996**, *6*, 183.

[Sal00] M. Salomon, J. Christie, E. Knieb, U. Lempert, W.R. Briggs, *Biochemistry* **2000**, *39*, 9401.

[Sal01] M. Salomon, W. Eisenreich, H. Dürr, E. Schleicher, E. Knieb, V. Massey, W. Rüdiger, F. Müller, A. Bacher, G. Richter, *Proc. Natl. Acad. Sci. USA* **2001**, *98*, 12357.

[San00a] A. Sancar, *Annu. Rev. Biochem.* **2000**, *69*, 31.

[San00b] G. B. Sancar, *Mutat. Res.* **2000**, *451*, 25.

[San03] A. Sancar, *Chem. Rev.* **2003**, *103*, 2203.

[San84] A. Sancar, G.B. Sancar, *J. Mol. Biol.* **1984**, *172*, 223.

[San87] A. Sancar, F.W. Smith, P.F. Heelins, *J. Mol. Biol.* **1987**, *262*, 15457.

[San94] A. Sancar, *Biochemistry* **1994**, *33*, 2.

[Schüt01] T.A. Schüttrigkeit, U. Zachariae, T. von Feilitzsch, J. Wiehler, J. von Hummel, B. Steipe, M.E. Michel-Beyerle ChemPhysChem **2001**, *5*, 325.

[Sel98] C. Selby, A. Sancar, *Photochem. Photobiol.* **1998**, *69*, 105.

[Sha02] D. Shalitin, H. Yang, T.C. Mockler, M. Maymon, H. Guo, G.C. Whitelam, C. Lin, *Nature* **2002**, *417*, 763.

[Shi79] O. Shimomura, *FEBS Lett.* **1979**, *104*, 220-222.

[Spe96] S. Speiser, *Chem. Rev.* **1996**, 96, 1953.

[Sta00] R. Stanley, A. MacFarlane, *J. Phys. Chem.* **2000**, *104*, 6899.

[Str62] S.J. Strickler und R.A. Berg, *J. Chem. Phys.* **1962**, *37*, 814.

[Str78] L. Stryer, *Ann. Rev. Biochem.* **1978**, *78*, 819.

[Swa01] T.E. Swartz, S.B. Corchnoy, J.M. Christie, J.W. Lewis, I. Szundi, W.R. Briggs, R.A. Bogomolni, *J. Biol. Chem.* **2001**, *276*, 36493.

[Swa02] T.E. Swartz, P. Wenzel, S. Corchnoy, W.R. Briggs, R. Bogomolni, *Biochemistry* **2002**, *41*, 7183.

[Tam97[T. Tamada, K. Kitadokoro, Y. Higuchi, K. Inaka, A. Ysui, P.E. De Ruiter, A.P. Eker, K. Miki, *Nat. Struct. Biol.* **1997**, *4*, 887.

[Tho98] J.J. van Thor, A.J. Pierik, I. Nugteren-Roodzant, A. Xie, K.J. Hellingwerf, *Biochemistry* **1998**, *37*, 16915.

[Thr98] R.J. Thresher, M.H. Vitaterna, Y. Miyamoto, A. Kazantsev, D.S. Hsu, C. Petit, C.P. Selby, L. Dawut, O. Smithies, J.S. Takahashi, A. Sancar, *Science* **1998**, *282*, 1490.

[Tod96] T. Todo, H. Ryo, K. Yamamoto, H. Toh, T. Inui, H. Ayaki, T. Nomura, M. Ikenaga, *Science* **1996**, *272*, 109.

[Tod97] T. Todo, S.-T. Kim, K. Hitomi, E. Otoshi, T. Inui, H. Morioka, H. Kobayashi, E. Ohtsuka, H. Toh, M. Ikenaga, *Nuc. Acid. Res.* **1997**, *25*, 764.

[Tod99] T. Todo, *Mutat. Res.* **1999**, *434*, 89.

[Tra81] R. Traber, E. Vogelmann, S. Schreiner, T. Werner, H.E. Kramer, *Photochem. Photobiol.* **1981**, *33*, 41.

[Tsi98] R.Y. Tsien, *Annu. Rev. Biochem.* **1998**, *67*, 509.

[Vis87] A.J. Visser, A. van Hoek, T. Kulinski, J. LeGall, *FEBS Lett.* **1987**, *224*, 406.

[Vit99] M.H. Vitaterna, C.P. Selby, T. Todo, H. Niwa, C. Thompson, E.M. Fruechte, K. Hitomi, R.J. Thresher, T. Ishikawa, J. Miyazaki, J.S. Takahashi, A. Sancar, A. *Proc. Natl. Acad. Sci. USA* **1999**, *96*, 12114.

[Voi01] A. Voityuk, A.D. Kummer, M.E. Michel-Beyerle, N. Rösch, *Chem. Phys.* **2001**, *269*, 83.

[Voi98] A. Voityuk, M.E. Michel-Beyerle, N. Rösch, *Chem. Phys. Lett.* **1998**, *296*, 269.

[Vol99] M. Volk, A. Ogrodnik, M.E. Michel-Beyerle, in: *Anoxygenic Photosynthetic Bacteria*, R.E. Blankenship, eds M.T. Madigan, C.E. Bauer, Kluwer Academic Publishers, Dordrecht, **1999**, p. 595.

[Wac97] R.M. Wachter, B.A. King, R. Heim, K. Kallio, R.Y. Tsien, S.G. Boxer, S.J. Remington, *Biochemistry* **1997**, *36*, 9759.

[Wac98] R. Wachter, M. Elsliger, K. Kallio, G. Hanson, S. Remington, *Structure* **1998**, *6*, 1267.

[Wal00] M.A. Wall, M. Socolich, R. Ranganathan, *Nat. Struct. Biol.* **2000,** 7, 1133.

[Web02] S. Weber, C.W. Kay, H. Mögling, K. Möbius, K. Hitomi, T. Todo, *Proc. Natl. Acad. Sci USA* **2002**, *99*,1319.

[Web50] G. Weber, *Biochem. J.* **1950**, *47*, 114.

[Web99] W. Weber, V. Helms, J. McCammon, P. Langhoff, *Proc. Natl. Acad. Sci. USA* **1999**, *96*, 6177.

[Wel82] A. Weller, *Z. Phys. Chem. NF*, **1982**, *133*, 93.

[Wie00] J. Wiedenmann, C. Elke, K. Spindler, W. Funke, *Proc. Natl. Acad. Sci. USA* **2000**, 97, 14091.

[Wie01] J. Wiehler, J. von Hummel, B. Steipe, *FEBS Lett.* **2001,** *487*, 384.

[Wie02] J. Wiedenmann, A. Schenk, C. Rocker, A. Girot, K. Spindler, G. Nienhaus, *Proc. Natl. Acad. Sci. USA* **2002**, *99*, 11646.

[Win92] J.R. Winkler, H.B. Gray, *Chem. Rev.* **1992**, *92*, 369.

[Yan00] H.Q. Yang, Y.J. Wu, R.H. Tang, D. Liu, Y. Liu, A.R. Cashmore, *Cell* **2000**, *103*, 815.

[Yan96] F. Yang, L.G. Moss, G.N. Phillips Jr., *Nature Biotechnology* **1996**, *14*, 1246.

[Yar01] D. Yarbrough, R.M. Wachter, K. Kallio, M.V. Matz, S.J. Remington, *Proc. Natl. Acad. Sci. USA* **2001,** *98*, 462.

[Zha97a] X. Zhao, J. Liu, D.S. Hsu, S. Zhao, J.S. Taylor, A. Sancar *J.Biol.Chem.* **1997**, *272*, 32580.

[Zha97b] S. Zhao, A. Sancar, *Photochem. Photobiol.* **1997**, *66*, 727.

[Zho01] D. Zhong, A.H. Zewail, *Proc. Natl. Acad. Sci. USA* **2001**, *98*, 11867

12 List of Publications

1. **Picosecond Time-resolved FRET in the Fluorescent Protein from *Discosoma Red* (DsRed-WT)**

   T.A. Schüttrigkeit, U. Zachariae, T. von Feilitzsch, J. Wiehler, J. Von Hummel, B. Steipe, M.E. Michel-Beyerle, *Chemphyschem* **2001**, *5*, 325-328

2. **Picosecond Time-Resolved Fluorescence from Blue Emitting Chromophore Variants Y66F and Y66H of the Green Fluorescent Protein (GFP)**

   A.D. Kummer, J. Wiehler, T.A. Schüttrigkeit, B.W. Berger, B. Steipe, M.E. Michel-Beyerle, *Chembiochem* **2002**, *3*, 359-663

3. **Primary Photophysics of the FMN Binding LOV2 Domain of the Plant Blue Light Receptor Phototropin**

   T.A. Schüttrigkeit, C.K. Kompa, M. Salomon, W. Rüdiger, M.E. Michel-Beyerle, *Chem. Phys.* **2003**, *294*, 501-508

4. **The Novel Phenomenon of Light Induced Increase of Fluorescence in the Coral Protein AsFP595**

   T. Schüttrigkeit, T. von Feilitzsch, C. Kompa, M.B. Agranat, K.A. Lukyanov, A. Savitsky, M.-E. Michel-Beyerle, in preparation

Danksagung

Zuerst möchte ich meiner Chefin Frau Prof. Dr. M. E. Michel-Beyerle danken, daß sie es mir ermöglicht hat, selbständig an so vielfältigen und interessanten Projekten mitzuarbeiten und dafür, daß sie regelmäßig die Knoten in meinen Denkweise entwirrt hat.

Mein weiterer Dank gilt unseren Kooperationspartnern Dr. J. Wiehler und Dr. habil. B. Steipe für den unerschöpflichen Vorrat an GFP-Proben. Prof. A. Sancar und seinen Doktoranden für die Photolyase und Cryptochromproben. Dr. M. Salomon für die LOV2-Domäne und Dr. A. Savitsky und seinen Kollegen in Moskau für das AsFP595-Protein nebst zahlreicher Mutanten.

Mein besonderer Dank gilt weiterhin:

Christian "Grizzly" Kompa für den Anfängerunterricht in Sachen Laserspektroskopie, seine unermüdliche Hilfsbereitschaft und die regelmäßigen Schokosemmeln.

Andreas "Hasi" Kummer für die Einweisung in akribische stationäre Probencharakterisierung, die gute Zusammenarbeit am GFP-Projekt und interessante Einblicke in die Fauna der Publinger Au.

Gabile Dietrich und Michaela Reischl für die Hilfe in der undurschaubaren Bürokratie der TU, viel Kaffee und guten Zuspruch.

Till "Freisprech von Telnet-Heißluft" von Feilitzsch für die gute Zusammenarbeit am AsFP595 und die neuesten Telefontarife.

Thomas "DocL" Langenbacher für die Übertragung des Photolyase-Projekts und dafür, daß ich von ihm gelernt habe, wie man Forschung nicht betreiben sollte.

Stephan "Bärli Pooh" Hess, Mirco "ConnyMaus" Götz, Bill Davis, Reinhard "Kalle" Haselsberger, Gagik Gurzadyan und Rainer Feick für das nette Arbeitsklima und das internationale Flair.

Alex Ogrodnik dafür, daß er das "Schwarze Loch" immer wohl besetzt hatte und Pancho Tzankov für die DNA-Messungen.

Meinen Knechten und Mägden Kjerstin Bruus-Jensen, Martin Bortenschlager, Clemens Wagner und Martin Ortner für die stationären Messungen an GFP und den RFPs.

Matthias "Checker" Stecher, daß er das Praktikum erträglich gemacht hat.

Und ganz wichtig: Ralph für seine unendliche Geduld und den Rückhalt während diverser Schreib- und Lernkrisen.